ROYAUME DU MAROC
Université Mohammed V - RABAT -
جامعة محمد الخامس – الرباط –
Faculté des sciences
كلية العلوم
CENTRE D'ETUDES DOCTORALES - SCIENCES ET TECHNOLOGIES

N° d'ordre **3225**

THESE

En vue de l'obtention du : ***DOCTORAT***

Structure de Recherche : **Laboratoire de Matière Condensée et Sciences Interdisciplinaires (LMCScI)**
Discipline : **Physique**
Spécialité : **Sciences des matériaux et Modélisation des systèmes**

Présentée et soutenue le 12/07/2019 par :

Abdelmajid KADIRI

Modeling and study of magnetic properties of nanoparticles assemblies: Monte Carlo analysis.

JURY

Abdellah EL KENZ	PES, Faculté des sciences, Université Mohammed V, Rabat	Président/ Rapporteur
Youssef EL AMRAOUI	PES, Faculté des sciences, Université Mohammed V, Rabat	Directeur de Thèse
Hamid EZ-ZAHRAOUY	PES, Faculté des sciences, Université Mohammed V, Rabat	Co-Directeur de Thèse
Abdelmajid AINANE	PES, Faculté des sciences, Université Molay Ismail, Meknès	Rapporteur/ Examinateur
Abdelilah BENYOUSSEF	PES, Membre résident de l'Académie Hassan II des Sciences et Techniques, Rabat	Examinateur
Lahoucine BAHMAD	PES, PES, Faculté des sciences, Université Mohammed V, Rabat	Examinateur
Abdeljalil RACHADI	PA, Faculté des sciences, Université Mohammed V, Rabat	Invité

Année Universitaire : **2018/2019**

Acknowledgements

This thesis has been carried out at " Laboratory of Condensed Matter and Interdisciplinary Sciences (LaMCsI) " Faculty of Science, Mohammed V University – Rabat, under the supervision of Pro.fYoussef EL AMRAOUI and Prof. Hamid Ez-ZAHRAOUY.

On this page, I would like to express my very great appreciation, deep gratitude and sincere thanks to my supervisor Prof.Youssef EL AMRAOUI for giving me this opportunity to learn from his valuable expertise and to have fruitful discussions with him. He patiently provided the vision, encouragement and advice necessary for me to proceed throughout my research period. It is my privilege to be his student.

As for my Co-director Prof. Hamid Ez-ZAHRAOUY , I would like to express my sincere gratitude and deep respect. You had always trusted and encouraged me. Thank you for putting me on the successful track and providing all the support at all levels.

Also, I would like also to offer my thanks to the thesis committee for reviewing my thesis and giving their insightful and useful comments and suggestions.

I would like also to express my thanks to Prof. Abdellah EL KENZ, from the Faculty of Science in Rabat, for reporting and reviewing this thesis and for agreeing to chair the jury. It is an honor for me to have him as president of the jury of this defense.

I would like to extend my thanks to Prof. Abdelilah BENYOUSSEF for the interesting discussions and contributions, he always had time to answer my questions.

I would like to thank Prof. Abdelmajid AINANE, from the Faculty of Science Meknès, for reporting and reviewing this PhD thesis, I express my gratitude for his participation in the jury of this thesis despite his occupations.

I would also like to extend my thanks to Prof. Lahoucine BAHMAD, from the Faculty of Science in Rabat, for reviewing this thesis.

I would also like to extend my thanks to Prof. Abdeljalil RACHADI, from the Faculty of Science in Rabat, for reviewing this thesis ,his encouragement and the very constructive discussions.

I would like also to offer my special thanks to all the professors of our laboratory for their valuable suggestions and discussions.

Résumé

Les nanoparticules magnétiques ont été largement étudiées pour leurs applications variées, allant du stockage d'information aux applications biomédicales. Cette multitude de fonctionnalités des nanoparticules magnétiques est due à leurs tailles nanométriques qui génèrent des phénomènes atypiques. Dans ce contexte plusieurs travaux théoriques et expérimentaux ont été consacrés à l'exploration des propriétés magnétiques de ce type de matériaux. Cependant, plusieurs problèmes ne sont pas encore résolus, en particulier la nature des interactions intra et inter-nanoparticules ainsi que les différentes morphologies des nanoparticules.

Cette thèse porte sur l'étude des propriétés magnétiques des nanoparticules en fonction de la température, à l'aide de la simulation numérique Monte et Carlo. Les effets de la dispersion, la morphologie des nanoparticules, les interactions surface-Cœur intra-nanoparticule et les interactions entre les nanoparticules ont été étudiés pour différentes tailles. Ainsi pour des nanoparticules cubiques, la température de critique, l'aimantation rémanente, les champs coercitifs et le cycle Hystérésis, dépendent fortement, des couplages d'échange, de l'anisotropie magnétique et de la taille des nanoparticules. De plus la température de compensation prend lieu pour des valeurs bien précises des interactions magnétiques surface-cœur et entre particules, en bon accord qualitatif avec les travaux expérimentaux.

Mots clés : *Nanoparticules magnétiques, nanocubes ,propriétés magnétiques, modèle d'Ising,effets de taille, diagrammes de phases, simulation Monte Carlo.*

Abstract

Magnetic nanoparticles were widely studied for their varied applications, ranging from information storage to biomedical applications. This multitude of functionalities of magnetic nanoparticles is due to their nanometric sizes, which generate atypical phenomena. In this context, several theoretical and experimental works have been devoted to the exploration of the magnetic properties of this type of material. However, various problems have not yet been solved, in particular the nature of the intra- and inter-nanoparticle interactions as well as the different morphologies of the nanoparticles.

This thesis focuses on the study of the magnetic properties of nanoparticles as a function of temperature, using numerical Monte Carlo simulation. The effects of dispersion, the morphology of the nanoparticles, the intra-nanoparticle interactions and the interactions between the nanoparticles have been studied for different sizes. Thus, for cubic nanoparticles, the critical temperature, the residual magnetization, the coercive fields and the Hysteresis cycle strongly depend on the exchange couplings, the magnetic anisotropy and the size of the nanoparticles. Moreover, the compensation temperature takes place for very precise values of magnetic interactions Core-Shell and between particles, in good agreement, qualitatively, with the experimental works.

Keywords : *Magnetic nanoparticles, nanocubes, magnetic properties, Ising model, size effects, phases diagrams, Monte Carlo simulation.*

Résumé détaillé

Au cours de ces deux dernières décennies, l'étude des matériaux à structures nanométriques a connu un intérêt grandissant en raison de leurs nombreuses propriétés physiques et applications technologiques, qui sont en général plus intéressantes que celles des matériaux massifs. Les nanoparticules magnétiques représentent un secteur d'innovation technologique pour la fabrication des dispositifs nanométriques fonctionnalisés. Elles sont véritablement devenues des briques élémentaires dans l'élaboration des nouvelles technologies. Ce qui ressort de la plupart des études est que le nanomonde recèle des surprises liées à l'effet de la taille qui conduit à avoir une augmentation du rapport surface-volume. En effet Leurs structures atomique et électronique dépendent de leur taille et présentent une évolution intermédiaire entre les deux états extrêmes de la matière, l'atome et le solide massif, ce qui entraîne l'apparition de propriétés physiques (magnétiques, optiques, etc. . .) très impressionnantes. Le domaine des nanotechnologies peut se vanter d'être l'un des rares à réunir des scientifiques issus de très nombreux domaines (physiciens, biologistes, médecins, chimistes etc...).

Vu le progrès de la science, la nanotechnologie est devenue très importante, car elle utilise la manipulation de la matière à une échelle dans laquelle les matériaux présentent des caractéristiques et fonctionnalités différentes : Les nanosciences se sont concentrées d'une part sur de nouveaux concepts et sur la recherche fondamentale à savoir la physique pour générer des nanoparticules avec des nouvelles fonctionnalités. D'autre part, la chimie pour la génération de nanoparticules avec des propriétés adaptées via différentes méthodes de synthèse. Les activités de recherche sur les nanoparticules les plus actives dans le monde comprennent des études fondamentales pour la génération, le traitement, la caractérisation et la modélisation; recherches sur des nanoparticules magnétiques; études sur les particules métalliques et composites; études et techniques d'auto-assemblage.

Depuis les travaux pionniers de Frenkel et Dorfman, les propriétés atypiques des nanoparticules magnétiques n'ont cessé de passionner les scientifiques de tout horizon, les progrès réalisés dans les approches expérimentales de même que les progrès en simulation numérique liés aux performances croissantes des moyens informatiques ont permis des avancées significatives pour caractériser des systèmes à l'échelle atomique. Les progrès dans ce domaine ont eu un impact technologique majeur pour des applications très variées, telles que: la spintronic, Le stockage d'information, la biotechnologie, capteurs magnétiques, le traitement et le diagnostic des maladies. .. et s'étendent à tous les domaines scientifiques. De plus, la complexité croissante de ces applications entraîne la conception de nouveaux nanomatériaux et ainsi l'invention de nouvelles générations de nanoparticules magnétiques en terme de structure, taille propriétés physiques. Par exemples, les nanoparticules magnétiques monodomaines à anisotropie iniaxiale pourraient permettre de stocker plusieurs petabit 1015 bit par cm2 dans un avenir proche .

Dans le domaine des biotechnologies, les particules magnétiques sont de plus en plus utilisées dans diverses applications telles que l'hyperthermie magnétique qui est né au sein du domaine biomédical précisément pour lutter contre le cancer. Face à la Résistance à la mort cellulaire des tumeurs et à la difficulté de les guérir, en effet les chercheurs ont besion d'innover de nouveaux techniques destructeurs à la palette de traitements déjà disponibles, tels que la chirurgie, la chimiothérapie, la radiothérapie, etc. alors Les nanoparticules magnétiques, apparaissent comme des plateformes multifonctionnelles extrêmement prometteuses. De plus, sous l'action du champ magnétique appliqué, les nanoparticules magnétiques ont une sensibilité magnétique unique, Elles peuvent être utilisées par exemple en imagerie médicale, comme agent de contraste permettant de faciliter l'identification de tumeurs, elles peuvent également servir de vecteurs transportant des médicaments à des endroits spécifiques du corps (drug delivery), ou encore en hyperthermie magnétique, afin de détruire ou fragiliser des cellules cancéreuses.. En surface, les nanoparticules magnétiques peuvent posséder une excellente biocompatibilité, ce qui convient aux applications médicales. Alors pour une fonctionnalisation biologique de leurs surfaces, les particules magnétiques peuvent être recouvertes d'espèces biologiques ou chimiques greffées à leurs surfaces, ce qui leur permet d'interagir et se lier avec une entité biologique ciblée, offrant ainsi la possibilité d'un "marquage" d'espèces biologiques.
Des travaux de recherche récents portant sur des capteurs magnétiques et des nanoparticules ayant des applications en biomédecine et leur détection par des capteurs magnétiques sous-tendent ces efforts, Il existe plusieurs types de techniques de détection magnétique, notamment les capteurs spintroniques basés

sur la magnétorésistance géante (GMR), la magnétorésistance à tunnel (TMR).
Dans la littérature, la majorité des nouvelles technologies dans les différents domaines nécessite de savoir synthétiser de tels objets. Actuellement, les efforts sont dirigés vers le contrôle de l'élaboration et de la synthèse de ces nanoparticules de façon à piloter leurs propriétés. Il est alors nécessaire de créer et optimiser des protocoles de synthèse de manière à avoir des objets de taille nanométrique contrôlée, avec une multitude des propriétés magnétiques dues à leurs tailles. En plus de la maturité des domaines des nanotechnologies qui engendrent des matériaux avec des mesures spécifiques, les études expérimentales apportent aussi des nouveaux défis concernant la synthèse de ces matériaux avec les normes désirées, et cela nécessite aussi l'accompagnement d'un progrès dans la modélisation de tels systèmes et la caractérisation des nanoparticules. En effet, il est indispensable de concevoir et simuler des modèles de spins permettant de tirer pleinement profit de la richesse des propriétés que recèlent ces modèles, cela va relativement réduire les couts des synthèses sachant qu'a priori, ces études théoriques vont apporter aux expérimentateurs une vision claire en terme de contrôle des tailles et des propriétés des systèmes en se basant sur des résultats théoriques.

En faisant référence à la problématique suscitée ci-dessus et pour contribuer à la formulation de ces problèmes. Nous pouvons citer les objectifs de cette thèse suivants : Nous proposons d'élaborer des modèles de spins qui portent sur des nanoparticules magnétiques avec des formes cubiques qu'ils soient en interaction ou isolés et avec différentes morphologies. L'étude théorique est faite en utilisant les méthodes de simulation Monte Carlo. Nous allons chercher à explorer les propriétés magnétiques de ce type des nanoparticules et les manipuler.

L'objectif de cette thèse était d'étudier le comportement des propriétés magnétiques des nanoparticules isolées ou en interaction, Tout au long de cette étude nous avons considéré des nanoparticules cubiques possédant une anisotropie uniaxiale. Nous avons cherché à contrôler les propriétés magnétiques d'ensemble des nanoparticules .les effets des différents facteurs ont été considérés qu'ils sont intrinsèques comme la constante d'anisotropie ou extrinsèques comme la température et le type d'excitation externe.

En premier lieu nous avons présenté les généralités sur le magnétisme et les nanoparticules magnétiques, nous avons discuté de leurs propriétés générales et magnétiques et leurs intérêt dans le domaine biomédicale, le stockage d'information et les capteurs magnétiques grâce à ces dites propriétés et leurs structures et morphologies. Nous avons ensuite présenté et décrit le modèle hamiltonian d'Ising que nous avons utilisé dans nos travaux .Nous avons également décrit la méthode Monte Carlo .Les fondamentaux concernant Monte Carlo ont été exposé , allant de principe d'application aux calculs de mesures à l'équilibre en passant par la mise en œuvre de l'algorithme de Metropolis. Nous allons maintenant résumer les principaux résultats chapitre par chapitre.

Dans le chapitre 4, nous avons étudié les propriétés magnétiques, les diagrammes de phases de l'etat fondamentale, à l'examen des diagrammes de phases à l'état fondamental et à l'exploration de l'aimantation partielle ou totale, de la susceptibilité et de la chaleur spécifique en fonction de la température et le comportement critique de la simple pérovskite P bV O3 avec spin S = 1/2 qui est un matériau important utilisé comme composants dans les appareils électronique. L'étude est faite par la simulation Monte Carlo en utilisant le modèle d'Ising 3D. En balayant sur les différentes valeurs réduites des interactions d'échange et du paramètre réduit de l'anisotropie magnétique. Il a été montré que les diagrammes de phases du système dépendent des paramètres mentionnés ci-dessus. Ces résultats correspondent à l'élaboration et à la discussion des phases stables. De plus, la température de transition déterminée dans cette étude (TN 182K) est en bon accord avec la valeur expérimentale TN = 190K. La transition de température augmente également avec l'augmentation de la valeur absolue des interactions de couplage d'échange (Jab, Jc). En outre, en étudiant les effets de la taille du système, nous avons constaté que le pic de la susceptibilité magnétique augmente lorsque la taille du réseau augmente. Pour étudier le comportement critique du matériau mis en évidence, nous avons été amenés à calculer les exposants critiques correspondants à la longueur de corrélation, à l'aimantation totale et à la susceptibilité magnétique.

Dans le chapitre 5, en utilisant la simulation de Monte Carlo, nous avons étudié un nanocube d'Ising à spin (5/2; 3/2; 5/2) en trois couches. Nous avons étudié les effets des couplages d'échange,

le paramètre de l'anisotropie, le champ magnétique externe, la taille du rapport d'épaisseur r sur les propriétés magnétiques et thermodynamiques. Les diagrammes de phases sont obtenus pour différents couplages d'échanges réduits $J2/J1$ (interaction $\sigma - \sigma$), $J3/J1$ (interconnexion entre couches $\sigma - S$) et paramètre réduit d'anisotropie $D/J1$, où les couplages d'échange entre spins σ et entre les spins S respectivement $J1$, $J2$ sont considérés comme ferromagnétiques, tandis que le couplage d'échange intercouche $J3$ est considéré comme antiferromagnétique. Selon les résultats, il est démontré que le système peut afficher le comportement de compensation. Pour le système actuel, on vérifie si le point de compensation (Tcom) apparaît dans le système, en fonction de l'existence du couplage d'échange critique $J2/J1$ et du paramètre anisotrope $D/J1$.

Dans le chapitre 6 dans la première section nous avons étudié les effets de taille et les paramètres de couplage et d'anisotropie sur les propriétés magnétiques des nanoparticules ferromagnétiques d'Ising spin-1.Le système étudié a la particularité d'être un cube de Rubik composé de nanocubes identiques .Ceci a été réalisé en utilisant la simulation de Monte Carlo dans le cadre du modèle d'Ising 3D . Il a été démontré que les diagrammes de phases dépendent des paramètres du système et sont affectés non seulement par la taille du nanosystème, mais également par sa taille. En effet, en fonction du couplage d'échange réduit, deux régimes ont été observés où la température critique réduite diminue et augmente, respectivement. Le système présente les transitions de phases du second ordre à des températures finies. De plus, On a appliqué un champ magnétique externe et nous étudions les boucles d'hystérésis pour les basses valeurs sélectionnées de la température. On a constaté que la réponse de l'aimantation à la force du champ magnétique montre des comportements d'hystérésis avec des boucles simples où le champ coercitif magnétique réduit s'amincit jusqu'à disparaître lorsqu'on passe de t = 0,1 à t = 5. Enfin, la variation du champ coercitif en fonction des tailles a mis en évidence un phénomène bien connu de nanomatériaux magnétiques à interactions dipolaires, où le champ coercitif augmente, atteint un maximum puis diminue à zéro lorsque la taille des nanoparticules diminue. Cependant, dans notre cas, nous n'avons pas trouvé de champ coercitif réduit à zéro pour les petites tailles. Nous avons attribué ces phénomènes à la structure et à la nature de notre système. Nous avons trouvé que nous résultats sont qualitativement en accord avec d'autres travaux.
Dans la deuxième section et dans le même contexte des nanocubes ,on a étudié les propriétés magnétiques de chaîne des nanocubes magnétiques (NCCM) de spin-1 ont été étudiées par les simulations de Monte Carlo. Les propriétés magnétiques ont été déterminées en faisant un balayage des valeurs des paramètres du système. Les températures de transition réduites sont établies pour différentes tailles de cube de NCCM (Lc * Lc * Lc). Il en ressort que la température de transition réduite augmente avec l'augmentation de la taille du cube (Lc). Comme deuxième résultat, la magnétisation par rapport à l'anisotropie réduite pour différentes valeurs de l'interaction d'échange réduite, de la taille du NCCM, du champ magnétique externe réduit ainsi que de la température réduite. Les cycles d'hystérésis magnétique sont trouvés pour différentes valeurs de température réduite, différentes valeurs d'interaction d'échange ainsi que pour différentes anisotropies réduites. Le champ magnétique coercitif augmente avec l'augmentation du couplage d'échange réduit et de l'anisotropie réduite, tandis que le champ coercitif diminue lorsque la température réduite augmente.

Dans la troisième section, nous avons étudié les propriétés magnétiques d'un nanosystème ayant une structure de cube de Rubik constitué par des nanocubes de morphologie core/shell, avec spin-1/2 dans le core et spin-3/2 sur le Shell. Ceci est simulé par la méthode Monte Carlo en utilisant le modèle Ising 3D basées sur un algorithme de Metropolis. Nous avons étudié les effets des paramètres de système sur les diagrammes de phase pour différentes tailles de système et les comportements d'hystérésis lors de l'application du champ magnétique externe. On a observé que les couplages d'échange et l'anisotropie magnétique affectent les diagrammes de phase. L'augmentation des interactions d'échanges positifs entre les spins core et shell, sur un et entre nanocubes d'autre part, a la particularité d'augmenter la température critique, en favorisant la phase stable (3/2, 1/2). La même phase est également avantagée par valeurs positives de l'anisotropie magnétique. Pour chaque phase on a présenté la configuration des spins de notre système étudié. De plus, l'augmentation de la taille du système a pour effet d'augmenter la température critique, comportement typique observé avec nanosystèmes. L'étude du comportement par hystérésis a montré que les couplages d'échange et l'anisotropie magnétique contrôlent la coercivité.

Finalement, ce travail démontre qu'il est possible de contrôler l'ordre magnétique dans les NPS

cubiques en jouant sur les tailles et les nombres des nanoparticules. De plus, les résultats obtenus pourront servir comme point de comparaison pour des calculs théoriques sur ces types de systèmes afin de mieux comprendre la relation entre leurs propriétés magnétiques et les facteurs structuraux et de la taille .

List of Figures

List of Tables

Contents

General introduction

Over the past two decades, there has been an increasing interest in the study of nano-structured materials [1–5] thanks to their many physical properties and technological applications, which are generally more interesting than those of solid materials. In fact, the magnetic nanoparticles are still a field full of potentials because of the fact that technological innovations are most likely to be made in this field for the fabrication of functionalized nano-metric devices. They have truly been seen as the basic stepping stones to the development of new technologies [1, 6], and this fact is what the wide majority of research studies have proved through finding that the nano-world contains astonishing surprises in terms of the effect of size; and this, in turn, leads to an increase in the surface-to-volume ratio. Their atomic and electronic structures depend on their size [7–9]and at the same time present an intermediate evolution between the two extreme states of matter, the atom and the massive solid. Indeed, this leads to the appearance of very impressive physical properties (magnetic, optical, etc.) [10–14]. So, the field of nanotechnology is undoubtedly one of the few sectors able to bring together scientists from many fields (physicists, biologists, doctors, chemists etc.) [15–18].

Given the progress of science, nanotechnology has become very important because it uses the manipulation of matter on a scale in which materials have different characteristics and functionalities: nanosciences have focused on one hand on the research in fundamental physics to study and explore other phenomena for nanoparticles that will lead to new features. On the other hand, the development and the synthesis of nanoparticles with properties adapted to the requirements of technological applications via different synthesis methods.in the same context, one of the most active research activities in the world has been devoted to the synthesis, fundamental study and modeling of so - called magnetic nanoparticles [19–22].

Since the pioneering works of Frenkel and Dorfman [23], the atypical properties of magnetic nanoparticles have continued fascinating scientists from all different fields. For instance, the progress made in both experimental approaches and numerical simulation which is related to the increasing performances of computing resources have led to significant advances in characterizing systems at the atomic scale. The headway made in this field has had a major technological impact on a wide range of applications such as: Spintronic [24–26], information storage [27–29], biotechnology [30–33], magnetic sensors [34–36], disease treatment and diagnosis [37, 38]. Actually, this impact concerns all the scientific fields. In addition, the increasing complexity of these applications leads to the design of new nano-materials and as a result this caused the emergence of new generations of the magnetic nanoparticles in terms of structure, size and physical properties: Monodomain magnetic nanoparticles with iniaxial anisotropy is enabled to store several petabit (10^{15} bits per cm^2) in the near future .

In the field of biotechnology, the magnetic nanoparticles are increasingly used in various applications such as the magnetic hyperthermia [39–42] which was born within the biomedical field with precisely the aim to fighting against cancer. Faced with the resistance to cell death of tumors and the difficulty of curing them, researchers need to innovate new effective and destructive techniques to be added to the existing variety of already-available treatments, such as surgery, chemotherapy, radiotherapy, etc. Besides, under the action of the applied magnetic field, the magnetic nanoparticles, which appear as extremely promising multifunctional platforms, have a unique magnetic sensitivity in the sense that they not only can be used, for example, in medical imaging [43–46] as a contrast agent to facilitate the identification of tumors, but also they can serve as vectors carrying drugs to specific areas of the body (drug delivery) [47–49] . On the surface, the magnetic nanoparticles can have excellent biocompatibility that

is suitable for medical applications [50, 51] see Figure 1. For biological functionalization of their surfaces, the magnetic particles can be covered with biological or chemical species grafted on their surfaces which allow them to interact and to bind with a targeted biological entity, and in this way they provide the possibility of "marking" of biological species [52, 53] .

Recent research on the magnetic sensors and nanoparticles with applications in biomedicine and their detection by the magnetic sensors crystallizes the huge efforts made in this respect [54, 55]. There are several types of magnetic detection techniques, including spintronic sensors, which are based on the giant magneto-resistance (GMR) [56, 57], and the tunnel magneto-resistance (TMR) [58, 59].

In the literature, the majority of new technologies in the different fields require the miniaturization of such objects. Currently, efforts are directed towards control of the elaboration and synthesis of these nanoparticles so as to control their properties. It is then necessary to create and optimize synthesis protocols in order to have objects of controlled nanometric size, with a multitude of properties magnetic due to their sizes. In addition to the maturity of the fields of nanotechnology that generate materials with specific measurements, experimental studies also bring new challenges regarding the synthesis of these materials with the desired standards, and this also requires the accompaniment of a progress in the modeling of such systems and the characterization of nanoparticles. Indeed, it is essential to design and to simulate spin models allowing to take full advantage of the richness of the properties that these models conceal, it will relatively reduce the costs of syntheses knowing a priori, these theoretical studies will provide the experimenters a clear vision in terms of size control and properties of the systems based on theoretical results.

Bearing in mind the problem raised above and as a contribution to the formulation of these problems, we would like to cite the following as the objectives of our thesis. Firstly, we propose to elaborate spin models that deal with the magnetic nanoparticles with cubic forms that are either interactive or isolated and with different morphologies. Secondly, the theoretical study is conducted using Monte Carlo simulation methods. In order to explore the magnetic properties of this type of nanoparticles and to manipulate them.

Besides the general introduction, this manuscript consists of two main parts so that we could meet the different objectives set for this dissertation. The first presents a state of the art with the purpose of presenting the theories and general properties of the magnetism of nanoparticles that will be used throughout this thesis. To cover all the necessary points so as to understand the importance of the new theoretical results obtained, this part consists of three chapters.

In the first chapter, we first introduce the history of magnetism along with its origin to set the context of our research questions. Then, before our describing the different forms of magnetic energies and the magnetic interaction that generates these energies, we deal with the different magnetic orders, each with its definition and properties. Finally, the hysteresis behavior is the last element tackled with.

In the second chapter, which is dedicated to nano-magnetism, we introduce the notion of magnetic nano-particles along with their properties and the phenomena related to atypical magnetic nanoparticles vis-à-vis those of the massifs. Afterwards, we pay special attention to the anisotropy of the nanoparticles. As a closing point of this chapter, we give a brief description of what is called core/shell type morphology for the magnetic nanoparticles.

The third chapter is devoted to the introduction of Monte Carlo (MC) simulation methods. We start with an introduction of some models of spins. Then, we present the basics of static MC simulation. Finally, we describe some algorithms for numerically generating Ising model configurations while focusing on the Metropolis algorithm.

For the second part, which is entitled "contributions", consists of three chapters. The first chapter which represents the case of a massive system, we study the magnetic properties of perovskite PbVO3. We through examining the effects of the couplings and size on the magnetization and susceptibility. Finally, we determine the critical coefficients.

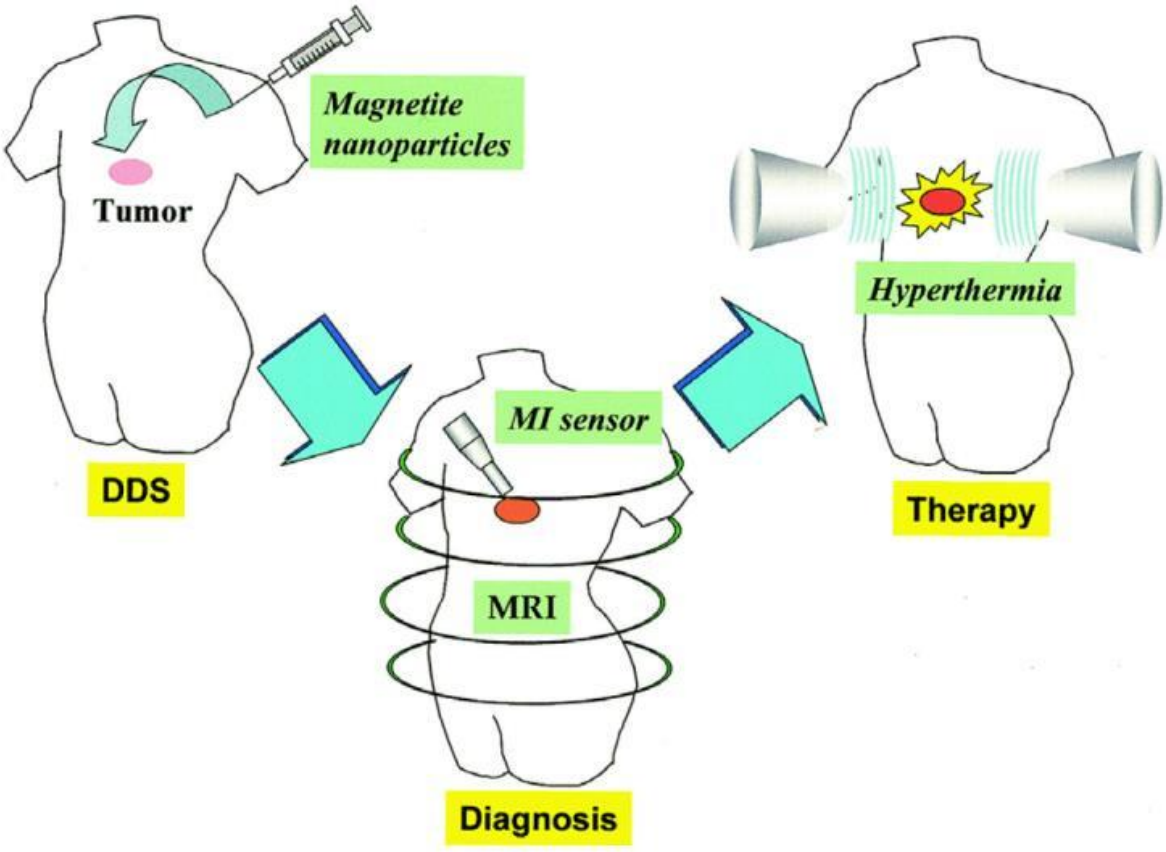

Figure 1: Scheme of the treatment strategy using magnetic nanoparticles [60]

The seconde chapter treats the case of an isolated magnetic nanocube with the combination of several magnetic elements in the form of a sandwich. In fact, the study here is concerned with a nanocube in multilayer magnetic form :two layers with spin-5/2 and a layer in the middle with spin-3/2 $(5/2, 3/2, 5/2)$ by concentrating on the anisotropy and coupling problems between the ferromagnetic and antiferromagnetic layers that can induce hysteresis loop offsets or magnetization reversals in the applied magnetic fields according to the processes which are sometimes complex. Also, we concentrate on the effect of the layer thickness on the critical and compensation temperatures .

The third chapter is dedicated to the case of assemblies of nanocubes. In the first section we present a theoretical study of the magnetic behavior of a set of ferromagnetic nanocubes in the form of a Rubik's cube, using the Monte Carlo method. Precisely, based on the Ising model, we simulate this set of the magnetic nanocubes that all carry spin-1. First, we study the effect of the size and number of nanocubes on the transition temperature of the system, by establishing phase diagrams for the different coupling values. Then, we present a transition temperature phase diagram as a function of anisotropy parameter. After that, we present the hysteresis behavior of the system under the effect of size. The second section is limited to the study of a spin-1 system in the form of a nanocubes chain, through focusing on the effect of anisotropy and size on the magnetic behavior of this system. Finally, the third section represents the study of an assembly of magnetic nanocubes that are in interaction with a core / shell morphology.

This thesis ends with a concluding section where we recall the main results and then present some perspectives which should constitute an interesting task for future investigations.

Part I

State of the art and basic concepts

Chapter 1

Magnetism background

1.1 Introduction

Since the dawn of time, magnetism intrigues the peoples and accompanies their history. Among the Greeks, Aristotle attributes the first scientific discussions on magnetism to the pre-Socratic philosopher Thales de Millet (600 BC). At the same time, the Chinese worked magnetite and made compasses for divinatory geomancy, for example to determine the optimal position of tombs and palaces. The discovery of a worked Olmec hematite suggests that this Central American people could also have used compasses to orient their temples, nearly a millennium before the Chinese ($<$ 1000 BC). The earliest treatises mentioning the practical use of magnetism, especially for navigation, date back to medieval times: in China (Shen Kuo, 1088), in Europe (A Neckam, 1190), then in the Arab world (1232). In 1269, the French engineer Pierre de Maricourt wrote the first detailed treatise on magnetism, describing in particular the laws of attraction and magnetic repulsion. From this date, all European explorers use the compass as a guide in the discovery of unknown regions of the globe, starting with Marco Polo and his brothers during their travels in China. Christopher Columbus follows suit 200 years later. As for LaPérouse, he will baptize his flagship "LaBoussole" in tribute to this tool, which has become indispensable to the sailor.

1.2 Mgnetic orders

Atoms in a massive magnetic material behave like little magnets, characterized by their magnetic moment. When a magnetic field (H) is applied, these elementary magnets orient themselves according to the field and the material then acquires a magnetization $M = \chi H$ (weak field) where χ is the magnetic susceptibility [1] [62] .

The magnetic moments can be oriented in different ways depending on the magnetic behavior of the material: diamagnetic, paramagnetic, ferromagnetic, ferrimagnetic or antiferromagnetic see Figure 1.1 [63]. In the case of the magnetic materials where the atoms don't interact with their neighbors, we speak of the non-cooperative magnetism. Atoms have a spontaneous macroscopic magnetization which is null.
There are two types of non-cooperative magnetism (Diamagnetism and Paramagnetism) :

1.2.1 Diamagnetism

The atoms have a zero permanent magnetic moment and acquire a weak moment induced in the presence of field. Their magnetization, induced by the field, is very weak and antiparallel to the field. The magnetic susceptibility χ, that is negative and of the order of 10^{-5}, does not depend on the temperature as illustrated in Figure 1.2 .

[1] The magnetic susceptibility χ is a dimensionless proportionality constant that indicates the degree of magnetization of a material in response to an applied magnetic field [61]

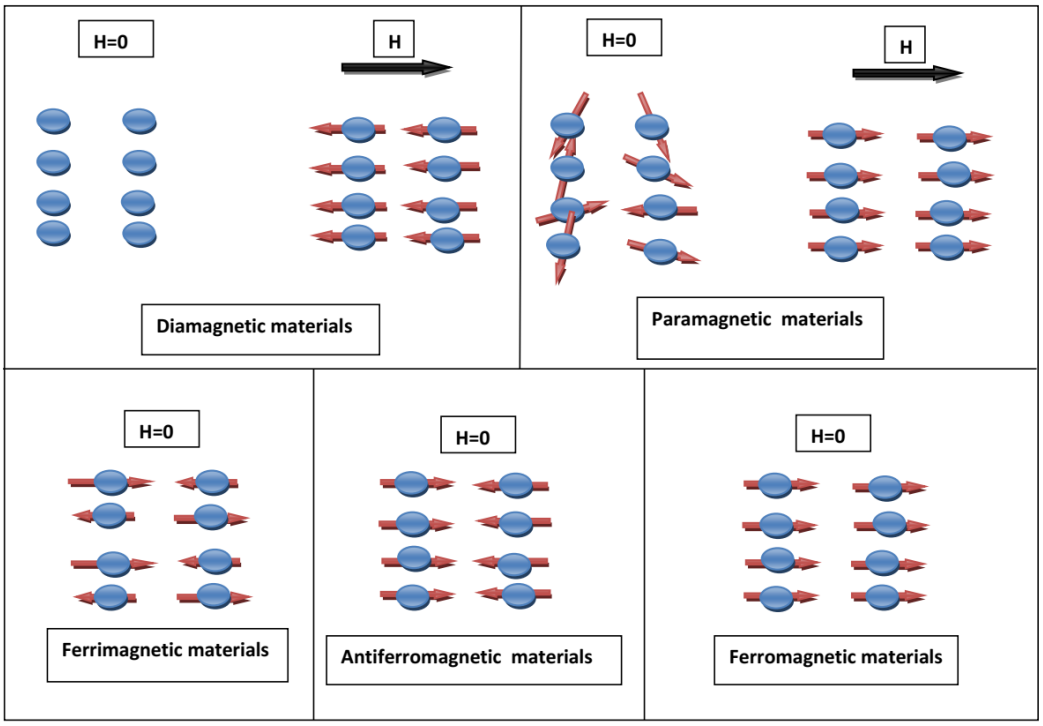

Figure 1.1: The different types of magnetic behaviors [64]

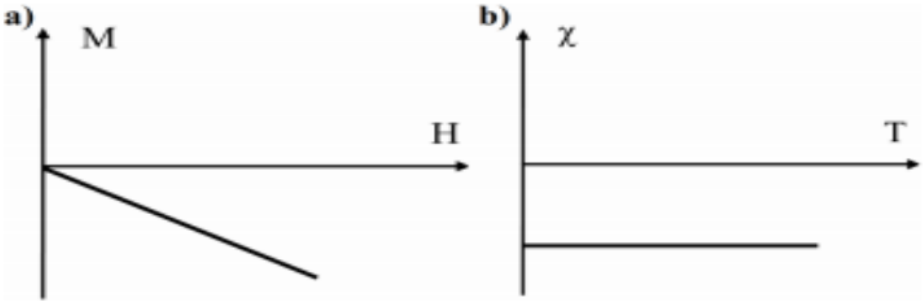

Figure 1.2: In (a) Magnetization as a function of the external magnetic field and in (b) the susceptibility as a function of temperature in the diamagnetic material.

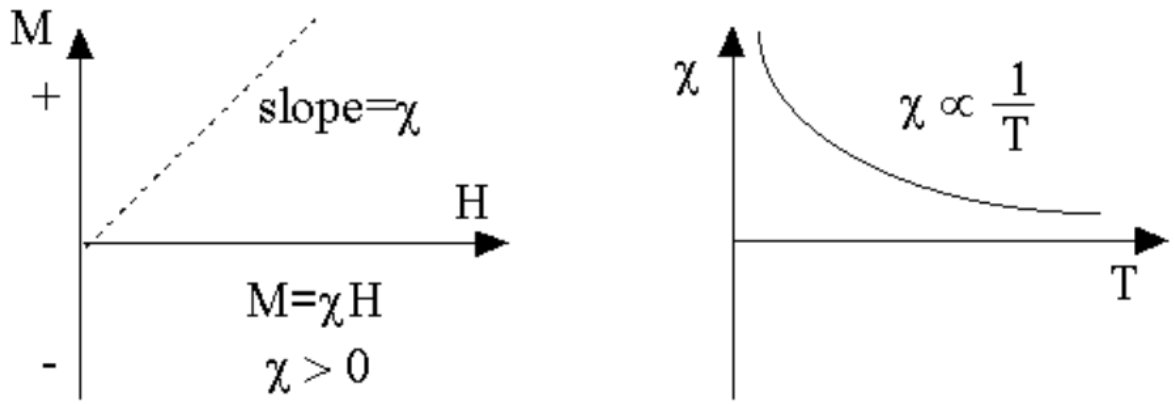

Figure 1.3: Magnetization as a function of the external magnetic field is on the left while the susceptibility as a function of temperature is on the right in the paramagnetic material.

1.2.2 Paramagnetism

The atoms have a non-zero permanent magnetic moment, and align themselves parallel to the applied field. The susceptibility χ is inversely proportional to the temperature T (Curie's Law) [65]: $\chi = C/T$, with C the Curie constant. χ is positive and of the order of $10^{-4} - 10^{-5}$ see Figure 1.3.

In the presence of interactions, the magnetic moments are spontaneously orientated in the absence of an external field. There are three types of cooperative magnetic behaviors(Ferromagnetism,Antiferromagnetism and Ferrimagnetism).

1.2.3 Ferromagnetism

The positive exchange interactions favor the parallel alignment of the magnetic moments of neighboring atoms. The susceptibility, instead of becoming infinite at $0K$ as in a paramagnetic order, it becomes infinite at a characteristic temperature, called Curie Temperature T_C (Curie-Weiss Law). Below this temperature, the interactions dominate the thermal agitation and spontaneous magnetization M_S appears in the absence of applied field.

1.2.4 Antiferromagnetism

Below a critical temperature T_N(Neel temperature) an ordered state of the magnetic moments appears. The moments are aligned in two equal and opposite magnetization subarrays, so that the total resultant magnetization is zero. Above the temperature of Néel, the thermal agitation leads to a susceptibility similar to that of a paramagnetic one.

1.2.5 Ferrimagnetism

Antiferromagnetism in which the carriers of moments are not equivalent. There is no further compensation for the magnetization of two sub-lattices and, below the order temperature T_C, spontaneous magnetization

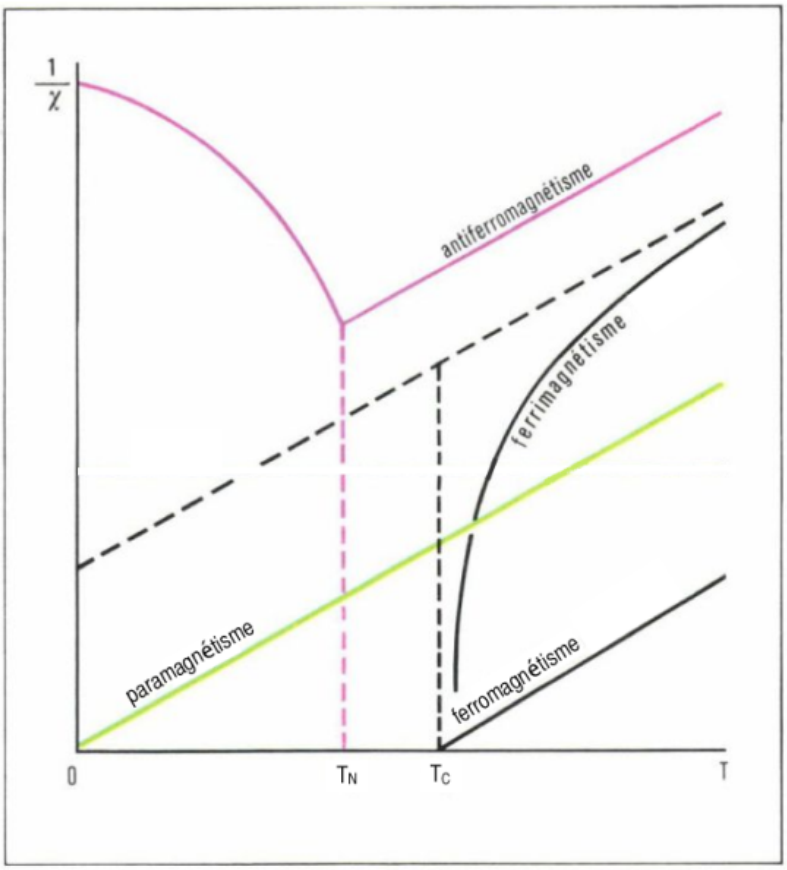

Figure 1.4: Variation of the inverse of the susceptibility according to the temperature of the different magnetic behaviors [66]

appears. Above this Curie temperature, the magnetic order is broken by thermal agitation and the material gradually regains a paramagnetic behavior.

1.3 Magnetic energies

We will now define the different magnetic energy terms used in the complete description of a magnetic system. The minimization of the total resulting energy makes it possible to predict the stable (fundamental) state of the system. We will describe in the following sections the formation of magnetic domains resulting from the competition of these energy terms.

The main distinction to be made between these energies is the distance they act on: very locally (short range) and therefore concern the nearest atomic sites, or at long range, they then influence the entire system. We will first describe the different terms of exchange interaction, then we will talk about the Zeeman energy of the system responding to the application of a magnetic field. Next, will describe the dipolar interactions within the system and will eventually describe the different terms falling within the expression of the magnetic anisotropy energy of the system.

1.3.1 Exchange energy

1.3.1.1 Direct symmetric exchange (isotropic)

That comes from the Coulomb repulsion between two electrons located on neighboring atoms (or on the same atom), and which becomes dependent on the spin state (up or down) because of the Pauli exclusion

principle [2]. It is a very short-range interaction that is responsible for the alignment of the magnetic moments and may be used, for example, to obtain a ferromagnetic phase.

The order of magnitude, the sign and the range of the interaction are dependent on the atoms and the crystallographic structure. Most commonly, in a phenomenological way, this interaction can always be written in the form:

$$e_{ex} = -1/2\mu_0 \sum_{\substack{ij \\ i \neq j}} \alpha_{ij} \overrightarrow{m}_i \overrightarrow{m}_j \tag{1.1}$$

Where α_{ij} are interaction coefficients between magnetic moments.

In the case of 3d transition metals, we see a special case where the orbital momentum μ_l [3] is minimized because of the crystalline field of the solid. This is called the extinction of the orbital moment. The spin-orbit [4] type interaction is then very weak or non-existent. The resulting magnetic moment therefore corresponds to the only moment of spin 8. The exchange energy is then written:

$$e_{exspin} = -\sum_{\substack{ij \\ i \neq j}} J_{ij} \overrightarrow{S}_j \overrightarrow{S}_j \tag{1.2}$$

where J_{ij} is the exchange constants between two neighboring atoms . This value is also called the exchange integral because it is proportional to the Orbital overlap [5], and vanishes if the overlap is nonexistent. It therefore depends on the distance between atoms and the type of orbitals that contribute to magnetism. When $J > 0$, a parallel alignment of the spin moments is favored, leading to a ferromagnetic configuration, $J < 0$ gives a configuration antiferromagnetic (when other energy terms are neglected).

The exchange of energy of a magnetic solid taht has a volume V is expressed in continuous form:

$$E_{exvol} = A_{ex} V M_s((\overrightarrow{\nabla} m_x)^2 + (\overrightarrow{\nabla} m_y)^2 + (\overrightarrow{\nabla} m_z)^2) \tag{1.3}$$

with $m_{x,y,z}$ the reduced component of the magnetic moment in the three directions of space and A_{ex} the exchange constant of the material considered by J/m ($A_{ex} \approx \frac{NJS^2}{2a}$ [68] ,with N the number of nearest neighbors, and S the total quantum number of spin). It is a function of the exchange integral J, but also of the distance between the moments, of the crystallographic structure of the solid, and the number of nearest neighbors.

This type of exchange is described as isotropic (or direct) exchange. For cases where the direct overlap is no longer possible due to the distance of the spins (then closer to the atomic nucleus), an indirect exchange interaction can maintain a certain magnetic order. by summarizing briefly the theory of this type of exchange : These two types of exchange interactions (direct and indirect) are called symmetrical interactions because energy is defined as the scalar product of two neighboring spins.

[2] The Pauli exclusion principle, discovered in 1925, states that no two identical fermions (e.g. electrons) may occupy the same quantum state. It was discovered before the Quantum mechanics [67]

[3] the trajectory (called orbital) of each of the electrons around the nucleus can be seen as a current loop inducing an orbital magnetic moment

[4] In quantum mechanics, the spin-orbit interaction qualifies any interaction between the spin of a particle and its motion

[5] Orbital overlap, i.e., mutual sharing of one or more electrons, can occur when two atoms are in close proximity to each other. The bonding resulting from such overlap is referred to as covalent bonding.

We will see later that it is also possible to define an exchange of anti-symmetric type, whose the energy (discrete) will depend on the vector product of two spins.

1.3.1.2 Indirect symmetric exchange

As mentioned above, this type of exchange occurs when the overlap of orbitals is impossible. The magnetic order is then realized step by step. Indirect symmetric exchange is at the origin of of various types of interactions such as super-exchange, connecting the electrons of two magnetic atoms through hybridization with oxygen orbitals (in the case of insulating magnetic compounds), or the Ruderman-Kittel-Kasuya-Yosida (RKKY) interaction.

It is this term RKKY that can explain the exchange interaction in rare-earth magnetic materials. In these materials, the orbitals responsible for magnetism are $4f$ orbitals whose spatial expansion is very small and therefore no direct overlap with neighboring atoms is allowed. The exchange interaction is therefore done via conduction electrons located on spatially larger bands (s, p and d) which can therefore move from one atom to another. These electrons are polarized in contact with the field induced by the electrons of the orbitals $4f$ and then an indirect exchange interaction with the electrons $4f$ of the neighboring sites follows. It has been observed that the sign of this interaction varies with the distance between the different sites, thus causing an oscillating character of ferromagnetism. This indirect exchange interaction was then generalized to the multilayer type system connecting the electrons of two magnetic materials via the conduction electrons of a nonmagnetic metal.

1.3.1.3 Anti-Symmetric Exchange: Interaction of Dzyaloshinskii-Moriya

When the magnetic material is in contact with a highly couplage spin-orbit metal (SOC), and thus does not exhibit inversion symmetry (interface), the inter-atomic exchange described above can also possess an anti-symmetric component: the interaction of Dzyaloshinskii-Moriya (DMI). It was introduced by Dzyaloshinskii in 1958 [69], who advanced the thesis that there was a direct link between the magnetic configuration of a system and its crystallographic structure. For this, he was interested in the study of certain compounds, such as $\alpha - Fe_2O_3$ hematite, for which, despite their antiferromagnetic configuration ($J < 0$), a low permanent magnetic moment was measured at low temperatures. This weak magnetization component has been attributed to the breaking of symmetry within this solid. In 1960,Moriya later showed how to calculate this type of additional interaction [70]. He has considered it the expression of a super-exchange interaction by adding a spin-orbit interaction expressed in this crystal structure. Dzyaloshinskii and Moriya had described this interaction as anisotropic super-exchange before it took their names; it was as:

$$e_{DMI} = -\sum_{ij} D_{ij} \overrightarrow{S}_i \overrightarrow{S}_j \tag{1.4}$$

where D_{ij} being the vector DMI. Therefore this energy is minimized for orthogonal spins between them, this interaction therefore promotes non-collinear alignments of the magnetic moments. This interaction can be expressed in bulk materials whose crystalline structure does not have inversion symmetry. In this case, the effect is noticeable in each of the cells of the lattice. But it can also be expressed in the case where the interfacing between films breaks the symmetry. In this case, we can usually express the vector DMI as: $\overrightarrow{D}_{ij} = D_{ij}(\overrightarrow{n} \times \overrightarrow{r}_{ij})$. With $\overrightarrow{r}_{ij}$ the unit vector between the two sites i and j (still depending on the structure crystalline) and $\overrightarrow{n}$ is the normal vector on the magnetic surface. Therefore This DMI vector is as function as sites considered.

When the DMI dominates the other contbutions, this interaction imposes a direction of rotation of the spin moments which is fixed according to the considered interface. This leads to chiral magnetic orders within the structures such as the state of periodic domains in stripes, for which the magnetization everywhere has the same direction of rotation, or the skyrmionic state.

1.3.2 Magnetocrystalline anisotropy energy

In a material magnetically ordered , there is an energy that directs the magnetization (localized magnetic moments) along certain axes defined crystallographic properties, called directions of easy magnetization. This energy is called magnetocrystalline energy or anisotropy energy .

If we consider a crystal of cubic symmetry, the magnetocrystalline anisotropy energy Ecrist is given by the following formula:

$$E_{cris} = K_1(\alpha_1^2\alpha_2^2 + \alpha_2^2\alpha_3^2 + \alpha_3^2\alpha_1^2) + K_2\alpha_1^2\alpha_2^2\alpha_3^2 + ... \tag{1.5}$$

with K_i the constants of crystalline anisotropy which depend on the type of material and the temperature, and $\alpha_{1,2,3}$ the cosines of the angles that the magnetization does with the three axes of the reference linked to the cube.

1.3.3 Zeeman energy

When a magnetic material of moment $\overrightarrow{m}$ is subjected to an external magnetic field $\overrightarrow{H}$, a torque is exerted by $\overrightarrow{H}$ on the vector $\overrightarrow{m}$, corresponding to a density of energy:

$$e_Z = -\mu_0 \overrightarrow{m}.\overrightarrow{H} \tag{1.6}$$

From a microscopic point of view, the magnetic field $\overrightarrow{H}$ acts on the moments μ_l and μ_S and reduces the energy of the configurations for which these moments are oriented in the same direction as the applied field. In addition, the energy of the moment configurations opposite to the applied magnetic field is increased. For a volume sample of magnetization $\overrightarrow{M}$ this energy is written then$E_Z = -V\mu_0\overrightarrow{M}.\overrightarrow{H}$ with V is the volume of the magnetic material.

1.3.4 Dipolar energy

Through the Zeeman interaction term we obtain the expression of dipolar energy between two magnetic dipoles $\overrightarrow{m}_i$ and $\overrightarrow{m}_j$ situated at r_i and r_j respectively :

$$E_d(\overrightarrow{r}_{ij}) = -\overrightarrow{m}_j \overrightarrow{B}_i(\overrightarrow{r}_j) \tag{1.7}$$

Where :

$$B_i(\overrightarrow{r}_j) = \frac{\mu_0}{4\pi}\frac{1}{r_{ij}^3}\left[3\frac{(\overrightarrow{m}_i.\overrightarrow{r}_i).\overrightarrow{r}_i}{r_{ij}^2} - \overrightarrow{m}_i\right] \tag{1.8}$$

$B_i(\overrightarrow{r}_j)$ is the magnetic field produced at r_j by the dipole m_i ,$r_{ij} = \| \overrightarrow{r}_{ij} \|$, $\overrightarrow{r}_{ij} = \overrightarrow{r}_j - \overrightarrow{r}_i$ and $\mu_0 = 4\pi.10^{-7}$.

The equation (1.7) of expression of the dipole-dipole interaction become:

$$E_d(\overrightarrow{r}_{ij}) = \frac{\mu_0}{4\pi}\frac{1}{r_{ij}^3}\left[\overrightarrow{m}_i.\overrightarrow{m}_j - 3\frac{(\overrightarrow{m}_i.\overrightarrow{r}_{ij}).(\overrightarrow{m}_j)}{r_{ij}^2}\right] \tag{1.9}$$

The dipolar energy E_d, or shape energy (or magnetostatic or demagnetizing energies), describes the interaction between the magnetization distribution in the magnetic material, with the field induced by

this magnetization. This field is locally opposed to magnetization and is commonly called demagnetizing field.

This interaction is very dependent on the orientation of the magnetization with respect to the shape of the system, and is equivalent to anisotropy in the case of particular dimensions. This is called anisotropy of form. In the case of thin films, for example, the thickness of the material is often less than its lateral dimensions and the demagnetizing field induces "magnetic charges" on the interfaces.

1.4 Hysteresis loop

1.4.1 Definition

Hysteresis loop is the response curve of magnetic materials, at through which, they keep the memory of all their magnetization states previous through the elementary domains. It is J.A.Ewing who has shown this specific behavior in the case of Iron, and that he called it hysteresis which means delay of the effect on the cause (here, the magnetization on the field applied) [71, 72]. The hysteresis cycle of a ferromagnetic material depends on the mobility of the Bloch's walls [6], itself is a function of magnetic energies and the applied field. So it can be considered as a characteristic of the material and in any case a well detailed mathematical model is necessary. Hysteresis is the delay in demagnetization and the deduction of the characteristic of the magnetic induction B (H) of the magnetic material. So the hysteresis cycle is the plot of the induction as a function of the applied external H field as illustrated in Figure 1.5.

$$B = \mu_0(H + M) = \mu_0(1 + \chi)H = \mu H \tag{1.10}$$

Where μ_0 represents the magnetic permeability of of free space .

1.4.2 Curve of first magnetization

When applying a magnetic field outside this material, the magnetic domains whose orientation is close to that of H increase at the expense of those whose orientation is opposite to that of H. The Bloch's walls are moving therefore in the material. Each cycle of hysteresis is defined by 4 parameters. We will define each of these parameters by referring to the curve (Figure 1.5):

- **Saturation field(H_S)**

  When applying a external magnetic field on this material, Magnetic domains whose orientation is close to that of H increase at the expense of those whose orientation is opposite to that of H. The Bloch's walls are moving therefore in the material. At the limit, when the external magnetic field reaches a critical value H_S , the single crystal consists of only one domain ferromagnetic whose orientation is the same as that of H.

- **Saturation magnetization(M_S)**

  The saturation magnetization M_S represents the maximum value reached when the applied magnetic field is strong (see Figure 1.5) All the magnetic moments are then aligned in the direction of the applied field and we observe a saturation on the magnetization curve.

- **Remanence magnetization (M_r)**

  When the intensity of the H field decreases to zero, the magnetic domains tend to reappear (AB curve, Figure 1.5) however, since the displacement of Bloch's walls is not instantaneous because of magnetic anisotropy; a non-zero magnetization M_r manifests in the material (point B, Figure 1.5). This value M_r is called remanent magnetization.

[6] the boundary between two domains in a magnetic material marked by a layer wherein the direction of magnetization is assumed to change gradually from one domain to the other

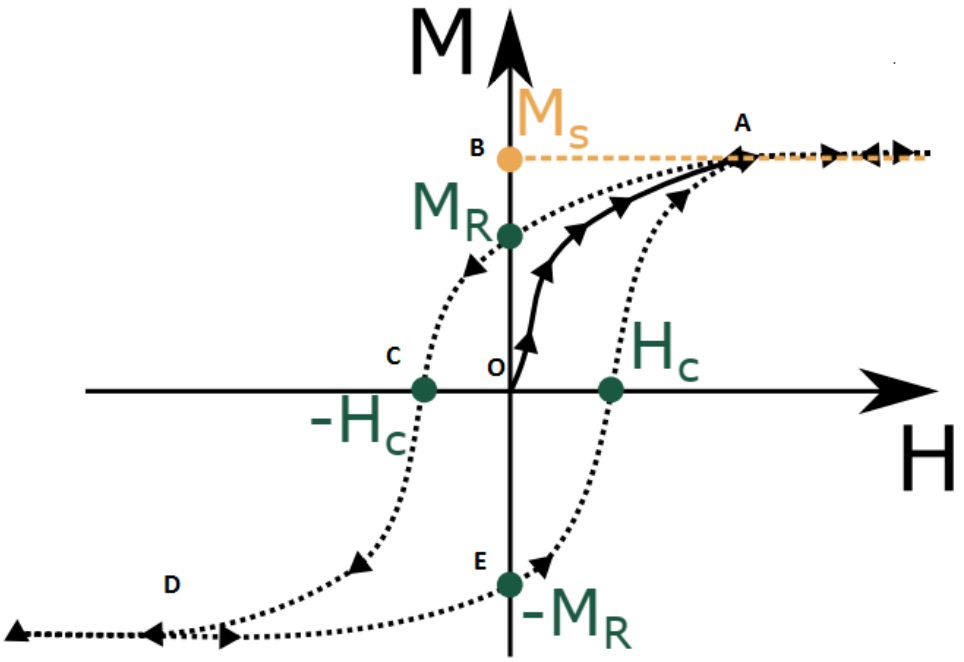

Figure 1.5: Magnetization curve (hysteresis cycle) of a ferromagnetic material (ABCDEFA)(in dotted lines). Curvature of the M (H) curve for a material initially demagnetized (or first magnetization curve) in a continuous line (OA). Different quantities characterize a magnetically tick: the saturation magnetization Ms, the coercive field Hc and the remanent magnetization Mr

- **Coercive field (H_C)**

  We must actually apply a magnetic field opposite to that of the field of the first magnetization so that the magnetization is zero (curve BC, Figure 1.5). The value of the field which generates this zero magnetization corresponds to the coercive field. The value of this field allows again to distinguish the large classes of ferromagnetic materials. Indeed, a soft material will have a low coercive field value (typically $< 1mT$), while it will be very high for a hard material ($> 60mT$).

  The shape of this cycle depends on the nature of the material, the processes of magnetization , induction and the geometry of the sample. Finally, this cycle deforms according to flow and frequency conditions.

  The area of the hysteresis cycle represents the energy expended per unit volume of the material, to reorient the magnetic moments of the domains and move the Bloch's walls, during a complete cycle of variation of external magnetic field. This energy dissipates in the form of heat.

1.4.3 Magnetic Hysteresis Loops for Soft and Hard Materials

1.4.3.1 Soft Magnetic Materials

Soft magnetic materials (see Figure 1.6) are those in which the coercive field is low . For these materials, when the external field varies, no obstacle is opposed to the displacement of the Bloch's walls and the reorientation of the magnetic domains, in other words these materials have few defects in their crystal structure, as well as reduced anisotropy. They are characterized by a very high permeability, a High saturation magnetization M_s, low coercive field and low losses by hysteresis (low surface area of the hysteresis loop). A soft magnetic material is used when it has to canalize a variable magnetic flux at high frequencies. The magnetic material must react quickly and frankly to small variations of the inductor field without undergoing heating or without its reaction being too sensitive to the field frequency. For

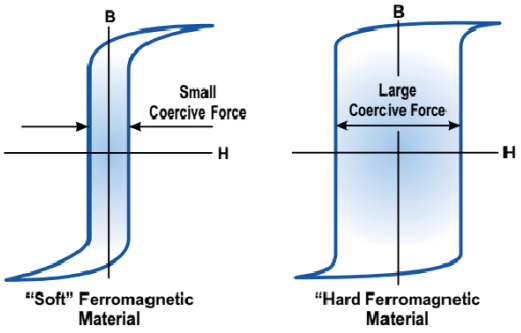

Figure 1.6: Loop of Soft material presented on the left and cycle of the Hard material illustrated on the right [73]

this purpose soft magnetic materials are used in cores (or magnetic circuits) of transformers, motors and generators, in precision inductances of electronic circuits, magnetic screens.

1.4.3.2 Hard Magnetic Materials

Hard magnetic materials (see Figure 1.6)are those characterized by high a coercive field, a high remanent magnetization and wide hysteresis cycle. In these materials, we try to hinder as much as possible the reorientation of the magnetic moments in the Weiss domains [7], as well as the displacement of the walls of Bloch see . This is why eutectoid steels in the quenched state (martensitic structure) are frequently used to produce permanent magnets. Thus a permanent magnet of good quality will be characterized by a high value of the magnetic anisotropy necessary for the persistence of a important part of the spontaneous magnetization (remanent) and the high value of coercive field.We use hard magnetic materials when the magnetic field generated by the material remains obligatorily stable over time and remains if possible high, and it is the same in the presence of parasitic external magnetic fields. They are used in permanent magnets, lifting magnets, loudspeaker cores, low power electric motors, magnetic lenses for cathode ray tubes.

[7] Weiss domain or magnetic domain, is a region of a material in which the magnetic moments are oriented in the same direction, the magnetization is therefore uniform.f

Chapter 2

Nanomagnetism

2.1 Magnetic properties of nanoparticles

The major difference between the nanoparticles and their bulk materials is the number of atoms associated. For nanoparticles moste of atoms are located at the surface Figure 2.1, For example: fcc-Co nanoparticles with diameter around 1.6nm with a lattice constant 0.36nm, will have about 200 atoms and 60 of them will be at the surface [7]. As a result the reduction of the size of materials on the nanometric scale exhibit new physical and magnetic properties different from that of bulk materials see Figure 2.2.

Two main magnetic contributions manipulate the magnetic behavior of a single nanoparticle. The first one is due to atoms located at the surface of a particle as we mentioned in the general introduction, the second one is the magnetic behavior due to the finite-size of a particle. It is a commonly accepted assumption to represent a nanoparticle as a combination of the core (where, the spins are ordered below a critical temperature, and magnetic behavior is the same as in bulk) and the shell (where the spins are disordered even at the lowest temperature). The magnetic behavior of the core and shell is quite difierent, leading to the competition resulting in a final magnetic state of a nanoparticle. For smaller particles the surface efiects become dominant due to the larger number of spins at the surface, while in case of large particles, the magnetic behavior of the core is dominant.

2.1.1 Magnetic domains

Ferromagnetic materials are often structured in magnetic domains called Weiss domains separated by bloch walls Figure 2.3. if the energetic cost of the formation of the walls is small compared to the energy difference between the mono-domain state and the multidomain state ,then a multidomain structure is energetically favorable.More the size of magnetic object is small, more it will tend to be monodomain. Below a critical size, the existence of a wall is no longer energetically favorable and the magnetic material has a new magnetic structure named macrospin. Indeed the transition to the single domain state is obviously a size dependent effect, which can be probed by a number of experimental techniques. Figure 2.5 qualitatively illustrates the dependence of the coercivity field Hc on the particle size. Below a critical size (which depends on the material) the Hc is zero and a superparamagnetic behavior (see below) is observed, which indicates the single domain magnetization state. The peak around the critical size is broad due to the particles size distribution. The critical size at which a particle becomes single domain is a result of competition between exchange coupling and magnetostatic energy, and therefore depends on the geometry, anisotropy, and saturation magnetic moment M_S of the particle. For a magnetic sphere with a cubic cell, the first estimate of this critical size was proposed by Kittel [8] by comparing the energy needed to create a bloch wall and the reduction of magnetostatic energy by creating domains. If the anisotropy is weak, the critical radius Figure 2.4 beyond which the nanoparticle is multidomains is then written:

$$R_c \approx \frac{9\sigma_\omega}{4\pi M_s^2} \tag{2.1}$$

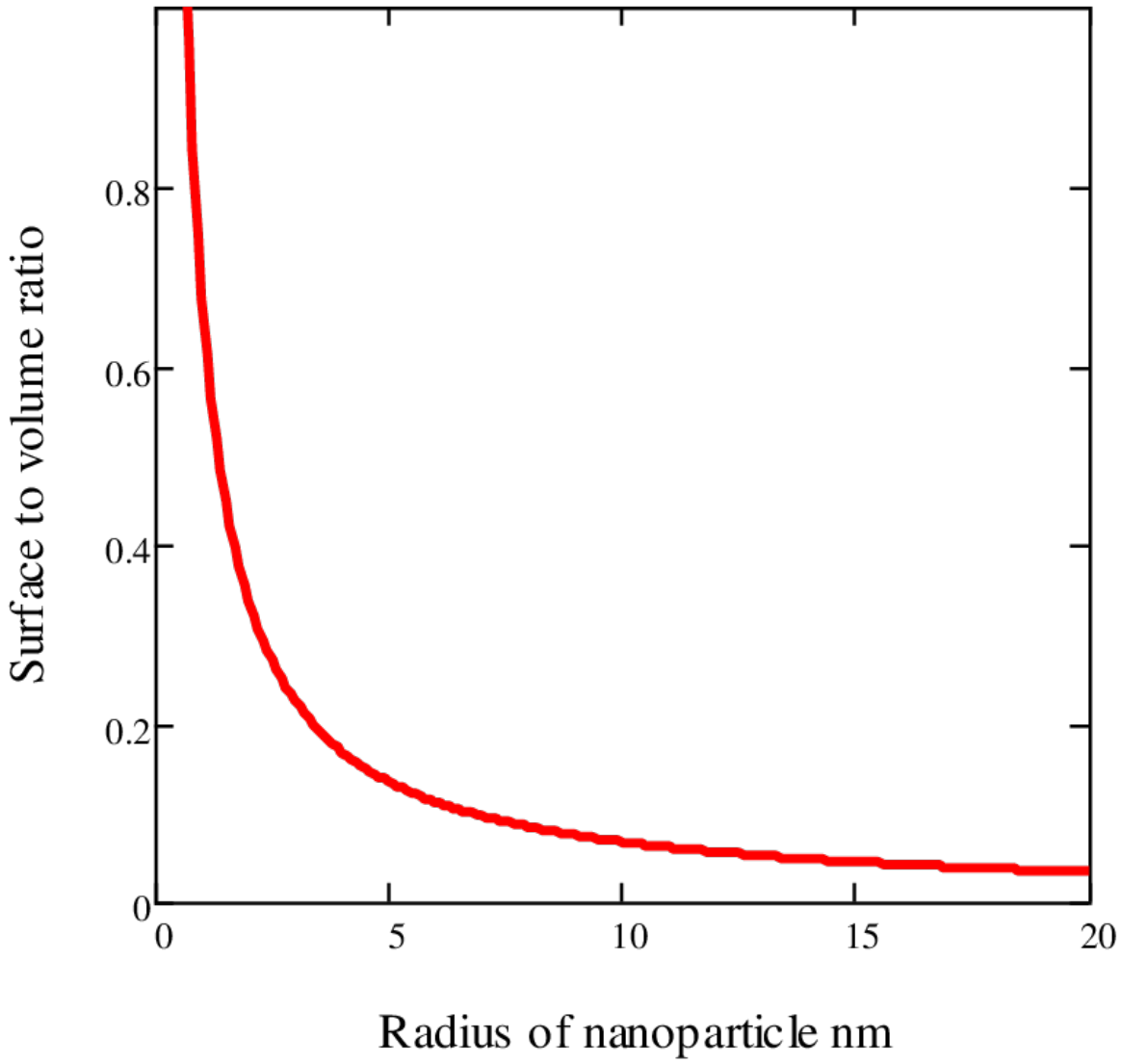

Figure 2.1: Surface to volume ratio of silicon nanoparticles versus radius. [74]

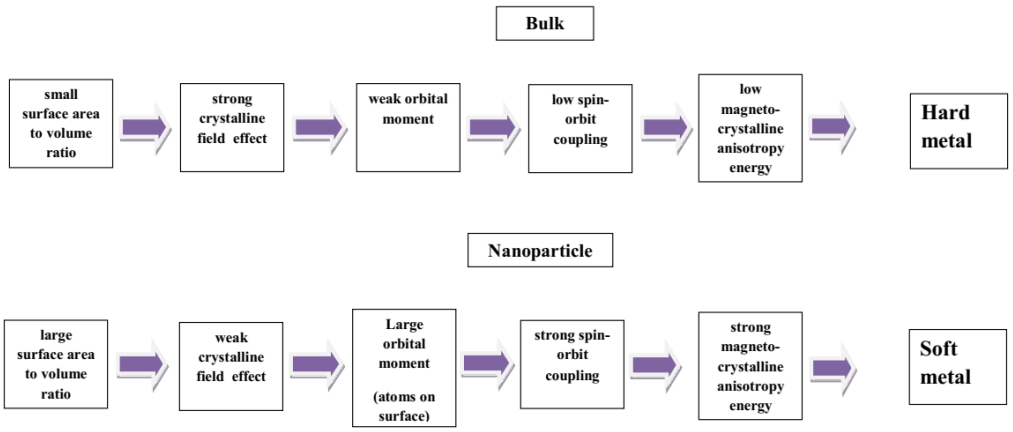

Figure 2.2: An assessment of the different size effects on the magnetic behavior of a transition metal in the massive state and at the nanoscale.

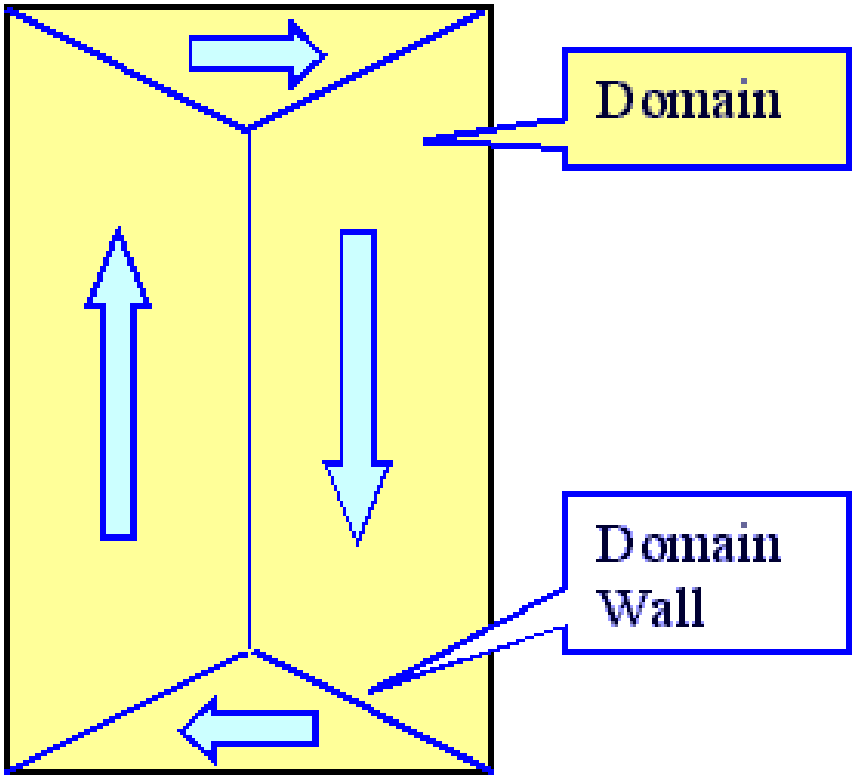

Figure 2.3: Magnetic domains are regions in a crystal with different directions of the magnetizations, they must by necessity be separated by domain walls [75]

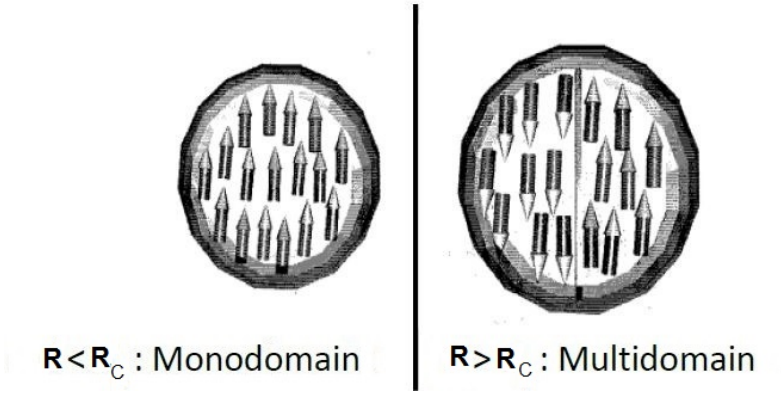

Figure 2.4: Schema of a spherical nanoparticle which, according to its radius, follows (a) a single domain configuration $R < R_c$ or (b) multidomain $R > R_c$ [77]

where $\sigma_\omega = 4\sqrt{AK}$ is the energy of the surface of a bloch wall and M_s is the saturation magnetization, $A = J_{ex}S^2/a$ is the exchange stiffness constant and J_{ex} the exchange integral and a the lattice parameter of the cubic lattice. Typically, R_c is 15 nm for iron and 58 nm for cobalt.However according to Brown [76], this approach does not ensure the existence of a single domain and does not allow an accurate evaluation of the critical radius.Indeed kittel compared the energy of a monodomain particle to that of a multidomain particle with very specific structures.its approach therefore does not take into account any other possible structure that could have a different energy. Kittel has therefore proved that it is possible for a particle to be a single domain beyond a certain radius, but he has not found a radius beyond which the particle is necessarily monodomain.Using a formalism borrowed from micromagnetism, Brown first calculated a radius R_0 below which the monodomain state is the one of lower energy.

$$R_0 = 3.6055\sqrt{\frac{2A}{4\pi M_s^2}} \tag{2.2}$$

Then he calculated two critical rays beyond which the state of lower energy is necessarily multidomain. In the case of a weak main constant of K_1 anisotropy:

$$R_1 = \frac{4.5292\sqrt{2A}}{\sqrt{4\pi M_s^2} - 5.6150K_1} \tag{2.3}$$

In the case of a stronger $K2$ anisotropy constant:

$$R_2 = \frac{9\sqrt{2A(K + 8\pi M_s^2)}}{8(3\sigma - 2)M_s^2} \tag{2.4}$$

With $\sigma = 0.785398$.

Gubin [29] provides R_C ,R_0,R_1 and R_2values for different materials:

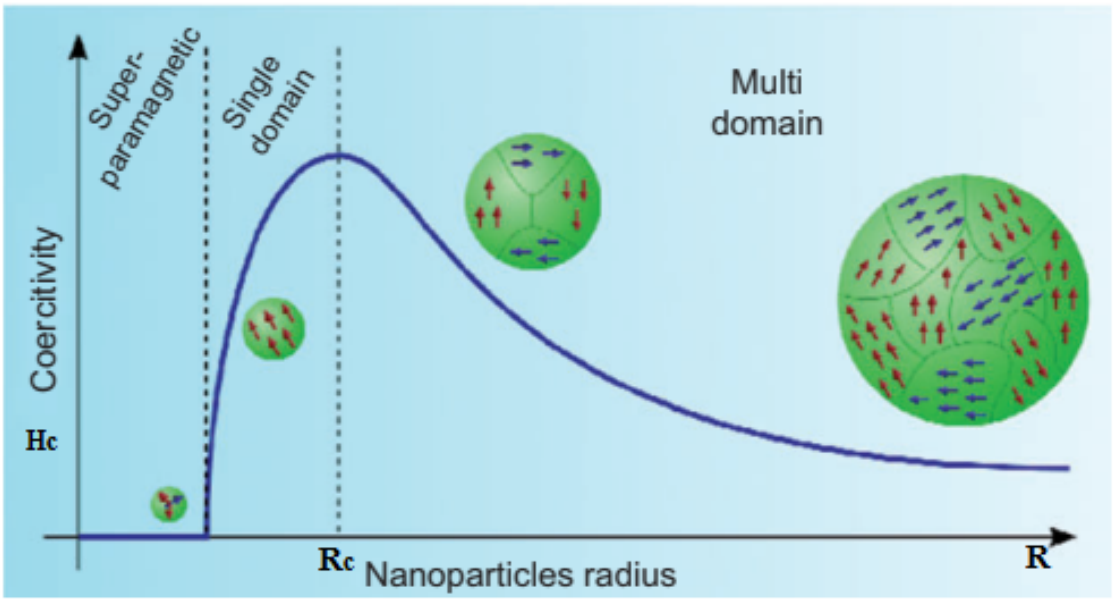

Figure 2.5: Schematic illustration of the coercivity-size relations of small particles [9].

Table 2.1: kittel and brown critical radius values of different materials

.	$M_s(emu/cm^3)$	$K(10^4 erg/cm^3)$	$A(erg/cm)$	$R_C(nm)$	$R_0(nm)$	$R_1(nm)$	$R_2(nm)$
Co	1430	430	1	58.1	15.1	51.4	146
Fe	1710	45	1	13.1	8.4	11	116.5
Ni	483	4.5	1	52.1	29.8	39.1	412.9

Nevertheless, it has been shown that these critical rays can vary according to the temperature and the external field [78]

2.1.2 Magnetic anisotropy of nanoparticles

For a single domain of nanoparticle the effective magnetic anisotropy is the resultant of magnetocrystalline , shape and surface anisotropy energies [79].

2.1.2.1 Magnetocrystalline anisotropy

For single domain nanoparticles with uniaxial anisotropy, the magnetocrystalline anisotropy energy is written:

$$E_u = K_u V sin^2\theta \tag{2.5}$$

Where K_u the effective uniaxial anisotropy constant, V the volume of the particle, and θ the angle between the magnetization and the axis of symmetry. his expression describes two minimum energies ($\theta = 0 \text{et} \pi$) separated by an energy barrier $K_u V$.

2.1.2.2 Anisotropy of shape

In addition to the magnetocrystalline anisotropy, shape anisotropy can be induced in the case of non spherical monodomain particles. The discontinuity of the magnetization on the surface of the particles

leads to the creation of a demagnetizing field. In the case of an ellipsoidal particle [80] the shape anisotropy energy is:

$$E_f = \frac{1}{2}\mu_0 V(N_x M_x^2 + N_y M_y^2 + N_z M_z^2) \tag{2.6}$$

where μ_0 the permeability in vacuum, V is the volume of the particle, $M_{x,y,z}$ the components of the magnetization and $N_{x,y,z}$ the demagnetizing field factors, relative to the axes x,y and z of the ellipsoid.Demagnetizing field factors verify equality $N_x + N_y + N_Z = 1$ For a spherical single domain nanoparticle, the shape anisotropy energy is zero.

2.1.2.3 Surface anisotropy

For a single domain nanoparticule particle, also the anisotropy energy depends on the surface interactions. As the size of the particles decreases, the surface magnetic contributions may become larger than those of the nanoparticles themselves. The surface anisotropy energy will then be dominant with respect to magnetocrystalline and shape anisotropy energies. For a spherical particle of diameter d, the effective anisotropy constant K_{eff} follows the empirical law:

$$K_{eff} = K_v + \frac{S}{V}K_s = K_v + \frac{6}{d}Ks_s \tag{2.7}$$

with K_v the volume anisotropy constant,v the volume of the particle , S the surface of the particle , K_s the surface anisotropy constant.The anisotropic energy of E_a particle Ea is defined by:

$$E_a = K_{eff}V \tag{2.8}$$

Effective anisotropy is therefore sensitive to particle size variation through the second term of the equation2.8. Since nanoparticles are rarely independent, other contributions to effective anisotropy may be added, such as dipolar interactions between nanoparticles or with the dispersion medium [81].

2.1.3 Superparamgnetism

If the nanoparticle is sufficiently small, it becomes monodomain and its magnetization is then uniform. If this nanoparticle possesses a uniaxial anisotropy, in the absence of an external magnetic field, its magnetization can be in two stable orientations parallel to the axis of anisotropy. From an energy point of view, these two orientations are separated by a barrier $\Delta E = K_{eff}V$. When the temperature gets high enough that $K_B T \sim \Delta E$. The magnetization of the nanoparticle can pass from one magnetization to another spontaneously. For the Neel-Brown model, the nanoparticle is considered fixed in space and has a uniaxial anisotropy. The exchange constant J is assumed to be very large in front of thermal energy $K_B T$ so that atomic spin fluctuations are neglected and therefore the magnetization norm is constant. The reversal of magnetization is done by the uniform rotation. Finally, the energy barrier due to the anisotropy is supposed to be very large in front of the thermal energy. Therefore the system spends most of its time in one of the two minimums of energy.Then according to this model, if the system is in a metastable state at $t = 0$, the probability that it is still in the same state at time t is $e^{-t/\tau}$ where τ t is the relaxation time following an Arrhenius law [1]:

$$\tau = \tau_0 e^{\frac{K_{eff}V}{K_B T}} \tag{2.9}$$

where $\tau_0 \sim 10^{-11} - 10^{-9}$s .Thus, the magnetic moment carried by the nanoparticle is returned more rapidly than the temperature is high. If the nanoparticle is sufficiently large, if its anisotropy is sufficiently high, or the temperature is low enough, then τ becomes longer than the experimental measuring time τ_m . We can then measure the magnetization of the nanoparticle and determine its orientation. We then say that the magnetic moment is blocked. On the contrary, if the nanoparticle is sufficiently small,

[1] In chemical kinetics, the Arrhenius law makes it possible to describe the variation of the speed of a chemical reaction as a function of temperature.

or the temperature becomes rather high, then τ may be shorter than the measuring time, and although the nanoparticle has a non-zero magnetization, the measured average magnetization will be zero. These behavior is the superparamagnetic regime. As with standard paramagnetism, thermal noise randomly alters the orientation of the magnetic moment. In the case of a nanoparticle, the magnetic moment is worth several thousands Bohr magneton and that is why we speak of superparamagnetism.

The temperature that defines the boundary between two regimes is called the blocking temperature noted T_B. We can find an analytical expression for T_B from the equation 2.9 and we put $\tau_m = \tau(T_B)$:

$$T_B = \frac{K_{eff}V}{K_B Log(\frac{\tau_m}{\tau_0})} \tag{2.10}$$

These formulas are valid only for an isolated monodomain nanoparticle. In a set of nanoparticles, it is known that the dipolar interactions modify the blocking temperature [82, 83]. Also, in a sample of nanoparticles not all have exactly the same size. The whole is polydisperse (in opposition to monodisperse). There is a distribution of rays, which then produces a distribution of blocking temperatures.

2.1.4 The effect of surface

The surface effects of nanoparticles is considered as a main element that paly a major role in magnetic properties of nanoparticles . This influence of surface is due to a strong increase of the surface-to-volume ration of atoms, relative to the bulk. When the size of the nanoparticle decreases the ratio increases. However The reduction of the total number of the nearest neighbors around a single atom of surface and the lack of translational symmetry at the particle boundaries can introduce frustration and spin disorder. Therefore, the competition between both magnetic orders will lead to the magnetic ground state of a nanoparticle which will be difierent from the simple assumption of a single domain with a perfect magnetic ordering corresponding to the bulk solid.

2.2 Core/shell morphology

Nanoparticles with core/shell morphology are nanostructres that have the core are and shell wich may be composed of several nanomaterials(the nanometer particle size regime ranging from 20 to 200 nm) is depicted in. These nanostructure morphology include a core surrounded by a shell. The core and shell can be made by inogrganic materials (silicia ,metal..) or organic. Also the core/shell nanostructure can be composed of more than two materials. Core/shell nanoparticles are multifunctional materials with unique properties that can be obtained from either core or shell material and can be altered by changing either the constituting materials or the ratio between core and shell [84].

Thanks to the new synthesis techniques, it is currently possible to prepare core/shell nanoparticles with different shapes. As a result thes shapes have attracted more attention because of their unique and novel properties. As it is illustrated in the Figures 2.6, there is a diversity of core/shell nanoparticles shapes. The most common ones is the spherical (Figure 2.6.(a)) and cubic(Figure 2.6.(c)) shapes .Other differents core/shell are formed differently than that of spherical shape .Figure 2.6.(d) shows a moveable core particle within a uniformed hollow shell particle .Multiple small core coated by shell are nanoparticles that have a single shell maaterial is coated onto many small core partioles together (Figure 2.6.(e)). nanomatryushk nanostructures are nanoparticles with cencentric nanoshells of alternative coating of dielectric core and metal shell material onto each other (Figure 2.6.(f)) [85].

2.2.1 Classification of Core/Shell Nanoparticle

There are a wide varieties of core /shell nanoparticles available with their wid rang of application .depending on their material nature, core/shell nanoparticles coulde be classified into four main several groups (Figure 2.7):

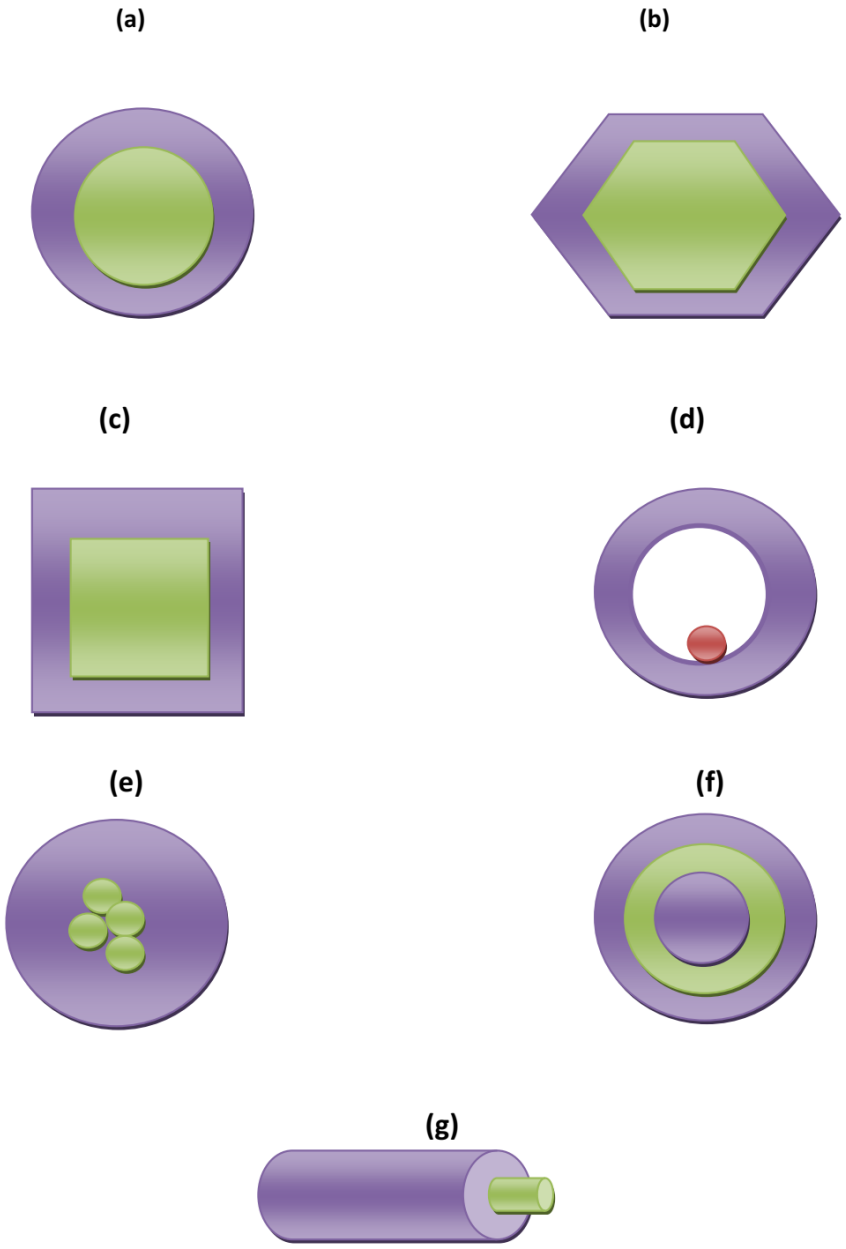

Figure 2.6: Different shapes of core/shell nanoparticles [86]

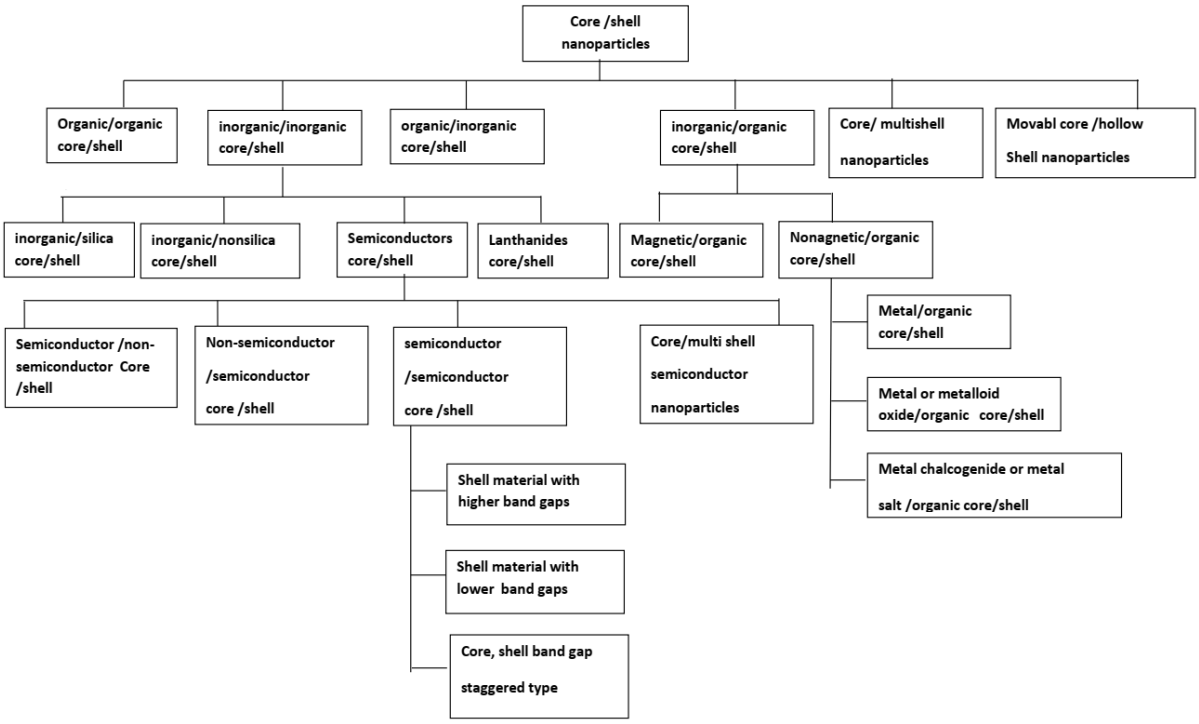

Figure 2.7: Types of core/shell nanoparticles [86]

- inorganic /inorganic.
- inorganic/organic.
- organic/inorganic.
- Organic/organic.

Chapter 3

Models and Methods

3.1 Introduction

The physics of condensed matter is particularly interested in the study of phase transitions (magnetic, superconducting, superfluid, ferroelectric, etc.) that appear in physical systems formed of a very large number of strongly coupled particles. These transitions make it possible to highlight the various configurations of the system under consideration, to explore the domains of existence and to determine its critical behavior [87].

Exchange interactions tend to align or anti-align particles (spins) to minimize the exchange energy of the system. They make it more difficult to calculate the partition function, but also, favor the appearance of a spontaneous local or global magnetic order below a certain temperature, called Curie temperature for ferromagnetic systems and Néel temperature for antiferromagnetic and ferrimagnetic systems. In 1929, Heisenberg showed that these interactions are due to a combined effect of Coulomb's repulsion and Pauli's expulsion principle [88]. In sum, the interactions designated within its systems are an intrinsic property and therefore can not be ignored or considered as a mere disturbance, as is the case in diluted media, and this is precisely the difficulty of their study. Two possibilities are thus possible to study the properties of infinite or semi-infinite physical systems:

- The first is to consider all the interactions of the system and to determine the partition function, solving the Schrödinger equation of quantum mechanics. The calculation of the partition function consists of summing a very large number of states. At the thermodynamic limit, this number is infinite and the sum becomes difficult to calculate. Models for which partition functions are exact analytic expressions are rare.
- This leads to the second possibility of neglecting the irrelevant details of the interactions between the particles of the system by adopting a theoretical model. Theoretical models are in fact the simplified representations, at the microscopic scale, of the physical systems (with N particles in interactions) making it possible to analyze them, to explain them and to predict some macroscopic aspects.

Several models have been introduced by theoretical physicists to study the magnetic phase transitions of ordered and disordered complex systems. Among these models, the most standard are: The model of Heisenberg [88], Ising [89], Blume-Capel [90] or Baxter-Wu [91], etc. which can be modified according to the needs of a study. However, these models, in addition to being used to describe the magnetic systems for which they were originally designed, are also used in the description of other systems such as multi-component fluids and ternary alloys [92].

Another aspect that must imperatively be addressed is the digital aspect, because the theoretical models previously described, are analyzed numerically and use numerical methods or approximations. Rightly today, because of continuous advances in computer technology, digital modeling and simulation could be considered as a third lever for scientific inquiry after pure theory and experimentation. Indeed, the tools of numerical modeling and simulation of different structures of materials and their properties,

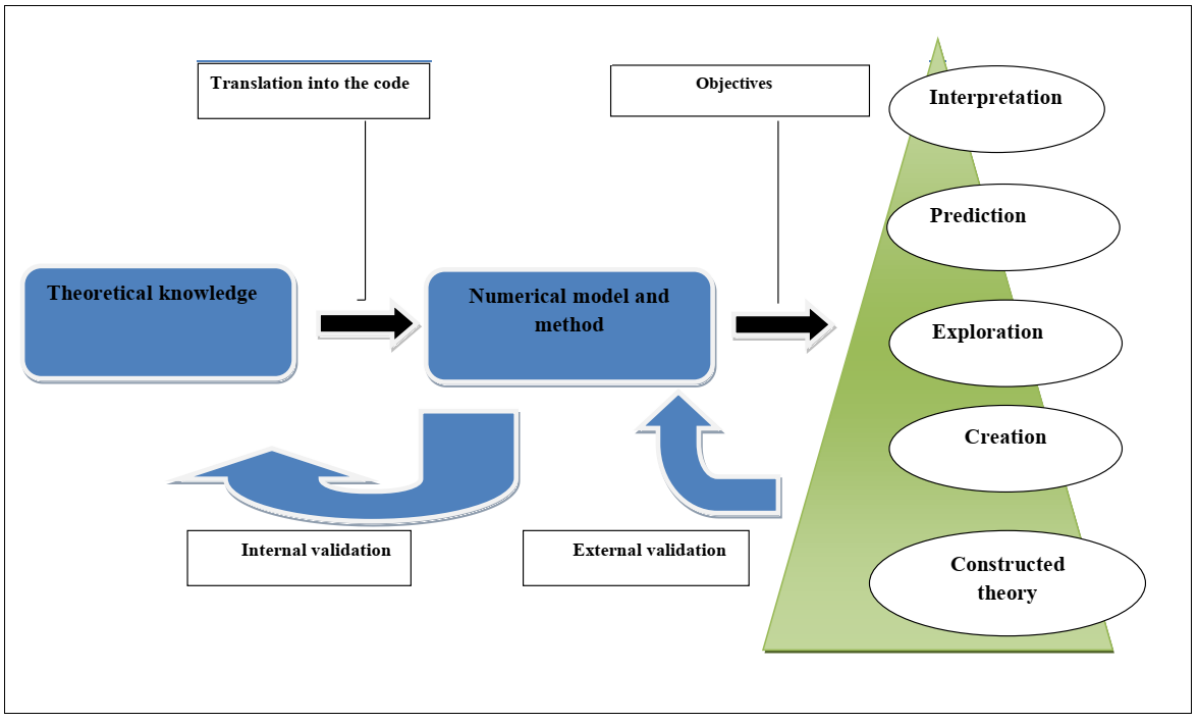

Figure 3.1: The simplified process of research in modeling and numerical simulation

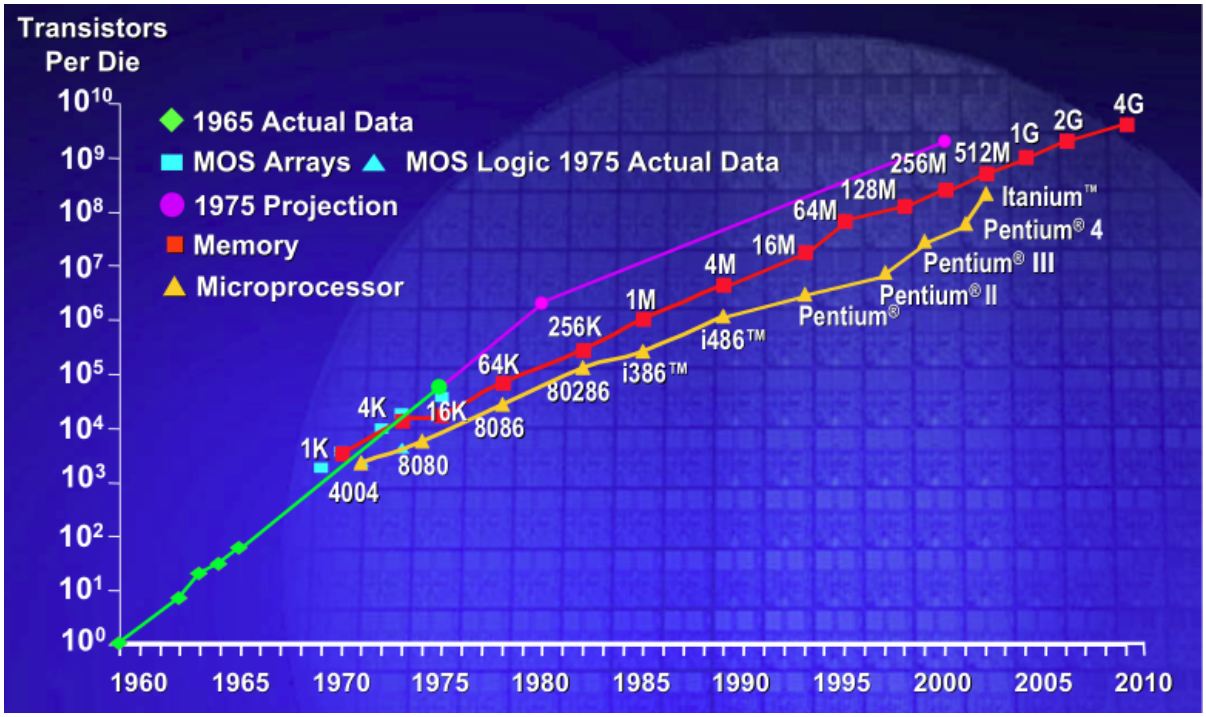

Figure 3.2: Moore's law from 1970 to 2010. Exponential growth of processors [93]

on different scales are very useful and valuable for the development of materials and their applications. Since they offer acceptable accuracy in predicting the properties of materials, they are widely used for:

- Interpret experimental results.
- Develop new materials, difficult to test experimentally, such as nanomaterials and determine their physical and chemical properties.
- Determine the properties of materials under extreme conditions (temperature, pressure, etc.) that are experimentally inaccessible.
- Determine the properties of complex systems that are unmanageable by microscopic mathematical models.
- Compare the theory of experimentation and suggest doing tests to save money (in cases where calculations are easier and faster) and time as well as for the validation of the theory.

The simplified process of research in numerical modeling and simulation of a Part and the interest of numerical models on the other hand are indexed in Figure 3.1: The researcher must translate the theoretical knowledge (TK) into the calculation model code (CMC). In the translation process, the terms and relationships of the researcher's TK are operationalized as the concrete structural relationships, variables and initial conditions of the CMC. CMC can be any type of mathematical or computational approach and requires full specificity before it works..

Modeling tools such as modern methods of electronic structure, mean field approximation, effective field approximation, and Monte Carlo simulations have proven to be the product of decades of intense research, stimulated by at least two equally important factors: First, the powerful digital algorithms that form essential elements of digital physics tools, including modern electronic structure codes. Some of these algorithms are the most popular and are ranked in the top 10 algorithms of the 20th century [94], as listed in the following Table 3.1:

1946 : The Metropolis Algorithm
1947 : Simplex Method
1950 : Krylov Subspace Method
1951 : The Decompositional Approach to Matrix Computations
1957 : The Fortran Optimizing Compiler
1959 : QR Algorithm
1962 : Quicksort
1965 : Fast Fourier Transform
1977 : Integer Relation Detection
1987 : Fast Multipole Method

Table 3.1: Top 10 algorithms of the 20th century

The second factor is the dramatic increase in material capabilities and storage of modern computer systems through the miniaturization of microelectronic devices. Moore's law in 1965 predicted an exponential growth in computing power (see Figure 3.2) when microelectronic devices smaller than the sublithographic range would be produced.

For example, in 2013, Tianhe-2, the supercomputer located in Guangzhou, People's Republic of China, at the National University of Defense Technology, was ranked fastest in the world with a record of 33.86 petaflops (1015 Flops, floating-point operation per second or flops or flop / s is a unit of measure for the speed of a computer system.) [95]

In this chapter, we are interested in the numerical simulation models and methods that we will apply in the study of spin model systems. First, we recall the difference between classical spin and quantum spin. Next, we describe Ising's model as a model of classical spins. Finally, we analyze the approximation methods, in particular the Monte Carlo method associated with the Metropolis algorithm.

3.2 Quantum and classical pins

The spin models depend essentially on the degrees of freedom and the atomic interactions observed in the system under consideration. There are several spin models, they can be of quantum or classical nature:

- The classical spin models are the discrete spin models, that is to say, the spins can only take finite values. This is the case of the Ising model [89, 96] and the Potts model [97, 98].
- On the other hand, quantum spin models are continuous spin models; spin can theoretically take an infinite number of values, forming a continuous set. Very often, they are designated by classical vectors.

  Among the quantum spin models, we can cite: The XY model with 2D unit vectors, the classical Heisenberg model with 3D unit vectors [99], the Baxter models [100], etc.

3.2.1 Ising model

In 1920, W. Lenz proposed to one of his students, Ernst Ising, a simple spin model to qualitatively explain ferromagnetic-paramagnetic phase transitions in a one-dimensional magnetic system [96]. Ising developed and solved exactly by the method of the transfer matrix (elementary calculus) this model that now bears his name and presented it in his thesis in 1925 [89].

The Ising model is defined as an extremely efficient simple model for studying phase transitions, in particular in magnetic systems, quantitatively and qualitatively. It is based on the representation of the studied system in the form of a fixed network of particles having a S_i magnetic moment, discernible and subjected to exchange and external field interactions. The Hamiltonian who describes the model is:

$$\mathcal{H} = -J \sum_{<i,j>} S_i * S_j - h \sum_i S_i \tag{3.1}$$

Where, the first term is the summation on the interactions between near neighbor spins. J is the exchange interaction constant between the spins S_i and S_j of sites i and j of the network.
if:

- $J > 0$the interaction is ferromagnetic,
- $J < 0$the interaction is antiferromagnetic,
- $J = 0$there is no interaction between S_i and S_j

The second term of the Hamiltonian is that of the summation on the interaction of each spin S_i of the lattice with the external magnetic field applied, h.If:

- $h > 0$ the spin S_i is aligned parallel to h,
- $h < 0$ the spin S_i is aligned antiparallel to h,
- $h = 0$ No external magnetic field is applied

It is known that ferromagnetism results from the interaction between the electronic spins of atoms. Considering that the magnetic moment is applied to each atomic spin, this interaction does not come from the coupling between the magnetic dipoles but rather from the exchange interaction which involves the Pauli exclusion principle and the electrostatic repulsion between the two. electrons. Thus, it can be expected that two electrons of parallel spins have an energy of less than two electrons of antiparallel spins. This difference in electrostatic energy results in the imposition of the coupling between the spins with an exchange interaction denoted J, as described above.

The resolution of the Ising model, originally, was performed in a 1D system, and later, the 2D Ising model was analytically solved in a null field, in the sense of the exact calculation of the energy

free by Lars Onsager, in 1944 [101]. Today, this model is easily solvable to 3D. At 1D, the magnetic susceptibility remains finite at any non-zero temperature, so the one-dimensional Ising model does not show a phase transition [102]. At 2D, the existence of a phase transition is manifested by a singular behavior of the thermodynamic functions or their derivatives. In 1955, Lee Yang confirms this phase transition by calculating the heat capacity and magnetization when the external field is zero.

The resolution of the Ising model to 3D is realized only by approximate solutions. Many approaches have been developed to study the magnetic properties of 3D systems and to determine magnitudes such as magnetization, susceptibility, specific heat, energy, critical temperature, critical exponents and phase transitions.

Among these approaches, we quote: the average field approximation, the effective field theory and the Monte Carlo method. We develop the basic concepts of Monte Carlo methods in the following section.

3.3 Monte Carlo simulations

The Monte Carlo method was developed by J. Von Neumann, S. Ulma and N. Metropolis by the end of the second world war to study the diffusion of neutrons in a fissile material, that is, within the framework of the Manhattan project (a secret project initiated by the Department of Defense of the United States for the research on the manufacture of the atomic bomb). N. Metropolis et al [103] carried out computer simulation of a simple liquid (hard disks moving in 2D) using probabilistic methods and thus proposed the name of "Monte Carlo " in reference to the famous casino in Monaco.
Other researchers, Alder and Wainwright [104], in their turn, carried out the simulation of hard spheres by focusing on the solid-liquid phase transition and observed the convergence of properties towards equilibrium. Monte Carlo simulations were then exported to several domains other than physics: In economics, Monte Carlo simulation techniques are used to model phenomena with a high degree of uncertainty of initial data such as the calculation of risk capital. In industry, the problems of space exploration and oil. In mathematics, to evaluate multidimensional integrals in the case of complicated bounds. In physics, to determine the thermodynamic, magnetic, transport properties, etc systems. The Monte Carlo simulation techniques follow a common regime whatever the field of application:

- Define an initial dataset.
- Establish a random process to generate the initial data according to a probability distribution.
- Calculate the quantities according to a deterministic framework, once the equilibrium is reached.
- Collect the results.

3.3.1 Principle of Monte Carlo simulation

Monte Carlo simulation is a numerical technique that, in equilibrium thermodynamics, allows the estimation of the average of a multidimensional integral. The first simulations were performed in the canonical ensemble and subsequently extended to the other statistical ensembles. The average of a physical quantity,G, in the canonical set is given by the relation:

$$< Q >= \frac{\sum_i Q_i e^{-\beta E_i}}{\sum_i e^{-\beta E_i}} \tag{3.2}$$

Where ,$e^{-\beta E_i}$ is the Boltzmann factor, that is, the probability density of the canonical ensemble . $\beta = \frac{1}{K_B T}$ with K_B, the Boltzmann constant. T is the temperature of the system. E_i is the potential energy.

In practice, the following considerations should be emphasized:

1. The simulation starts initially at almost zero temperature, in the ordered phase of an initial magnetic configuration.
2. A random sequence of accessible states (Markov chain) is generated in the space of the system configurations.
3. We sample by favoring the regions of this space where the Boltzmann factor is the highest (Metropolis algorithm).
4. The probability of a particular configuration of potential energy Ei is then proportional to $e^{-\beta E_i}$. In other words, the acceptance of a configuration of the Markov chain is weighted by a frequency proportional to the Boltzmann factor.
5. The probability of a particular configuration of potential energy Ei is then proportional to $e^{-\beta E_i}$ A property of equilibrium is then obtained as a simple average on the accepted configurations.

In sum, the principle of Monte Carlo simulation is based on the following basic ideas:

The choice of the sample

The thermal Monte Carlo method consists in choosing a sample, that is to say, a finite set that contains the dominant (stable) states. This operation is called: The important sample: It is based on the Markov chain. The process of the Markov chain consists in generating a series of configurations where the thermodynamic and structural properties are obtained by calculating the averages of the concerned quantities according to the Boltzmann distribution under the following terms:

1 A very large number of configurations are generated.

2 The passage of the system between two accessible states during the simulation is done randomly.

3 The probability of finding the system in a given state is equal to the weight of that state in the real system.

4 If Boltzmann's weight is large, it is taken as the probability of passage. It seems then necessary to define the rule of transition from a state to another: This is the simulation dynamics. In the Monte Carlo simulation, It is governed by the master equation3.3 that gives the probability variation for each state:

$$\frac{dp_a}{dt} = \sum_b \{P_b(t) * W(b \longrightarrow a) - P_a(t) * W(a \longrightarrow b)\} \tag{3.3}$$

where,
$P_{a(b)}$ is the probability that the system is in the state $a(b)$.

$W(a \longrightarrow b)$ is the probability of passage (transition) between a and b.$W(a \longrightarrow b)$ must satisfy the following condition:

$$\sum_a W(a \longrightarrow b) = 1 \tag{3.4}$$

5 When a particle leaves a state, the probability of that state decreases. However, when It reaches this state the probability of this state increases

The idea is to favor states where $P_{a(b)}$ has high values compared to those where they are close to zero; because it is difficult to calculate the average of a physical quantity G in an infinite set. Indeed, this calculus leads to inaccuracies because of the large number of degrees of freedom of the system. By considering a sample, $F = \{a_1, a_2, ..., a_N\}$ containing N states a, the estimate of the quantity Q (given in equation 3.2) of the canonical statistical set is the ratio:

$$Q_F = \frac{\sum_{i=1}^{N}(\frac{Q_{a,i}}{P_{a,i}}) * e^{-\beta E_{a,i}}}{\sum_{j=1}^{N}(\frac{1}{P_{a,j}}) * e^{-\beta E_{a,j}}} \tag{3.5}$$

When $N \to \infty$, the estimate of the quantity G becomes equivalent to its average, $Q_F =< Q >$. The states in the sample are not equiprobable, but distributed according to the distribution of probability:

$$P_{a,i,j} = e^{-\beta E_{k,i,j}}/Z \tag{3.6}$$

Z is the partition function.

Therefore, to improve the estimate, G_F, we choose this probability distribution. This is the most well-known form of the important sample.

$$Q_F = \frac{1}{N}\sum_{i=1}^{N} Q_{k,i} \tag{3.7}$$

Which is better than when all states are equiprobable.

The completion of the Markov process requires two additional conditions, namely, ergodicity and detailed balance.

Ergodicity

The ergodicity condition is that during the Markov process, the system can, at a given state, to pass, by any state after a long time. If, for example, all the transition probabilities from a given state are zero, then the ergodicity is violated. As a result, in equilibrium, the average value of a statistically calculated quantity is equal to the average of a very large number of measurements taken in time. The first value is that which can be measured experimentally. The ergodic hypothesis is therefore fundamental for a good connection between theory and experience.

The detailed balance

It ensures that the system is in equilibrium and remains there by the Boltzmann distribution and not by another. The particles that leave the equilibrium are replaced by an equal number of those that arrive there. This translates into the equation3.8:

$$\sum_a P_a * W(a \longrightarrow b) = \sum_b P_b * W(b \longrightarrow a) \tag{3.8}$$

From equation 3.4, we obtain afterwards:

$$\sum_a P_a * W(a \longrightarrow b) = P_a = \sum_b P_b * W(b \longrightarrow a) \tag{3.9}$$

For any set of probabilities of transitions that satisfies equation 3.9, the P_a distribution constitutes a state of equilibrium from the transitions observed in the (stationary) Markov process. Unfortunately, satisfying this equation does not guarantee to reach P_a from any state of the system [105]. This can easily be demonstrated by considering that $W(b \longrightarrow a)$ are the elements of Markov matrix M.

We write:

$$q_b(t+1) = \sum_a W(a \longrightarrow b) * q_b(t) \tag{3.10}$$

In matrix form:

$$Q(t+1) = M * Q(t) \tag{3.11}$$

When the Markov process reaches equilibrium, we find:

$$Q(\infty) = M * Q(\infty) \tag{3.12}$$

If the process reaches a limit cycle:

$$Q(\infty) = M^n * Q(\infty) \tag{3.13}$$

Where, n is the size of the cycle.

Under these conditions, it appears that equation 3.9 does not guarantee equilibrium. To overcome this difficulty, we impose the condition of the detailed balance, taken from 3.8, which has the advantage of eliminating the limit cycle:

$$P_a * W(a \longrightarrow b) = P_b * W(b \longrightarrow a) \tag{3.14}$$

If the process reaches a limit cycle:

At equilibrium $Q(t)$ tends to $P_{a(b)}$ when t tends to infinity Real systems obey the detailed balance.

From equation 3.14, we can write:

$$\frac{W(a \longrightarrow b)}{W(b \longrightarrow a)} = \frac{P_b}{P_a} = e^{-\beta(E_b - E_a)} \tag{3.15}$$

This shows that the Boltzmann distribution is the distribution observed at equilibrium. Thus, equations 3.5 and 3.14 are mandatory conditions that determine the choice of the transition probability $W(a \longrightarrow b)$

Acceptance

When switching from one state to another, an acceptance report must be defined. It makes it possible to find the good probabilities of transition from any Markov process. The condition $W(a \longrightarrow b) \neq 0$ is allowed. It always satisfies the detailed balance whatever its value. By posing the transition probability as:

$$W(a \longrightarrow b) = \pi(a \longrightarrow b) * R(a \longrightarrow b) \tag{3.16}$$

Where, $\pi(a \longrightarrow b)$ is the probability of selection; probability that the algorithm generates state b from a. $R(a \longrightarrow b)$, the probability of acceptance of this configuration change. The acceptance is arbitrary between 0 and 1. If $R(a \longrightarrow b) = 0$, for all transitions, then $W(a \longrightarrow b) = 1$. This gives us a total freedom of choice of the selection probability:

$$\frac{W(a \longrightarrow b)}{W(b \longrightarrow a)} = \frac{\pi(a \longrightarrow b) * R(a \longrightarrow b)}{\pi(b \longrightarrow a) * R(b \longrightarrow a)} \tag{3.17}$$

With, $\frac{R(a \longrightarrow b)}{R(b \longrightarrow a)} \in [0, +\infty[$, while $\pi(a \longrightarrow b)$ and $\pi(b \longrightarrow a)$ can take any values. To avoid that the algorithm is slow, we choose the acceptance close to 1. The best algorithm fits well $\pi(a \longrightarrow b)$ and puts $R(a \longrightarrow b) \simeq 1$.

3.3.2 Implementation of the Metropolis Algorithm

The Metropolis algorithm is very general. It can be applied to any model for which it is possible to generate random numbers and to associate there variations of energy. Ising's model meets these criteria. This algorithm is based on a stochastic Markovian stationary dynamics [106], defined above. From an initial configuration, a, characterized by the Boltzmann factor e $e^{-\beta E_a}$, a stochastic displacement of a particle is carried out in order to generate a new configuration b, a factor of Boltzmann $e^{-\beta E_b}$. This displacement is carried out with the transition probability, $W(a \longrightarrow b)$. Each configuration thus created by this process belongs to a finite set of states called: The state space of the system. Once the system is in equilibrium, the probability of passage $W(a \longrightarrow b)$ must be the same as $W(b \longrightarrow a)$. The Metropolis algorithm allows to determine the most suitable transition probability. The implementation of the algorithm of Metropolis follows the following steps:

1. From an initial configuration a of energy E_a, a new configuration is created randomly.
2. Each new configuration is tested to see if it should be rejected or accepted, in order to obtain the new configuration b of energy E_b (to remember).
3. Once the random displacements are carried out, one calculates the variation of energy $\Delta E = E_b - E_a$.

   If $\Delta E < 0$, the new configuration b is accepted. If $\Delta E > 0$, we generate a number randomly, r, between 0 and 1.Si $r < e^{-\beta \Delta E}$, the new configuration is accepted, otherwise the new configuration is rejected and the process is repeated until b is obtained. This procedure is represented in Figure 3.3.

4. To see the balance we follow a physical quantity, like the magnetization or energy. After equilibrium, it stabilizes, only fluctuations remain. In in some cases the system remains trapped in a local minimum of energy. To avoid it we start from different initial configurations

In the case of the Ising model, state b is generated from state a. by choosing at random in the network, a single spin, k, to return (the flip). The two states therefore differ by spin reversal, k. The difference in energy, $\Delta E = E_b - E_a$, in the absence of the external magnetic field is calculated from the expression of the Hamiltonian given in equation

$$E_b - E_a = -J \sum_{<ij>} S_i^b S_j^b + J \sum_{<ij>} S_i^a S_j^a = -J \sum_{<ik>} S_i^a (S_k^b - S_k^a) \tag{3.18}$$

If $S_k^a = 1$ then $S_k^b = -1$ and $S_k^b - S_k^a = -2$

If $S_k^a = -1$ then $S_k^b = 1$ and $S_k^b - S_k^a = 2$

then

$$S_k^b - S_k^a = -2S_k^a \tag{3.19}$$

And

$$E_b - E_a = 2J \sum_{<ij>} S_i^a S_k^a = 2JS_k^a \sum_i S_i^a \tag{3.20}$$

3.3.3 Mesures et erreurs

Once the system has reached equilibrium, the quantities most interested can be measured. The simulation program must run for a long enough time to reach this equilibrium, as we have already stated in the ergodic condition. This time corresponds to the steps or steps Monte Carlo (Monte Carlo steps, in English). The equilibrium can be identified by following the evolution of a magnitude such as magnetization or entropy (The entropy is maximal at equilibrium). For the Ising model, the Metropolis algorithm is used to calculate the thermodynamic quantities such as, magnetization, magnetic susceptibility or specific heat, by converging the system not to not towards a situation of equilibrium.

- The total magnetization of the state a is given by:

$$M_a = \sum_i S_i^a \tag{3.21}$$

We use, the difference of magnetization:

$$\Delta M = M_b - M_a = \sum_i S_i^b - S_i^a = S_k^b - S_k^a = 2S_k^a \tag{3.22}$$

hence

$$M_b = \Delta M + M_a = M_a + 2S_k^b \tag{3.23}$$

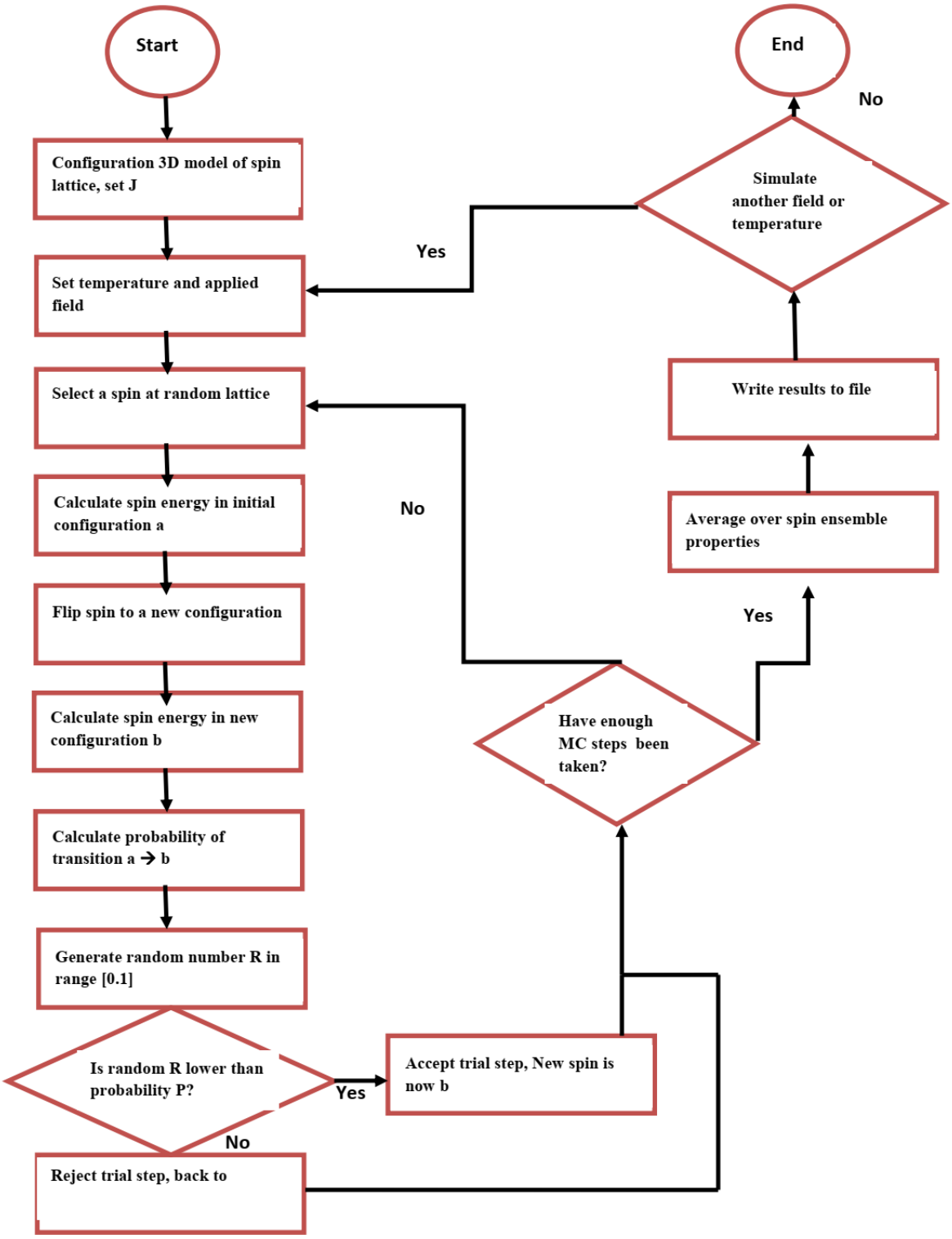

Figure 3.3: Flow diagram of a Monte-Carlo simulation with Metropolis algorithm [107]

- Magnetic susceptibility:

$$\chi = \frac{N}{\beta}(< M^2 > - < M >^2) \tag{3.24}$$

Where, N is the total number of spins corresponding to the size of the network.

- The specific heat:

$$C_v = \frac{\beta^2}{N}(< E^2 > - < E >^2) \tag{3.25}$$

There are two types of errors: statistical errors and systematic errors.

- Statistical error: This is the error on the average. In the Ising model, it results from thermal fluctuations. To obtain reliable results, an average must be taken on steps much larger than the number on which the Monte Carlo states are correlated. This becomes more difficult near the critical point due to a critical slowdown. If we suppose that the magnetizations Mi are independent, the best estimate of the statistical error is given by:

$$\sigma = \sqrt{\frac{\frac{1}{n}\sum_{i=0}^{n}(M_i - \overline{M})^2}{n-1}} = \sqrt{\frac{1}{1-n}(\overline{M^2} - (\overline{M})^2)} \tag{3.26}$$

The exact expression of σ is written:

$$\sigma = \sqrt{\frac{1 + \frac{2\tau}{\Delta t}}{1-n} * (\overline{M^2} - (\overline{M})^2)} \tag{3.27}$$

Where Δt is the time interval between two measurements and τ is the correlation time (time required for the system to go from one state to another, very different from the first one). If $\Delta t \gg \tau$, we find the previous equation.
Often $\Delta t \ll \tau$, where:

$$\sigma = \sqrt{\frac{2\tau}{t_{max}} * (\overline{M^2} - (\overline{M})^2)} \tag{3.28}$$

With $n = t_{max}/\Delta t.\sigma$ does not depend on Δt , so there is freedom of choice.

- Systematic errors: The sources of systematic errors in the simulation of the Ising model are the fact of:

- Wait for balance only for a short time.
- Do not run the system long enough after the balance

There is no general method for estimating these errors.

In addition to the Metropolis algorithm, there are two other algorithms of turnaround of a single spin by step, which are also widely used nowadays. These are the "hot-bath" and "glauber" algorithms [108]. These algorithms are sometimes called, update algorithms: In the model of Potts (whose Monte Carlo simulation is similar to that of Ising), at low temperature, the Metropolis algorithm is no longer effective. To overcome this difficulty, we use the hot-bath algorithm.

Notes: When implementing the Metropolis algorithm, the knowledge a number of practical details is an asset to get a code that works correctly:

- Initial configuration: It must not influence the final configuration. However, the balance can be reached more quickly if a good initial setup is chosen.
- Degrees of freedom: There are several ways to update degrees of freedom Freedom in the program. They may be chosen at random or according to a Random permutation, which can be updated. However, a simple sequential order fixed is also allowed. In network models, we can also update first the even sites, then all the odd sites, which is the usual choice in the vectorized codes.
- Boundary conditions: Different boundary conditions can be used:
- Periodic boundary conditions: The system is periodically repeated in all directions to imitate an infinite system.
- Free boundary conditions: These are used to describe the systems finished like nanoparticles.
- Random numbers: They are generated by pseudo-random number generators (RNGs), which can produce uniform distributed numbers whose values are very difficult or even impossible to predict using any deterministic rule. The quality of a RNG is measured by the difficulty of deriving the deterministic rule underlying their generation, the absence of correlations and a very long time. It is very important for a RNG to produce results reproducible for testing purposes and also portable between different computing platforms
- The effects of network size: Finite size effects. The networks considered in the Monte Carlo simulations, as digital tools limited by the memory of the computer, must have a finite size while the macroscopic properties are generally targeted. To take the limit of a size to infinity, one calculates, usually, an average for several different sizes of the network, then extrapolates the average to an infinite size.

The magnetic properties can be easily determined by normalizing the parameters of the Hamiltonian as a function of a parameter chosen upstream. The system parameters are then reduced parameters. This technique makes it possible to describe qualitatively the magnetic properties of the material studied as well as to predict phenomena such as the magnetic stability of the material, the phase transitions and the magnetic compensation. As part of our research, we used the Ising model combined with the Monte Carlo method to study the magnetic properties of spin models, in this case magnetic nancucubes assemblies and single nanocubes.

Part II

Contributions

Chapter 4

Calculated Magnetic Properties of the Compound $PbVO_3$

4.1 Introduction

From viewpoints of basic physics and application, multiferroics (MF) seem to be an interesting class of materials.The three or two (anti)ferroelectricity, (anti)ferromagnetism, and ferroelasticity are observed in the same phase in multiferroics.

In 1960–1970, (anti)ferroelectricity, (anti)ferromagnetism, and ferroelasticity were investigated, though they did not attract much interest because of the difficulties in manufacturing good samples and the very weak coupling between different order parameters. Because of the advanced preparation and characterization techniques multiferroics have seen a revival of interest in the last years [109]. Also, there are prospects of new features important for technical applications [110, 111].

Simple perovskite-like compounds ABO_3 ($A \in \{Pb, Bi\}; B \in \{V, Co\}$) lately were synthesized under high-temperature and high-pressure conditions in thin film and bulk forms; their electric and magnetic properties were examined and are considered two of the promising MF candidate materials [112–114]. The structural and electronic conditions in these compounds appear to favor a large desirable coupling between a ferroelectricity and a cooperative magnetism [115]. The result of large A and B atomic distortions in these materials is sizeable ferroelectric polarizations and peculiar magnetic properties [116, 117]. The PbMO3 perovskites exhibit an interaction between the Pb–6s,6p lone-pair hybrids and the transition-metal MO3 perovskite framework [118]. The AVO3 (A = Sr, Ba, and Pb)-type perovskite-based oxide compounds are very convenient, among which the prototype $PbVO_3$ shows unusual behaviors at high pressure [119–122]. The compounds AVO_3 are considered to have many potential applications in domains such as multiferroic arrangements, high-temperature solid oxide fuel cells, and high TN superconductivity [121]. Without being affected by their potential importance, relevant investigations on the AVO_3 compounds are relatively rare. Tetragonal PbVO3 has drawn much attention as a promising MF candidate material [123–127]. Antiferromagnetic (AF) insulator state with the C-type AF ordering is the most stable state for the two bulk $PbVO_3$ and $BiCoO_3$ referring to the electronic structure calculations [123, 127–129]. Vanadium oxide $PbVO_3$ newly produced [109, 110, 127] presents remarkable ferroelectric properties becoming a subject of intense studies, both theoretical and experimental within the ferroelectric community. In this paper, we have studied the magnetic properties of compound $PbVO_3$ by Monte Carlo simulation. With this method, we have obtained the diagram phases which are discussed and interpreted; the magnetizations, the susceptibly, the specific heat, and the critical temperature are analyzed and determined. We finished with calculation of the critical exponents.

4.2 Theoretical model and method

Our aim in this section is to determine the model and method of compound $PbVO_3$. The crystal structure of simple perovskite $PbVO_3$ is an undistorted tetragonal composite whose space group is $P4mm$. The

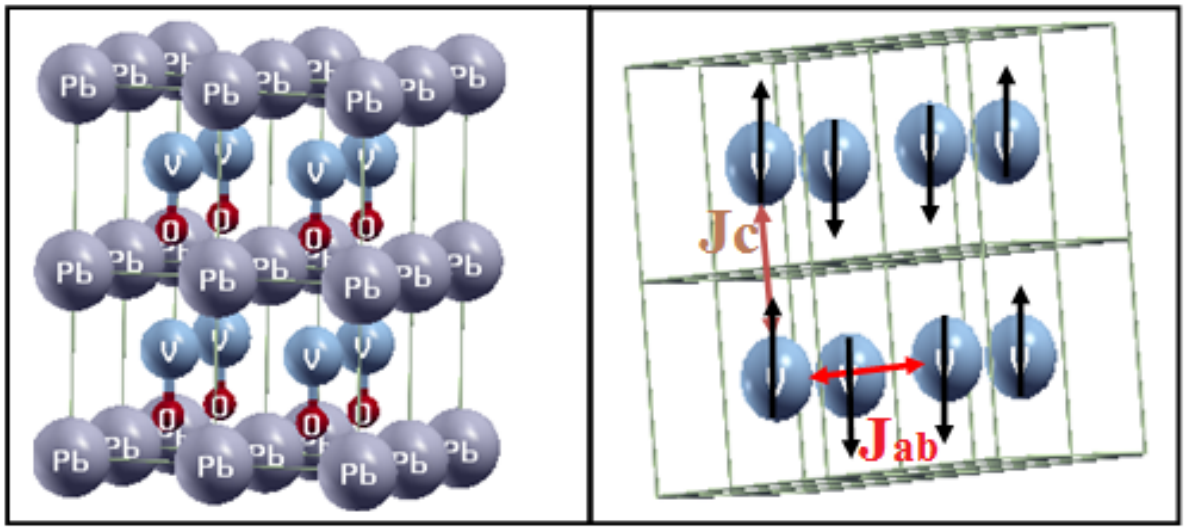

Figure 4.1: Structure of compound $PbVO_3$ in the left and the magnetic structure in the right $(2, 2, 2)$

parameters of this compound are $a = b = 3.8039$ and $c = 4.6768\mathring{A}$ as determined in [112]. The atomic positions are presented in (see Figure 4.1). The distribution of charges in this compound is given by $Pb^{+2}V^{+2}O^{-3}$. It is clear that Pb and O ions are not having a magnetic moment . As a result, the magnetic moment of this compound comes from the V ion with moment spin $S = 1/2$.

The magnetic structure of our system consists of two simple cubic sublattices with the classical Ising model described by the following Hamiltonian:

$$\mathcal{H} = -J_{ab} \sum_{\langle i,j \rangle} \sigma_i^A \sigma_j^B - J_c \sum_{\langle\langle i,k \rangle\rangle} S_i S_j - H(\sum_{i=1}^{N/2} \sigma_i^A + \sum_{j=1}^{N/2} \sigma_j^B) \tag{4.1}$$

Where

- $\langle i, j \rangle$ denote the first neighbors between σ_i^A, σ_j^B
- $\langle\langle i, k \rangle\rangle$ designed the second neighbors between $\sigma_i - \sigma_k$ (A–A or B–B)
- J_{ab} is the first exchange coupling interactions between $\sigma_i^A - \sigma_j^B$ and $J_{ab} = -337k$ [113]
- J_c is the second exchange coupling interactions between $\sigma_i - \sigma_k$ and $J_c = +38k$ [113].
- H stands for an external magnetic field.

The magnetic properties and the critical behavior of $PbVO_3$ are established and determined using the Monte Carlo method in combination with the Metropolis algorithm, for systems with linear size L. Cyclic boundary conditions on the lattice were imposed, and the configurations were generated by sequentially traversing the lattice and making single-spin flip attempts. The flips are accepted or rejected according to a heat-bath algorithm under the Metropolis scheme. Our data were generated with $3 * 10^5$ Monte Carlo steps per spin, discarding the first $2 * 10^4$ Monte Carlo configurations. Starting from different initial conditions, we performed the average of each parameter and estimated the Monte Carlo simulations, averaging over many initial conditions.

With this simulation method, we calculated the total magnetizations (M), energy (E) of the system, the magnetic susceptibilities (χ), the specific heat (Cv) and the critical behaviors which are as follows:

- The internal energy per site:

$$E_T = \frac{\langle H \rangle}{L^3} \tag{4.2}$$

- The partial and total magnetizations of the system are given by:

$$M_A = \frac{2\sum_{i=1}^{N/2} \sigma_i^A}{L^3} \tag{4.3}$$

$$M_B = \frac{2\sum_{i=1}^{N/2} \sigma_i^B}{L^3} \tag{4.4}$$

$$M_{Total} = \frac{|M_A - M_B|}{L^3} \tag{4.5}$$

- The magnetic susceptibilities and specific heat are given respectively by:

$$\chi = \frac{\beta}{L^3}\left(\langle M_{Tot}^2 \rangle - \langle M_{Tot} \rangle^2\right) \tag{4.6}$$

$$C_v = \frac{\beta}{L^3}\left(\langle E^2 \rangle - \langle E \rangle^2\right) \tag{4.7}$$

- The critical behaviors of the observable quantities are given by:

$$\chi_{max}(L) \sim L^{\frac{\gamma}{\upsilon}} \tag{4.8}$$

$$C_v max(L) \sim L^{\frac{\alpha}{\upsilon}} \tag{4.9}$$

where $\beta = \frac{1}{K_B T}$ and K_B is the Boltzmann constant, which is taken equal to its unit value in this work.

4.3 Results and discussions

4.3.1 Ground-State Phase Diagrams (T=0 K)

In this part of the study, the phase diagrams, which are illustrated in Figure 4.2, generated from our compound are going to be analyzed and discussed. Once more, it is necessary to indicate that we are inspired and motivated by $PbVO_3$ compound for a fixed and thermodynamic limit size, $N = L*L*L = 24*24*24$ spins and $S(V^{+4}) = 1/2$.
First of all, the illustration of the corresponding groundstate diagrams in the plane (J_{ab}, J_c) in the absence of the external magnetic field ($H = 0.0$) is made to demonstrate the influence that the exchange coupling on the stable states (see Figure 4.2.a). This figure shows that the stable phases are phase $(-1/2, -1/2)$, phase $(+1/2, +1/2)$, phase $(-1/2, +1/2)$, and phase $(+1/2, -1/2)$.

We plot Figures 4.2b, c to determine the stable configurations as the second and complementary facet of the analysis of the phase diagram. In Figure 4.2.b, it is deduced that phase $(-1/2, -1/2)$, phase $(+1/2, +1/2)$, phase $(-1/2, +1/2)$ and phase $(+1/2, -1/2)$ are the stable states. Also, in Figure 4.2.c, the stable phases are phase $(-1/2, -1/2)$ and phase $(+1/2, +1/2)$.
It is crucially important to indicate that the phase diagrams have been studied at null temperature while the magnetic properties shall be investigated at the non-null temperature in the following subsection.

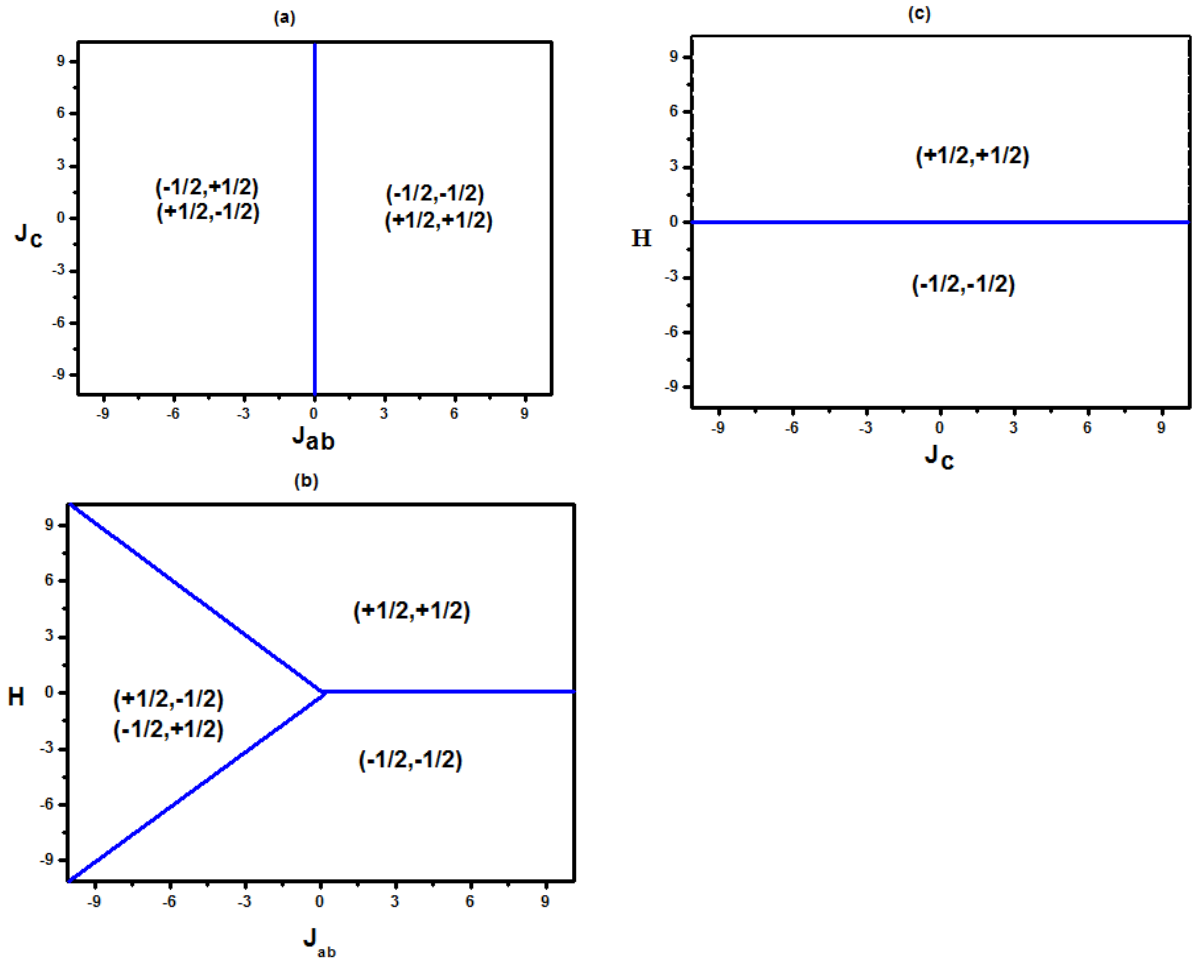

Figure 4.2: Ground-state phase diagrams displaying different stable phases in different phase diagrams: in a) the plane (J_{ab}, J_c) for $H = 0.0$ and $\Delta = 0.0$;b) in the plane (H, J_{ab}) for $J_c = 1.0$ and $\Delta = 0.0$;c) in the plane (H, J) for $J_{ab} = +1.0$, $\Delta = 0.0$

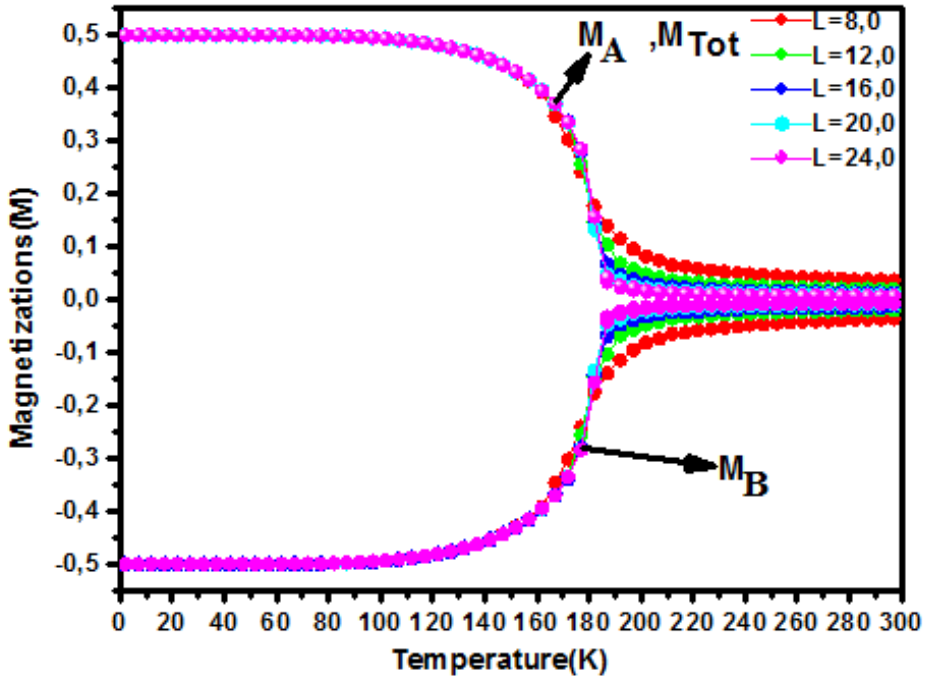

Figure 4.3: Partial (M_A; M_B)-total magnetizations as a function of temperature for various sizes: $L = 8, 12, 16, 20$, and 24, for $J_{ab} = -337K$ and $J_c = +38K$ of $PbVO_3$

4.3.2 Monte Carlo Results ($T \neq 0$)

In this section we investigated the $PbVO_3$ compound using Monte Carlo simulation with the application of the Metropolis algorithm in the framework of the threedimensional Ising model. The results obtained by this method are organized as follows:

Figure 4.3 displays the variation of the magnetization as a function of the temperature for the different values of the system size ($L = 8, 12, 16, 20$ and 24). It is evident that the system size goes through the variation from 8 to 24 for the values of the exchange coupling $J_{ab} = -337K$ and $J_c = +38K$. Put in another way, the main observation made here is that for the smaller sizes ($L = 8$ and 16) of the compound, the magnetization is in the condition of constancy and non-zero above the Curie temperature; however, for the other sizes ($L = 20$ and 24), we have concluded that the magnetization decreases by the increasing temperature until it vanishes at the Neel temperature $T_N \simeq 182K$. Moreover, it is observed that the second-order transition is present because of the continuity of the magnetization and this observation is important for determining the critical exponents. This transition temperature determined in this study is a good agreement with experimental value $T_N = 190K$ [112].

In the same line, Figure 4.4a,b these figures illustrated the peaks of the specific heat and the susceptibility, too. From these figures, we have observed that the peaks increase when the system size increases. More importantly, the peaks of the thermal magnetic susceptibility are located at the transition temperature whose determined value is $TN \simeq 182K$ as said before.

In the same context, we presented in this part of work the variation of the transition temperature versus the exchange coupling interactions, Figure 4.5a–f illustrated the impact of the exchange coupling interactions (J_{ab}, J_c) on the transition temperature. In Figure 4.5.a–c are plotted different values of J_{ab} with J_c fixed, and in Figure 4.5.d–f is illustrated J_{ab} fixed and J_c varied. From these figures, we deduced, when the absolute values of the exchange coupling interactions increase, the transition temperature increases too. Finally, we do the calculation of the critical exponents α, γ , and ν by first taking a logarithm to calculate the critical exponent ν from the slope $(1/\nu)$ of the linear fit as illustrated in Figure 4.6.a. By using the value of the critical exponent ν and taking the logarithm of (4.8) and (4.9),

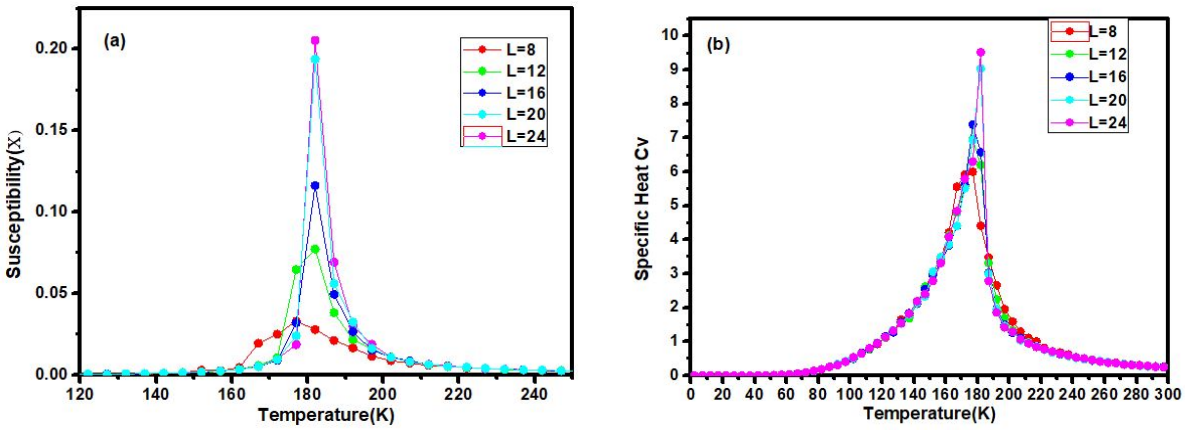

Figure 4.4: a)Susceptibility and b) specific heat as a function of temperature for various sizes: $L = 8, 12, 16, 20$, and 24; for $J_{ab} = -337K$ and $Jc = +38K$ of $PbVO_3$

we determine the critical exponents γ and α from the slopes (γ/ν) and (α/ν) of the linear fits as shown in Figure 4.6.b, c. The critical exponents obtained are $\nu = 0.66$, $\gamma = 1.26$, and $\alpha = 0.28$. By comparing with the universal values of the 3D Ising model $\nu = 0.632$, $\gamma = 1.23$, and $\alpha = 0.104$ [130], our critical exponents are near to them.

4.4 Conclusion

In conclusion, we obtained results by means of the investigation made into the PbVO3 compound with spin $S = 1/2$ which is an important material used as components in electronic devices. These results are the elaboration and discussion of the stable phases, the examination of the ground-state phase diagrams is made, and the partial– total magnetization, susceptibility and specific heat as a function of the temperature have been explored. Furthermore the transition temperature determined in this study $(T_N \simeq 182K)$ is in good agreement with experimental value $T_N = 190K$ Also the temperature transition increases with the increasing of the absolute value of the exchange coupling interactions (J_{ab}, J_c). Finally, the critical exponents have been determined. This has been achieved essentially by using Monte Carlo simulations (MCS) within the framework of the Ising model. We have succeeded in determining the magnetic properties of compound $PbVO_3$

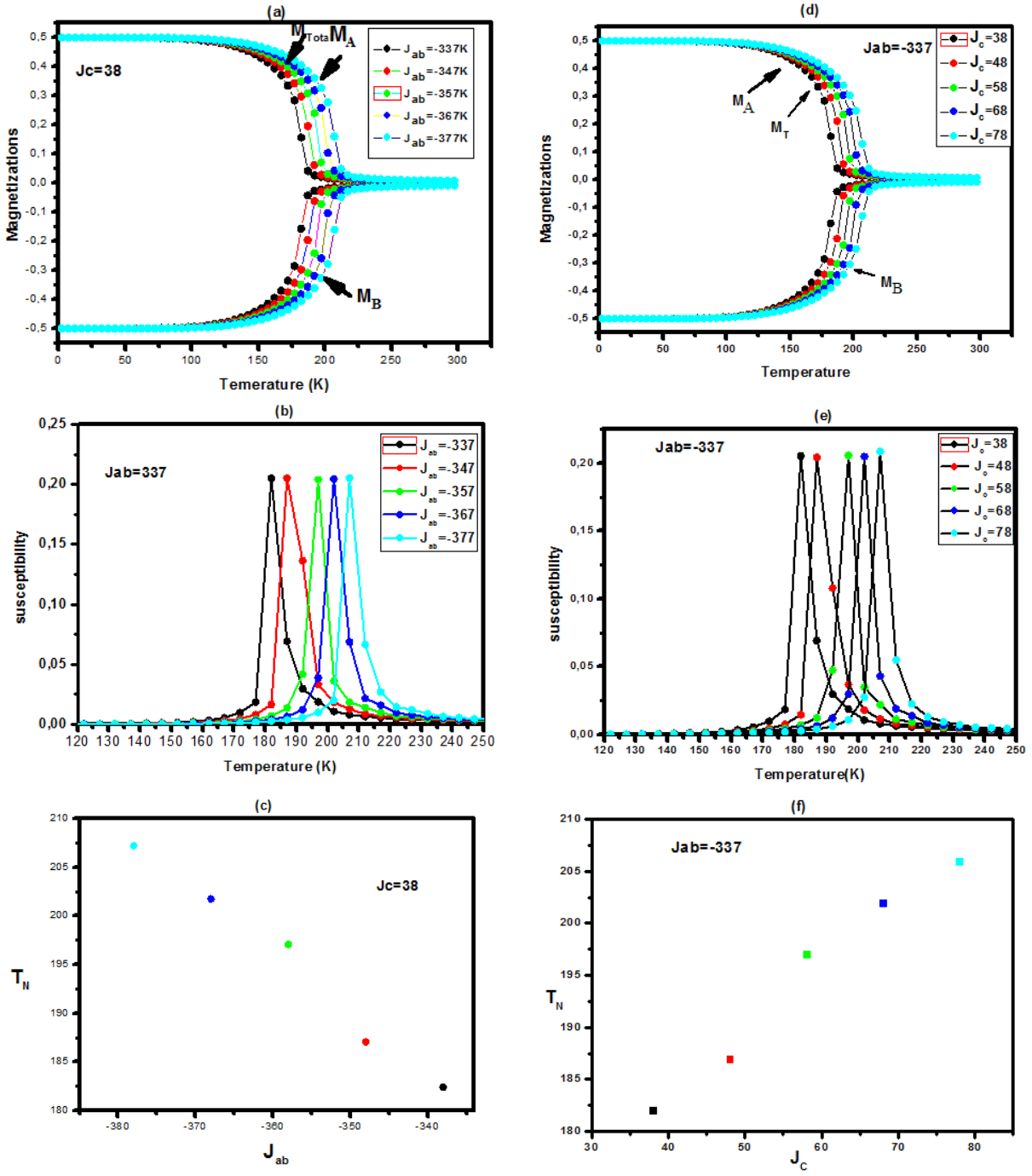

Figure 4.5: Variation of the transition temperature as a function of the exchange coupling interactions (J_{ab}, J_c)

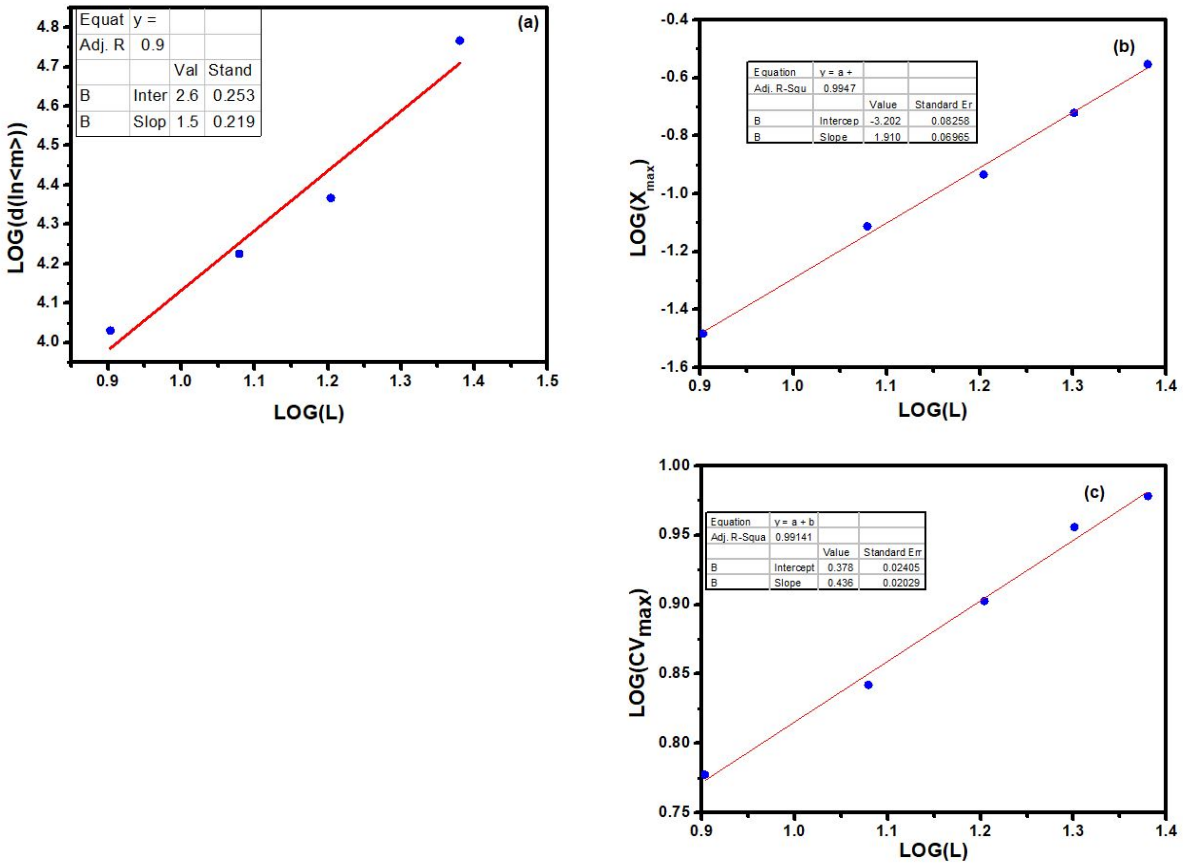

Figure 4.6: Critical exponents for values of the exchange coupling $J_{ab} = -337K$ and $J_c = +38K$ of $PbVO_3$ in the absence of the external magnetic. a *Log–log* plot of the maxima of $d(ln < m >)/d(1/KBT)$ as a function of the system size L. b *Log–log* plot of the maxima of the susceptibility versus the system size L. c *Log–log* plot of the maxima of the specific heat versus the system size L.

Chapter 5

Effect of thickness size on magnetic behavior of layered Ising nanocube with Spins (5/2,3/2, 5/2):Monte Carlo simulations.

5.1 Introduction

Magnetic nanoparticles (MNs) are undoubtedly of great interest to researchers because of their magnetic and morphological properties [1]. MNs have potential nanotechnological and industrial applications in the following domains: information storage [28, 131], biomedical applications [132], shielding [133], sensors [134, 135] and magneto-resistive devices [136]. The nanoparticles constituted by combining two or more magnetically coupled structures [21, 41, 137–142] (layers, core-shell...) leads to enormous applications because of the numerous physical and magnetic phenomena that occur. It is noteworthy, that each substructure may exhibit a different thermal behavior for its magnetization such as compensation points, i. e., temperatures below the critical point for which the total magnetization is zero while the individual substructures remain magnetically ordered [143, 144].

In today's climate of intensive nanotechnology research, several types of nanoparticles with combined magnetic substructures have been successfully synthesized such as nanocubes, nanowires, and nanofilms.

Well obviously experimental research progress of these magnetic nanoparticles is complete fewer opportunities without detailed theoretical investigations. In the same context many theoretical studies have been devoted to investigate the magnetic properties of magnetic nanoparticle by using different types of methods: Monte Carlo (MC) [145, 146] and micro-magnetic simulations [147]. A number of this was earmarked for the study of phase diagrams of compensation points. Particularly Layered [148, 149] magnetic systems seeing that it presents well the phenomenon of point of compensation and other like such as the giant magnetoresistance [150, 151] and the magnetocaloric effect [152–154] have important technological applications. In the same context there is also immense theoretical interest in investigating the magnetic properties of these kind of systems, to better understand the interactions between the characteristic behaviors of two- and three magnetic layers. Diaz et al confirmed that the compensation effect is favored by weaker interplanar couplings and by a more pronounced intraplanar coupling asymmetry studying a Ferrimagnetic 1/2-spin Ising bilayers by using Monte Carlo simulations [148]. Jiang et al have explored the magnetic properties of the ferromagnetic nanoparticles on a body-centered cubic lattice based on a classical Heisenberg spin Hamiltonian in which S=3/2 and σ=5/2 spins are distributed in the two interpenetrating square sublattices. They have discussed the occurrence of a compensation temperature in the system and its conditions. They also noticed the fact that compensation temperature of system vary as the particle size increases, and it becomes relatively independent of particle size when

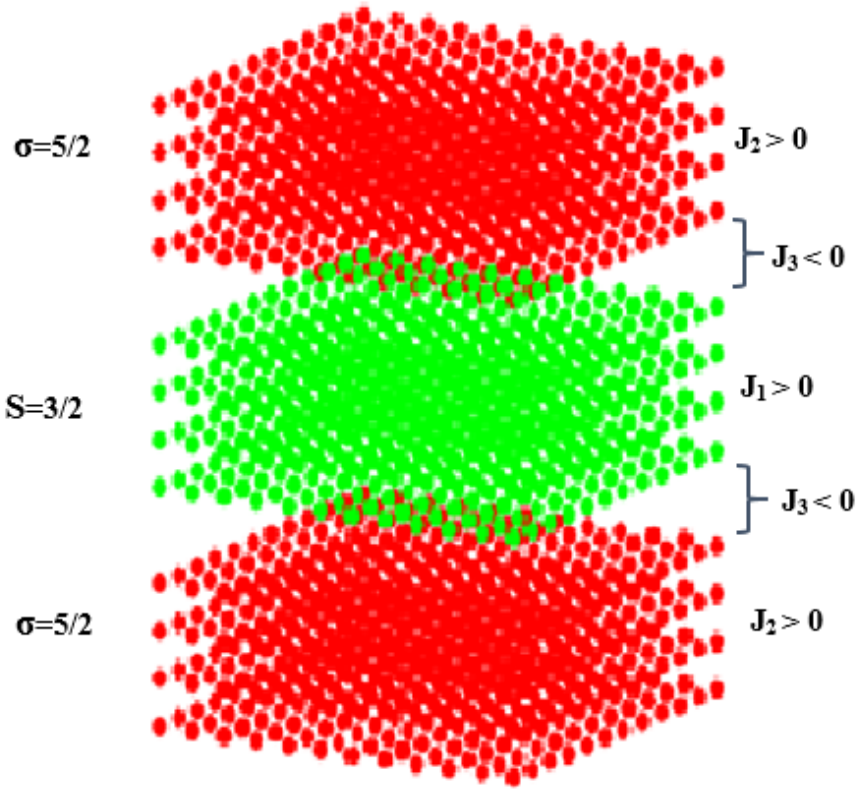

Figure 5.1: Trilayred Nanocube with: green color indicates layer with spin 3/2 and two others with red color for spin 5/2.

the particle size is increased further [155]. Yuksel et al have investigated the phase diagrams and thermal and magnetic properties of a ferrimagnetic nanoparticle which is defined on a simple cubic lattice with a ferromagnetic spin-3/2core which is interacting antiferromagnetically with a ferromagnetic spin-1 shell layer. More recently Lv [156] and Kanyoushi [157] have investigated the phase diagrams and the thermal variations of total magnetization for Ising bilayer. Other works have focused on magnetic trilayers [158, 159] and multilayers [160].

We utilized the Monte Carlo simulations to investigate what phenomena may be obtained in the Ising trilayers nanocube consisting of the two layers with spin-5/2 and one in the middle with spin-3/2. We examined the effects of exchange couplings, anisotropic parameter, and the thickness of the nanocubes layers on the behavior of critical, compensation temperatures, the phase diagram, and hysteresis loops.

This work is organized as follows. In section 5.2 , we define the model and present the method. The simulation results and discussion are presented in section 5.3, and finally we give our conclusions in section 5.4.

5.2 Theoretical model and method

Here, we considered a single nanocube system containing three alternating ferromagnetic layers. The middle one noted $L1$ is described by coupled spins $S = 3/2$ with thickness t_S while the two other layers noted $L2$ are described by coupled spins $\sigma = 5/2$ with thickness t_σ for each one. Spins are assumed to interact ferromagnetically inside layers while the spins between two adjacent layers are interracting antifroemagnetly (interlayers). We note the thickness ratio $r = \frac{t_\sigma}{t_S}$. The Hamiltonian which governs the

system studied is expressed by:

$$\mathcal{H} = -J_1 \sum_{\langle i,j \rangle} S_i S_j - J_2 \sum_{\langle k,l \rangle} \sigma_k \sigma_l - J_3 \sum_{\langle m,n \rangle} S_m \sigma_n - D \sum_i ((\sigma_i)^2 + (S_i)^2) - H \sum_i (\sigma_i + S_i) \tag{5.1}$$

Where S_i and S_j are nearest-neighbours, spins of sites i and j represent the layer $L1$ while σ_k and σ_l represent thus of layers $L2$. σ_m and σ_n denote interlayer spins of the following adjacent layers. J_1 and J_2 are exchange couplings between nearest neighbors of spins belonging to the $L1$ and $L2$ respectively. J_3 is exchange coupling interactions of nearest-neighbor spins are between consecutive adjacent layers . D is the magnetic anisotropy parameter, and H is the external magnetic field acting on all spins. The Hamiltonian (5.1) is solved numerically. In the following, we used normalized parameters: J_2/J_1, J_3/J_1, D/J_1 and H/J_1.

To compute the thermodynamic quantities, we used the Metropolis algorithm in the context of the Ising model. The lattice was considered with free boundary conditions, and the simulation was performed for different lattice sizes. The program ran a sufficient for an amount of time using 18.10^5 Monte Carlo steps (MCS) per spin, and the equilibrium was reached after 10^5 MCS steps per site. The magnetizations per site of $L1$ and $L2$ can be calculated by:

$$M_1 = \frac{1}{N_1} \sum_{i=1}^{N1} S_i \tag{5.2}$$

$$M_2 = \frac{1}{N_2} \sum_{i=1}^{N2} \sigma_i \tag{5.3}$$

While the total magnetization per site is:

$$M_T = \frac{M_1 N_1 + M_2 N_2}{N} \tag{5.4}$$

The magnetic susceptibility per site of the magnetic nanoparticle is defined as:

$$\chi = \beta(< M_T^2 > - < M_T >^2) \tag{5.5}$$

Where $\beta = \frac{1}{K_B T}$

We could obtain the compensation temperature T_{com} by looking for the point of intersection between the absolute values of the magnetizations of the layers by using:

$$(M_1(T_{com})) = -(M_2(T_{com})) \tag{5.6}$$

With $T_{com} < T_c$.

5.3 Results and discussions

In Figure 5.2, we represented total and partial magnetizations as functions of the reduced temperature and investigated the effect of the anisotropy parameter D/J_1 on phase diagrams of interest. We have found that for selected values -0.3, 0.0 and 0.3 of D/J_1, magnetizations decrease continuously until vanishing at a specific point before reaching the critical one. That denotes the phenomenon of magnetic compensation (see Figure 5.2.a). In fact, this phenomenon appears generally in the ferrimagnetic order

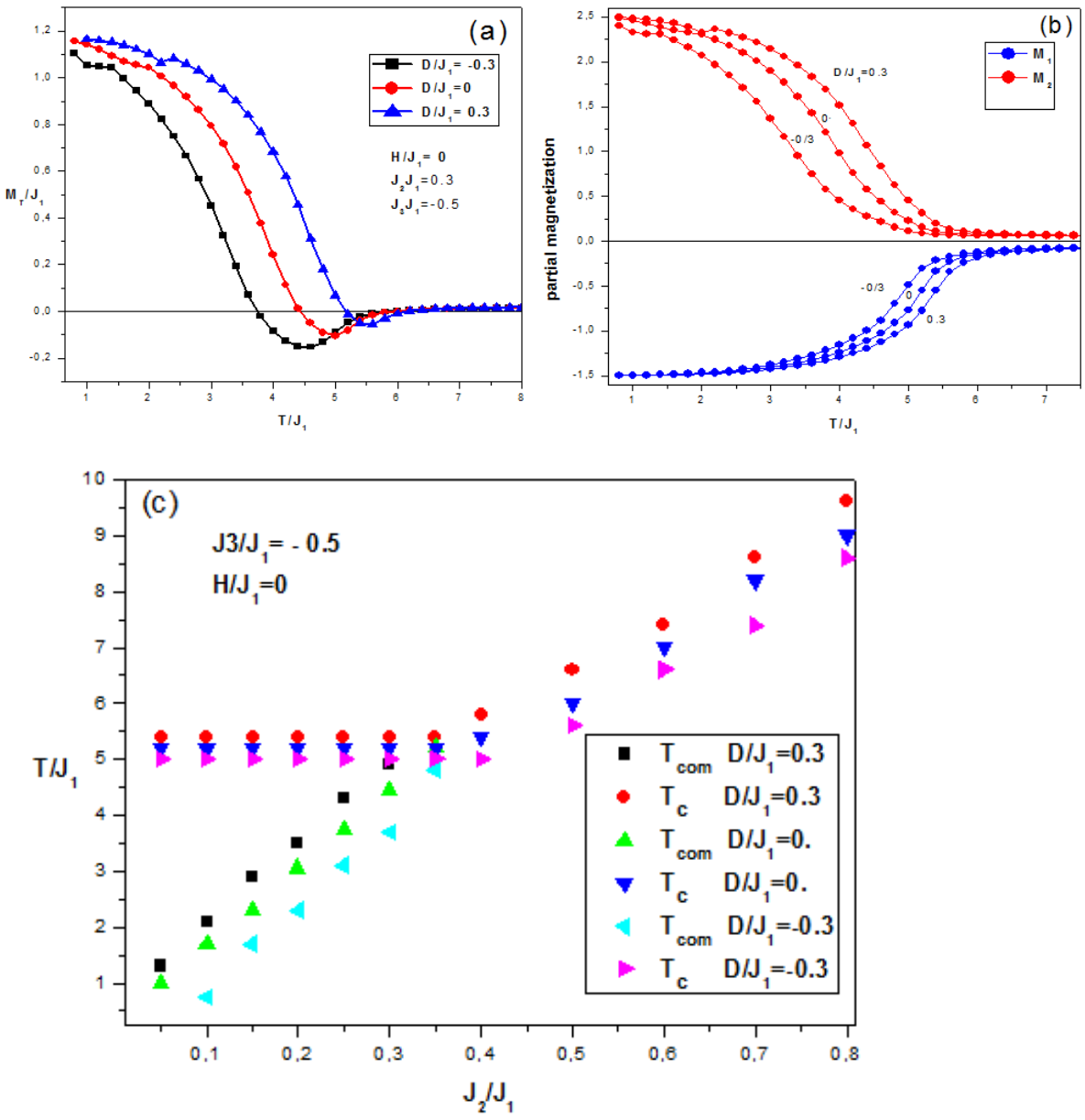

Figure 5.2: Effect of the anisotropy parameter D/J_1 on the temperature dependencies of (a) total magnetization M_T , (b) Layer spin-3/2 and Layers spin-5/2 magnetizations M_1 , M_2 For J_2/J_1 =0.3, J_3/J_1 = -0.5 and H/J_1 =0. (c) Phase diagram of the system in (T_c ,$T_{com} - J_2/J_1$) plane for D/J_1 = -0.3 ,0,0.3 and for the same parameters.

when the magnetization is plotted versus the temperature. The specific point in Figure 5.2.a is called by the compensation point; it corresponds to the intersection between a magnetization curve and the temperature axis and indicates the compensation temperature value. It is seen in (Figure 5.2.c) that the compensation temperature increases proportionally with D/J_1. Diaz and Branco reported a similar behavior when studying spin-1/2 Ising system containing three layers [149]. It is worth noting that the magnetic compensation is useful in the control of the magnetic stability of some magnetic systems used in spintronics.

Figure 5.3.(a-c) shows the effect of the thickness ratio $r = \frac{t_\sigma}{t_S}$ on the temperature dependencies of total magnetization M_T for J_2/J_1=0.2 ,0.45 and 0.8 , J_2/J_1=-0.5, H/J_1=0 and D/J_1=0. The compensation temperature have been observed at low values of $J_2/J_1 = 0.2$, see Figure 5.3.a which increases with increasing the thickness ratio r. Also, we show that for all values of J_2/J_1 the total magnetization M_T increases as we increase the thickness ratio r. Below J_2/J_1=0.8 a antiferromagnetic order have been appeared. The Figure 5.3.(d-f) presents the magnetic susceptibility χ of the nanocubes for J_2/J_1=0.2 ,0.45 and 0.8 , J_2/J_1=-0.5, H/J_1=0 and D/J_1=0. For J_2/J_1=0.2, we see tow peaks of the magnetic susceptibility χ in Figure 5.3.d, the first and second peaks are corresponding to the compensation and critical temperatures. For $J_2/J_1 > 0.45$ the compensation of the total magnetization disappear and the magnetic susceptibility χ presents one peak which corresponding to the critical temperature. The calculated critical temperature concur with result reported by N. De La Espriella et all [161] in studying magnetic behavior of a mixed Ising system $(3/2; 5/2)$ on a square lattice.

The effect of J_2/J_1 and the thickness ratio r on compensation and critical temperatures for $D/J_1 = -0.3, 0, 0.3$ and for the same parameters for layered nanocube are plotted in Figure 5.3.g, the system presents a compensation temperature below $J_2/J_1 = 0, 45$. For $J_2/J_1 > 0.45$ the critical temperature increases with increasing the thickness ratio r, but For $J_2/J_1 < 0.45$ to the compensation and critical temperatures increase with decreasing the thickness ratio r. The point (0.45-6) corresponding to tricritical point in the Phase diagram of the system in $(T_c, T_{com} - J_2/J_1)$. The critical temperatures of nanocube found are closed to their of Ising bilayer system consisting of the mixed $(3/2; 5/2)$ reported by M Keskin [162].

Figure 5.4.a shows the total hysteresis loops for different values of thickness ratio r when fixed $T/J_1 = 1$, $J_2/J_1 = 1$, $J_3/J_1 = -0.5$, and $D/J_1 = 1$. Under the influence of thickness ratio r, the total area of the hysteresis loop of nanocube systems increases with increasing the thickness ratio r, we found that the total hysteresis loop depends of the thickness of spin-5/2, also a fixed hysteresis loop have been observed for the partial hysteresis loop of buffer layer (spin 3/2) (see Figure 5.4.b), suggesting that the magnetization in this system governed by spin-5/2 layered. It is found that the hysteresis loop showing ferromagnetic behavior for all values of thickness ratio r.

The magnetic hysteresis loops behavior that we researched is of great importance for memory storage device development, high frequency device application, and academic study [163]. The resulting reduced total-partial hysteresis loops for several values of reduced anisotropy D/J_1 is determined in Figure 5.5.From these figures, we observed that the total system exhibits the triple loop when D/J_1=-1.5 while the sublattices S and σ present the single loop. We can conclude that the appearance of the triple loop in the total system is due to the combination of the both sublattice S and σ. when $D/J_1 = -1$ the hysteresis loop of total system changes and becomes a single loop and its area increase, also for sublattice S while the area of the sublattice σ decrease ,which comes from the variation in the hysteresis loops of the sublattice S. by increasing D/J_1 (for D/J_1=0 and 1) the single loop the triple hysteresis loop still exists in the system, also we can notice the existence of the magnetization plateaus in the hysteresis loops, meanwhile the sublattice S and sigma present a rectangular shape like the hysteresis behaviors in the ferromagnetic system. The area of the loop increases obviously, the same for S sublattice, while the area of σ sublattice is nearly unchanged. By describing the effect of anisotropy on coercivity and remanence of the system: increasing the reduced anisotropy parameter D/J_1 the coercivity of the system increases slightly at first, then increase abusively in continuous density, while the remanence remains virtually unchanged.

The Figure 5.6 illustrates the impact of the reduced exchange coupling interaction (between spin-5/2) J_2/J_1 of on the total and partial hysteresis loops with fixed $J_3/J_1 = -0.5$, $T/J_1 = 2$ and $D/J_1 = 0$. From This figure we can see that the shape of the hysteresis loops take a conspicuous change by increasing

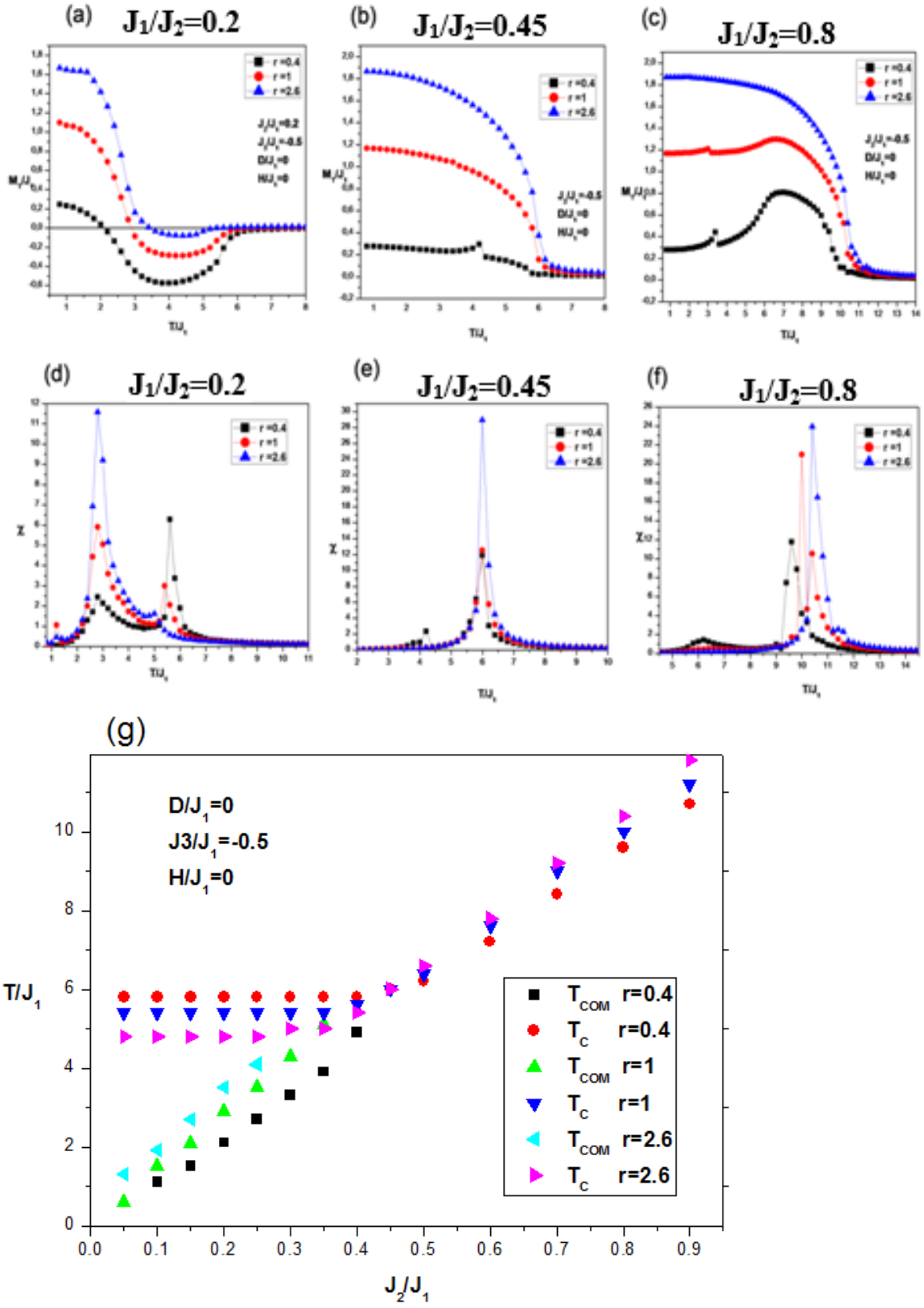

Figure 5.3: (a-c) Effect of the thickness ratio $r = \frac{t_\sigma}{t_S}$ on the temperature dependencies of the total magnetization M_T and (d-f) and magnetic susceptibility χ of the nanocube for $J_2/J_1 = 0.2$,0.45 and 0.8 , J_3/J_1 =-0.5, H/J_1 =0 and D/J_1 =0 (g) Phase diagram of the system in $(T_c, T_{com} - J_2/J_1)$ plane for $r = 0.4, 1$ et 2.6 for the same parameters.

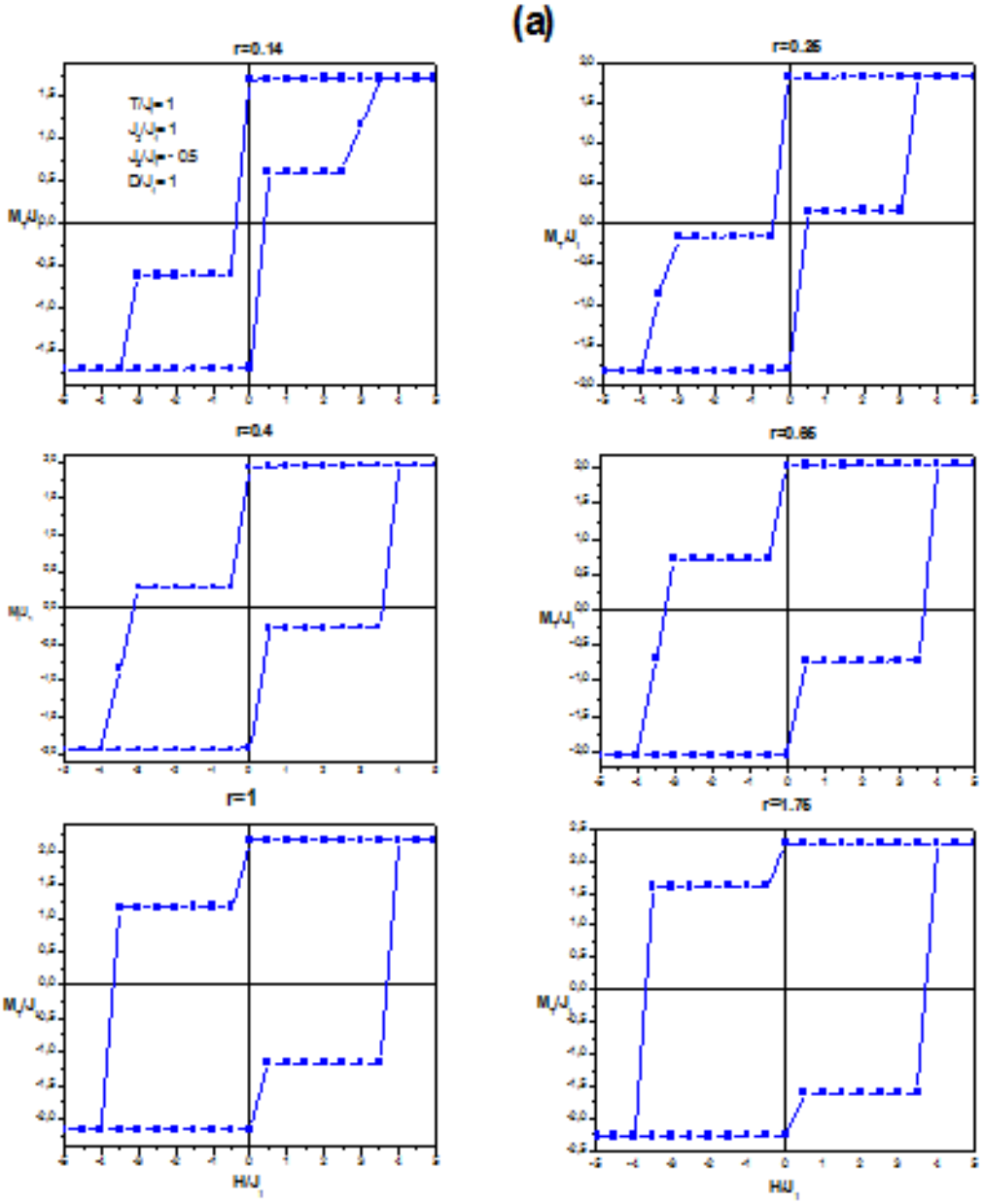
(a)
r=0.14
T/J1=1
J2/J1=1
J3/J1=-0.5
D/J1=1
r=0.25
r=0.4
r=0.86
r=1
r=1.75
H/J1

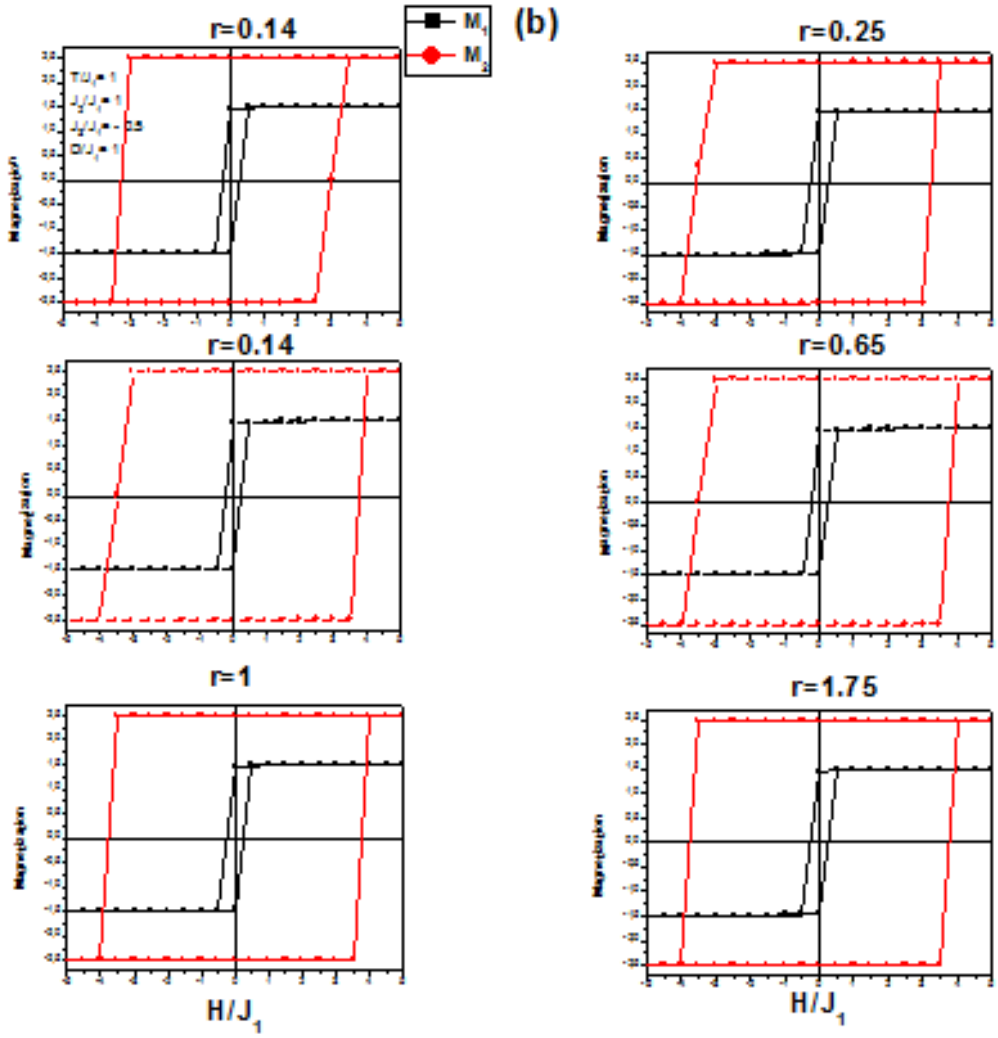

Figure 5.4: (a) Total (b) layer with spin-3/2 and layers with spin-5/2 magnetizations versus magnetic field calculated for different values thickness ratio r showing ferromagnetic hysteresis loops .

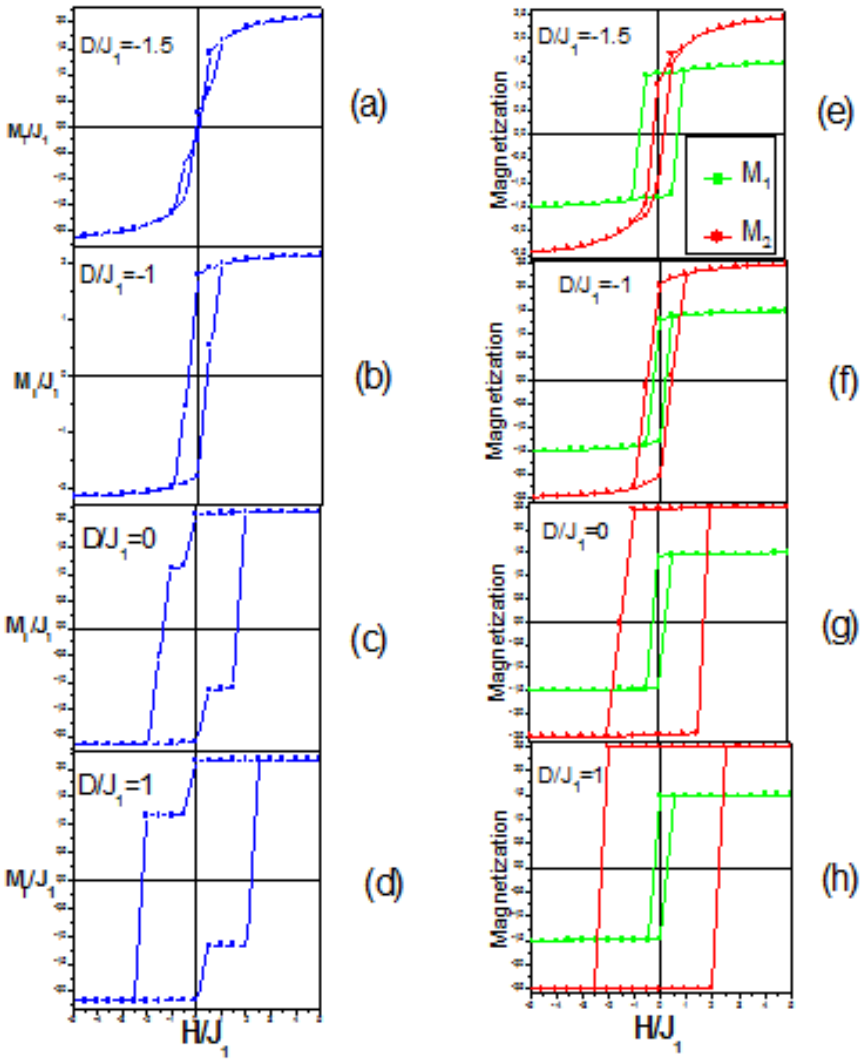

Figure 5.5: (a-d) Total(bleu line) , (e-h) both of layer with spin 3/2(green line) and layers with spins 5/2 (red line) magnetizations versus magnetic field calculated at T/J_1 =2 for different values of anisotropy parameter D/J_1 showing ferrimagnetic hysteresis loop.

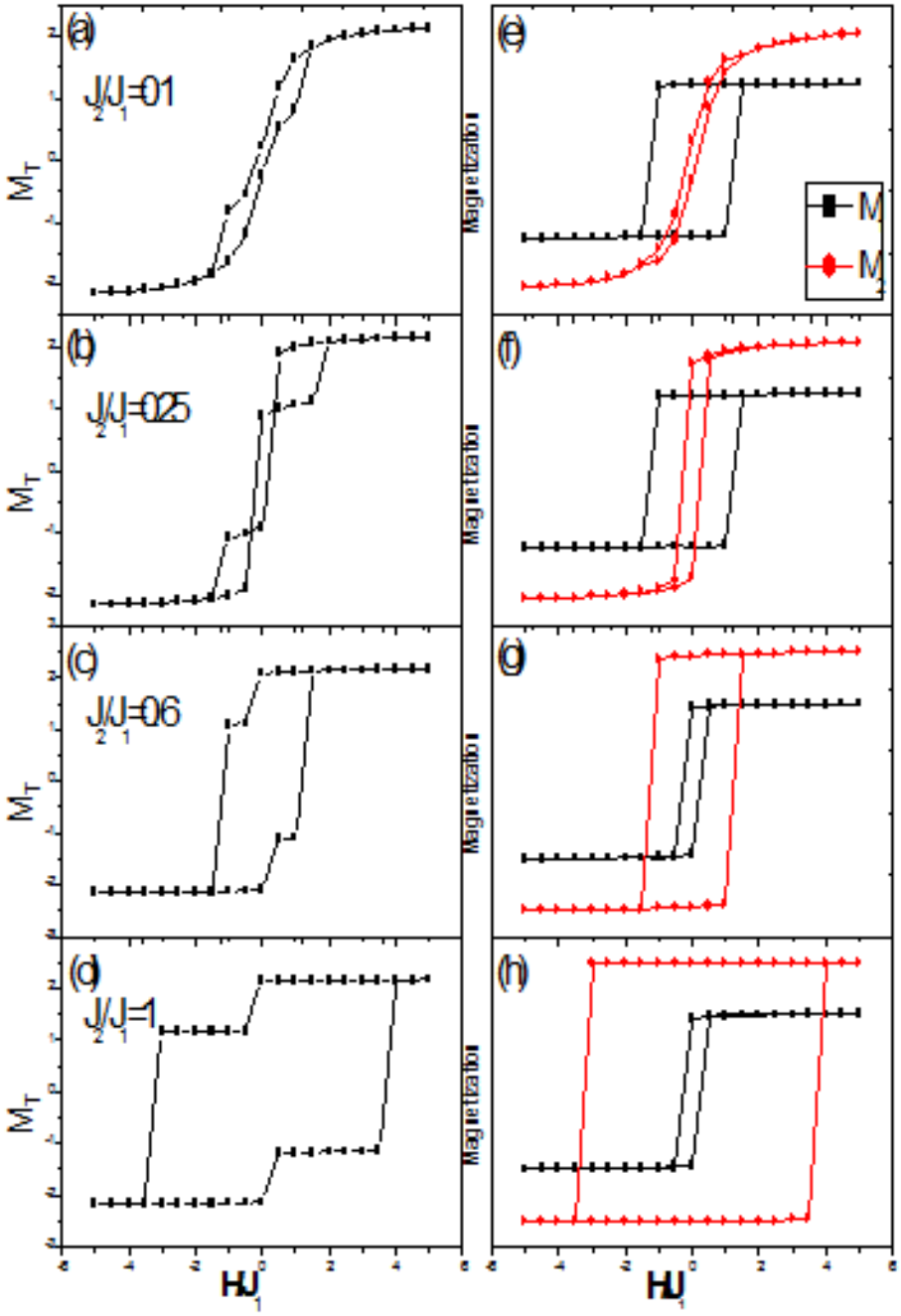

Figure 5.6: (a-d) Total(bleu line) , (e-h) both of layer with spin 3/2(green line) and layers with spins 5/2 (red line) magnetizations versus magnetic field calculated at T/J_1 =2 for different values of exchange coupling interaction J_2/J_1 showing ferrimagnetic hysteresis loop.

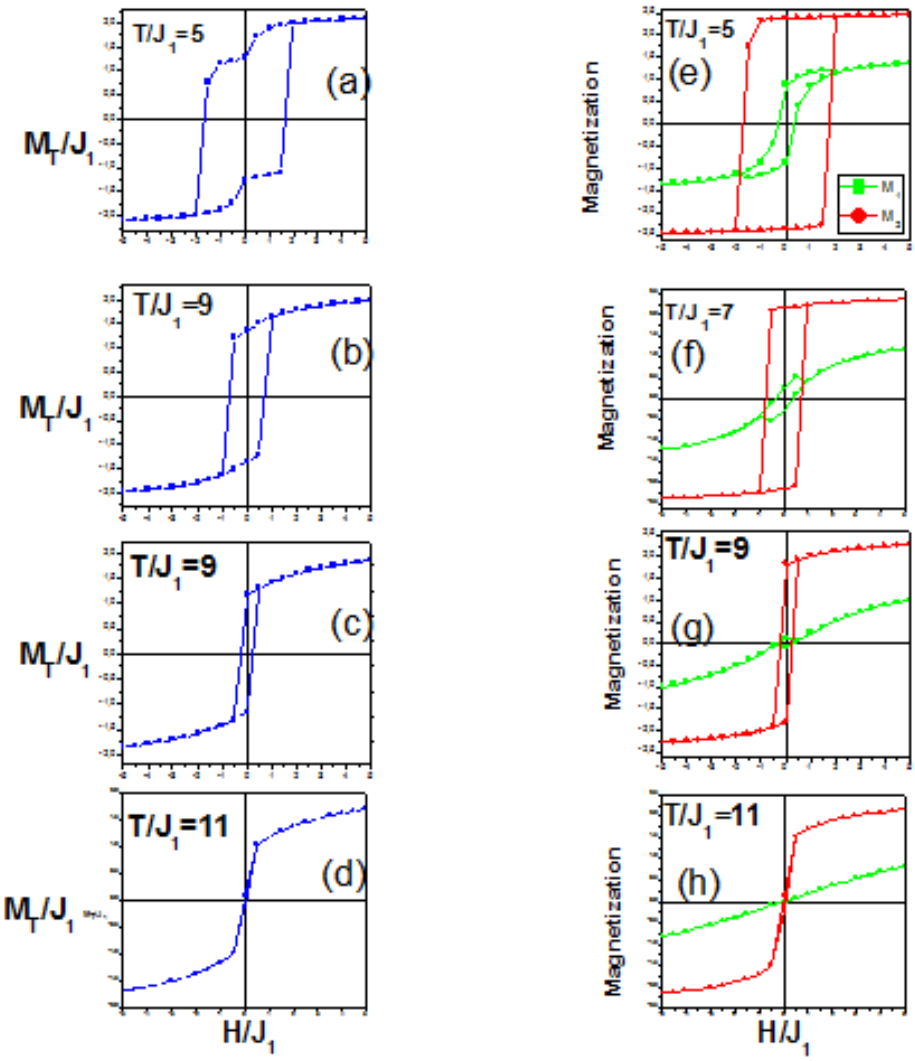

Figure 5.7: (a-d) Total (e-h) layer with spin 3/2 and layers with spins 5/2 magnetizations versus magnetic field calculated for different values of temperature T/J_1 showing ferromagnetic hysteresis loops.

J_2/J_1 from 0.1 to 1.0. that is The system may turn from the single hysteresis loop (J_2/J_1=0.1) into the triple hysteresis loops (J2/J1=0.25), conversely for the values of $J_2/J_1 > 0.25$ the hysteresis cycle of the system amounts to behaving in the same way as at the beginning it is to say: from the triple hysteresis loop ($J_2/J_1 > 0.25$) into the single hysteresis loops also magnetization plateaus begin to appear in the hysteresis loops. It can be seen that the total area of the hysteresis loops and remanence increase. Whereas the coercivity of the system first remain almost invariable from $J_2/J_1 = 0.1$ to 0.25, thereafter for ($J_2/J_1 > 0.25$) the coercivity exponentially increases.The obtained hysteresis loops are in a good agreement, quantitatively, with experimental results of FeCo alloy nanocubes reported by X. W. Wei [164]

Figure 5.7 shows the hysteresis loops for different values of T/J_1, when J_2/J_1 =1 , J_3/J_1=-0.5 and D/J_1=0 .We noticed that the coercive field decreases with the increasing of the reduced temperature ,from our simulated system, we found that the hysteresis loop may disappear at the reduced transition temperature (T/J_1=11), suggesting that the system expresses the supermagnetic phase. In Figure 5.7.(d,h) corresponding to T/J_1=11, it is clearly shown that the area of the hysteresis loop, the coercivity and the remanence decrease with increasing T/J_1, which is due to being weakened by the temperature. It is

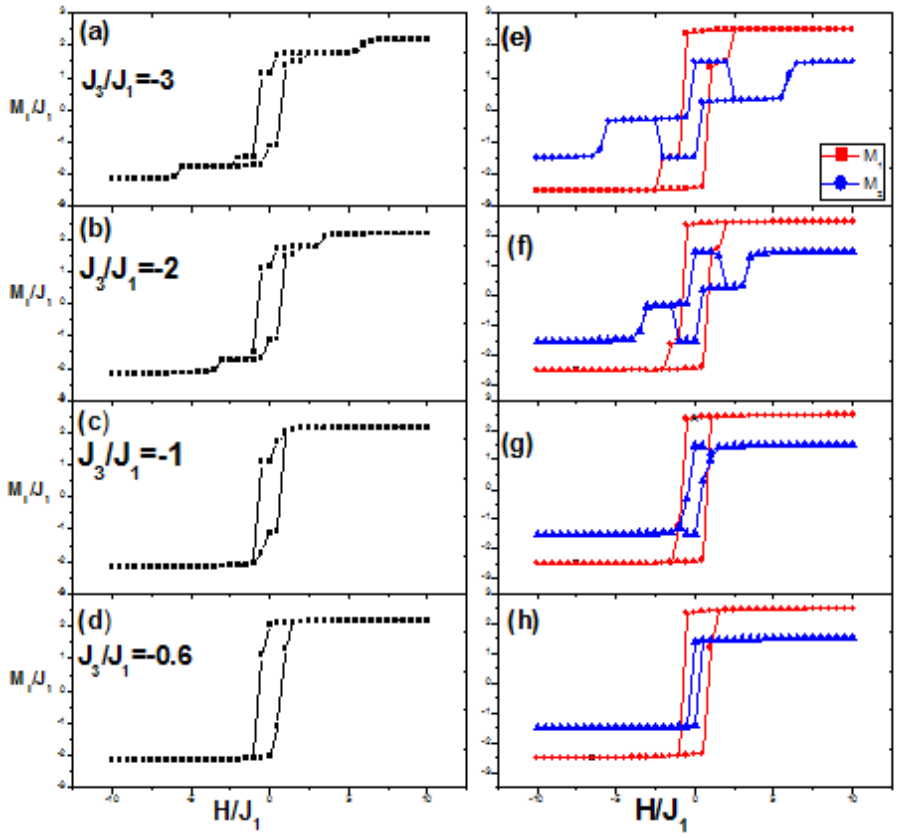

Figure 5.8: (a-d) Total (e-h) layers with spins 5/2 and layer with spin 3/2 magnetizations versus magnetic field calculated at $T/J_1 = 2$ for different values of inter layers exchange coupling interaction J_3/J_1 showing ferrimagnetic hysteresis loops .

worth mentioning that the hysteresis loop can express the step effect of low temperatures. For example, as shown in Figure 5.7 (a,e) corresponding to T/J_1=5, it can be noted the existence of magnetization plateaus in the hysteresis loops for different values of the external magnetic field T/J_1.

Figure 5.8 show the total and partial magnetization versus the applied external magnetic filed H/J_1 for different values of J_3/J_1 with fixed T/J_1=2 , D/J_1=-0.2, J_2/J_1=0.5 .Pour J_3/J_1 =-0.6 the partial magnetization hysteresis cycles show a ferromagnetic behavior even if the J_3/J_1 is negative. This returns to the competition between the ferromagnetic J_2/J_1 and the negative J_3/J_1 couplings. According to the coupling values, a barrier value of negative J_3/J_1, below this value the ferromagnetic behavior exists. To varying J_3/J_1 from -0.6 to -1 the loops of layers 5/2 retains the shape of a rectangle, but apart from -2 there is a slight change so that the cycle becomes shifted for layer it exhibits a single loop, but from J_3/J_1 = -2 it begins to form double loops under-triangles. This is due to the change of layers 1/2 states. We can say that the interlayer's interaction has an influence on layers 3/2 of middle more than those of 5/2.

5.4 Conclusion

We have studied a Single Ising nanocube system containing three alternated ferromagnetic layers .The studied system is described by spins (5/2;3/2;5/2). The interactions between pairs of spins of the same layer (L1-L1 or L2-L2 bonds) are ferromagnetic while the interactions between pairs of atoms of different layers ($S-\sigma$) are antiferromagnetic . The study is carried out through Monte Carlo simulations. We have investigated the magnetic and thermodynamic properties the system.the effects of anisotropy parameter

D/J_1 , temperature T/J_1 , inter layers exchange coupling interaction J_3/J_1 and exchange coupling interaction J_2/J_1 on the hysteresis loops are deterimned. We verified the occurrence of a compensation phenomenon and determined the compensation temperatures, as well as the critical temperatures of the model for a range of values of the Hamiltonian parameters and thickness ratio r. We present phase diagrams and a detailed discussion about the conditions for the occurrence of the compensation phenomenon. Our results are in a good agreement, quantitatively, with some theoretical and experimental results.

Chapter 6

Case of assemblies systems of nanocubes

6.1 Ferromagnetic Nanoparticles of Ising Spin-1 with a Rubik's Cube Structure: Monte Carlo Simulations.

6.1.1 Introduction

In recent years, magnetic nanostructure systems such as nanocubes [2, 3, 165, 166], nanodots [167–169], nanofilms [170], nanowires [105, 171–173], dendrimers [174–177], nanotubes [178, 179], and nanospheres [180] attracted the interest of researchers whether they are theoreticians or experimenters. This growing interest in these systems is mainly due to the importance given to the nanotechnologies and industrial applications in the following domains: information storage [27, 28], biomedical applications [181–183], shielding [184], sensors [185], permanent magnets [135], and magnetoresistive devices [186]. However, many theoretical studies have been devoted to investigating the magnetic properties of various types of magnetic nanoparticle systems mentioned above by using different types of methods such as Monte Carlo (MC) [143, 144, 144, 145], mean field approximation (MFA) [187, 188], effective field theory (EFT) [106, 189, 190], Green function formalism [191], cluster variation method (CVM) [192, 193], or micromagnetic simulations [147].

Nanocubes as one of the different shapes of nanoparticles have attracted an important part of theoretical and experimental studies. Nevertheless, more researches have been devoted to the synthesis of cubic nanoparticles with several methods during the last few years such as (iron/iron oxide core/shell [194], wustite-spinel (core)/(shell) [195], Fe [196], $Fe1-xO\ /Fe_{3-\delta}O_4$ (core/shell) [197], and Ni [198] CoxFe3-xO4 [199] Ag [200, 201].

Moreover, the spin systems permit the representing of these molecular materials in simple 2D or 3D models in order to study them theoretically by the aforementioned methods. In this connection, several studies on nanocubic spin systems have been carried out, but particularly on single nanoparticles. Due to the size of these nanosystems, several unusual thermal and magnetic properties which appear different from those of bulk systems have been obtained.

For the present work, its singularity is to study a spin-1 ferromagnetic 3D (multi-nanoparticles) system composed of several nanocubes under the form of a Rubik's cube. From this structure, interesting magnetic properties comparable to those observed in magnetic nanoparticles with dipolar interactions and non-collinearity of spins have emerged. These phenomena are due to the size effects. The outline of the remaining parts of this work is as follows: In Section 2, we describe the Hamiltonian model and the method used. In Section 3, we present results and discussions. Finally, in Section 4, we present the conclusion.

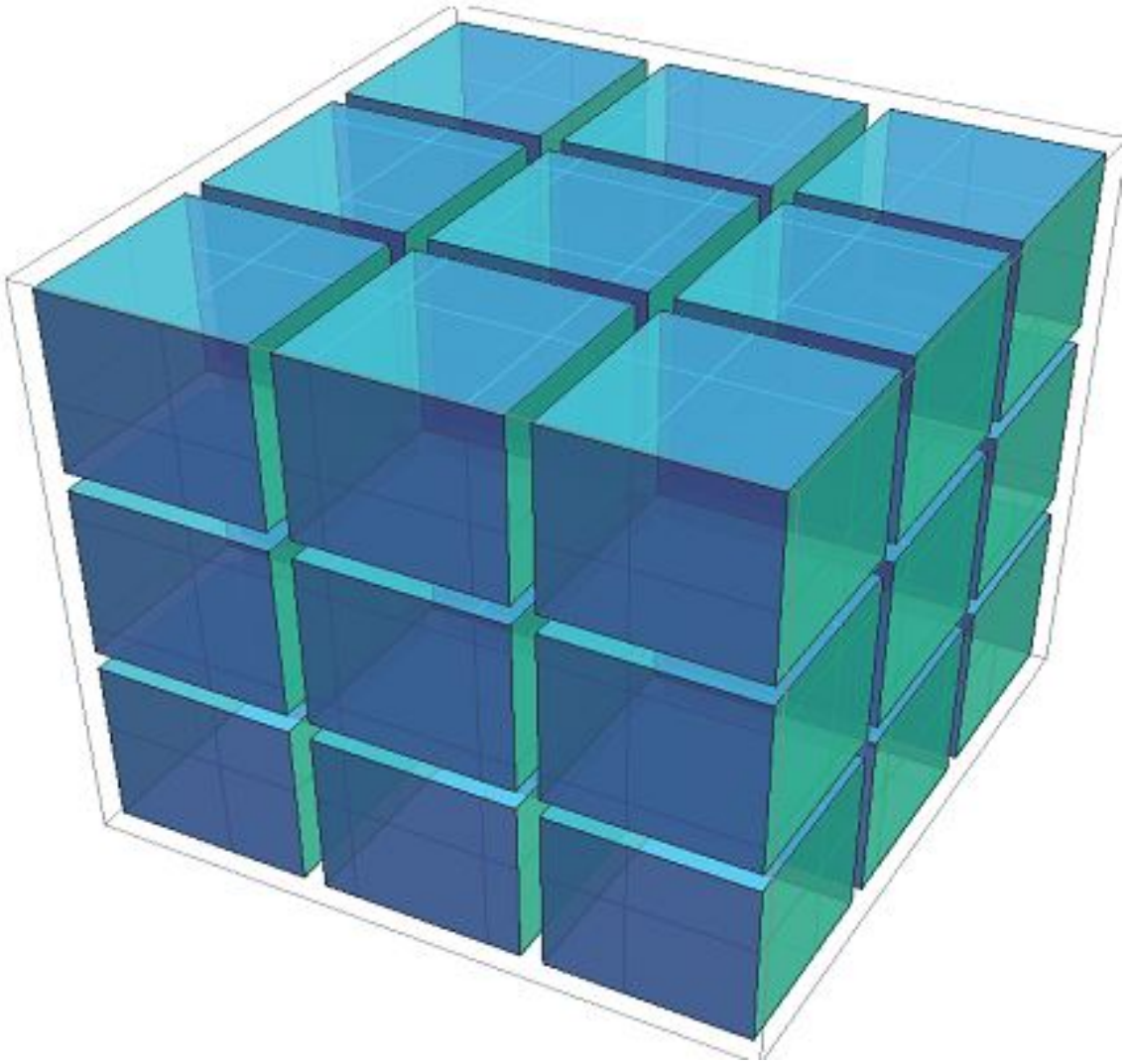

Figure 6.1

6.1.2 Theoretical model and method

Here, we considered the Rubik's cube as the structural model for the studied system. As shown in Figures 6.2.a, the model contains nidentical nanocubes of size Lnc grouped in a cubic nanosystem of size Lc. Each nanotube is described by mcoupled spins $S = 1$ which are assumed to interact ferromagnetically inside nanocubes as well as between two adjacent nanocubes (see Figure 6.2.b). The Hamiltonian which governs the system studied is expressed by:

$$\mathcal{H} = -J_1 \sum_{\langle i,j \rangle} S_i S_j - J_2 \sum_{\langle l,f \rangle} S_l S_f - \Delta \sum_i (S_i)^2 + H \sum_{\langle i \rangle} S_i \tag{6.1}$$

Where S_i and S_j are nearest-neighbor spins of sites i and j while S_l and S_f denote the nanocube side-last spin and the side-first spin of the following adjacent nanocube, respectively. J_1 and J_2 are exchange couplings between nearest neighbors, respectively, of spins belonging to a nanocube and of consecutive adjacent nanocubes in any direction x, y, or z. Δ is the magnetic anisotropy parameter, and H is the external magnetic field acting over all spins S_i. We solved numerically the Hamiltonian (6.1) in order to investigate the size effects and magnetic properties in the ferromagnetic nanoparticles of Ising

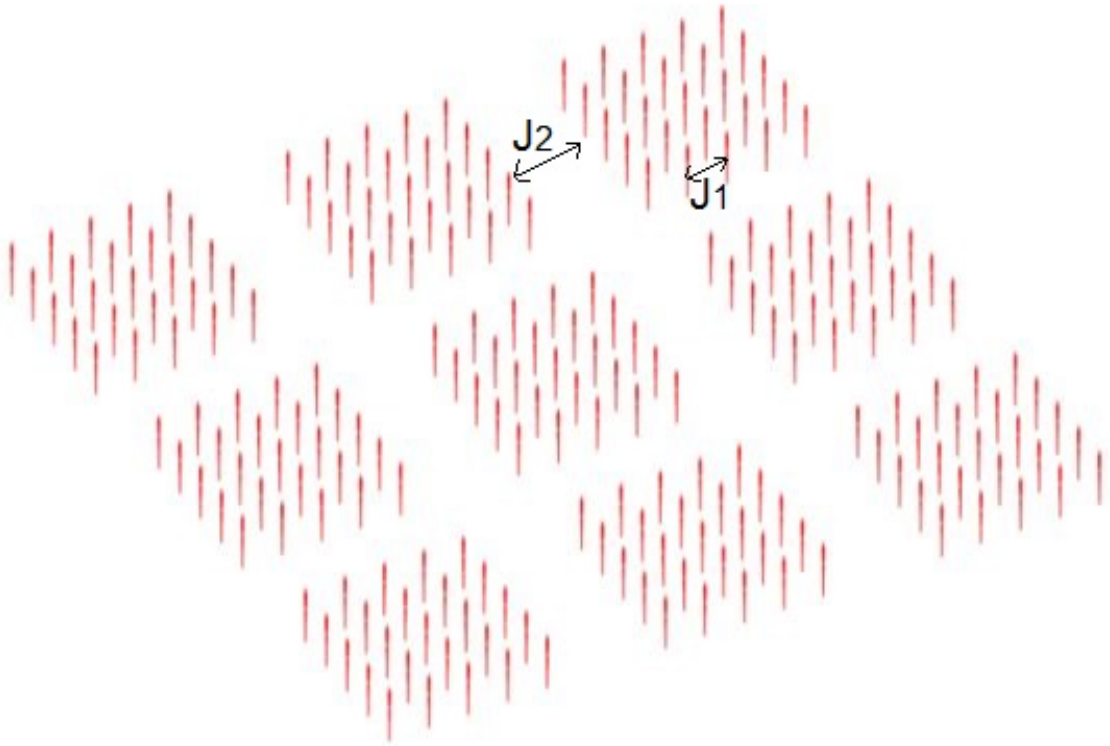

Figure 6.2: a) Rubik's cube as a group of identical nanocubes. b) Ferromagnetic arrangement in nanocubes

spin-1. For a theoretical study, we used in the following normalized parameters $\rho = J_1/J_2$, $\delta = \Delta/J_2$, and $h = H/J_2$.

To compute thermodynamic quantities, we have used the Metropolis algorithm in the context of the Ising model. We have considered the system lattice with free boundary conditions and performed the simulation for different lattice sizes. The program was turned long enough, and the equilibrium was reached after 12.10^5 MC steps per site. The total magnetization is expressed by:

$$M = \frac{1}{N} \mid \sum_i S_i \mid \tag{6.2}$$

Where $N = (n * m)$ is the total number of spins in all the lattice.

The magnetic susceptibility is given as:

$$\chi = \frac{N}{K_B T}(\langle M^2 \rangle - \langle M \rangle^2) \tag{6.3}$$

K_B is the Boltzmann's constant set to unity.

The relation links the magnetization and the susceptibility:

$$\chi = \frac{\partial M}{\partial H} \mid_{H=0} \tag{6.4}$$

H is the external magnetic field.

6.1.3 Results and discussions

In this section, we present the results of our work, which consists of the study of size effects and magnetic properties of the ferromagnetic nanosystem of spin-1. We have first investigated system parameter effects on the phase diagrams for different sizes of the lattice. Then, we have analyzed the hysteresis loops behavior. Finally, we have studied the size effects on the coercive field. The quality of the results obtained is largely attributed to the nature and structure of the studied system.

To show the effects of the system parameters on magnetic stability regions where spins are ordered, we present two types of phase diagrams in the $(L_{nc}, t_c = T_c/J_2)$, (L_c, t_c), and (δ, t_c) planes. From Eq. (3), we plotted the reduced critical temperature tc as functions of Lnc and L_c, respectively, for varying ρ and as a function of δ. In Figures 6.3, the phase diagram $L_{nc} - t_c$ is plotted for selected values $\delta = 0.1$ and $h = 0.0$ with sizes $L_c = 3$ and $L_{nc} = 3, 4, 5, 6$, and 7. The variation of the critical temperature displays a dual behavior due to the competition between the reduced exchange coupling effect and the size effect of nanocubes. First of all, we can see that for $\rho > 0.63$, the reduced critical temperature increases proportionally both to the exchange coupling and the nanocube size, which is a characteristic feature of ferromagnetic nanoparticles. However, for $\rho > 0.63$, the reduced critical temperature increases with the exchange coupling but decreases when the nanocube size increases. At $\rho = 0.63$, the size effect is blocked; the reduced critical temperature is constant for any nanocube size. The linear fits denote the set of critical points of second-order phase transitions. Thus, we show in Figures 6.4 the magnetic susceptibility versus the temperature for $\rho = 0.63$, $\delta = 0.1$, and $h = 0.0$ with sizes $L_c = 3$ and $L_{nc} = 3, 4, 5, 6$, and 7. It is found that the peak of the susceptibility increases with the nanocube size, giving the critical temperature $t_c = 21.20$ which agrees with Figures 6.3. The phase diagram $L_c - t_c$ in Figures 6.5 representing the variation of the reduced critical temperature as a function of the total nanosystem size is plotted for $\delta = 0.1$, $h = 0.0$, and $\rho = 0.4, 0.5, 0.6, 0.7, 0.8$, and 0.9 with sizes $L_{nc} = 3$ and $L_c = 2, 3, 4$, and 5. In spite of ρ values around 0.63, the increase of the reduced exchange coupling and the nanosystem size

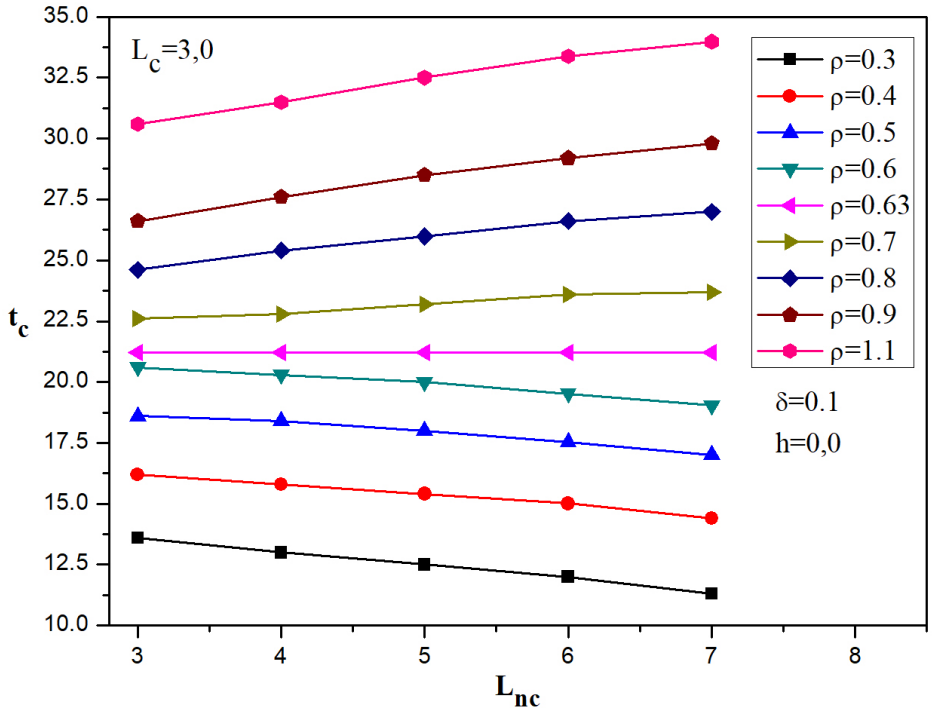

Figure 6.3: Reduced critical temperature as a function of the nanocube size for different values of the exchange coupling ρ. The constant linear fit corresponds to $\rho = 0.63$

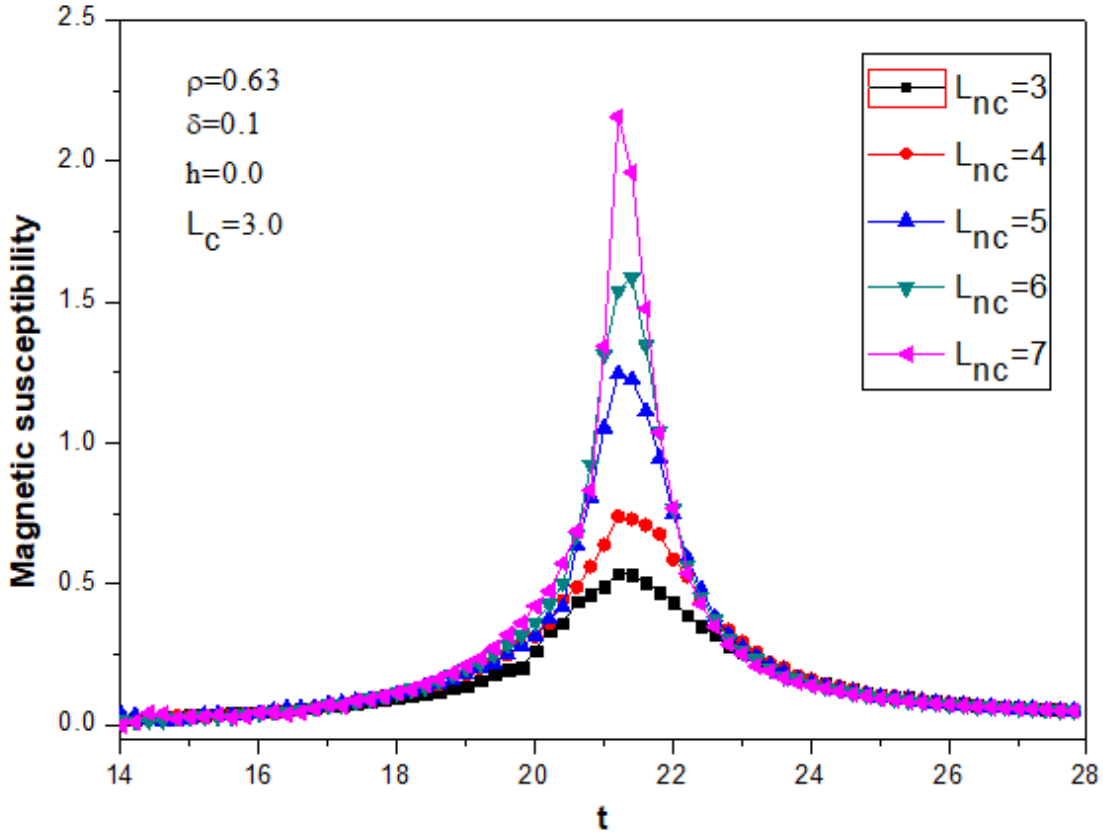

Figure 6.4: Magnetic susceptibility versus the reduced temperature for $\rho = 0.63$, $\delta = 0.1$, and $h = 0.0$ with sizes $L_c = 3$ and $L_{nc} = 3, 4, 5, 6$, and 7

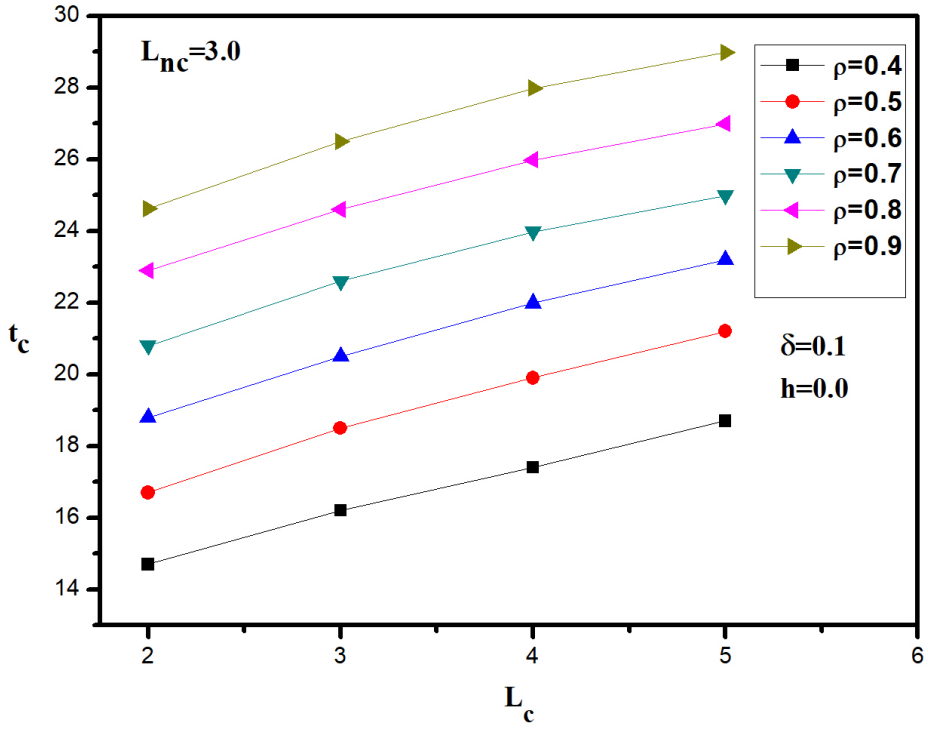

Figure 6.5: Reduced critical temperature as a function of the nanosystem size L_c for different values of the exchange coupling around $\rho = 0.63$

induces one of the reduced critical temperatures simultaneously, meaning that contrary to the first case, the nanosystem size effect does not compete with the reduced exchange coupling effect. These two effects favor the extension of the magnetic stability region.

The effect of the reduced magnetic anisotropy is presented in the diagram of the (δ, t_c) plane, where the dependence of the critical temperature to δ is brought out (Figures 6.6) for parameters $\rho = 0.1$ and $h = 0.0$ with selected sizes $L_c = 3$ and $L_{nc} = 3$ and 5. We can see that the critical temperature increases when δ increases from negative to positive values. Critical temperatures are lightly higher for $L_{nc} = 3$ than for $L_{nc} = 5$ in agreement with Figures 6.3 and Figures 6.5. Otherwise, they are lower and constant for negative low values of the reduced magnetic anisotropy; this phenomenon was observed before in another work [199]. The set represents a fit of second-order phase transition points, while in the present case, we did not observe first-order transition lines but, according to references [199], they can be predicted for the studied nanosystem.

Now, we apply an external magnetic field and we investigate the hysteresis loops for selected low values of the temperature. Thus, we show first in Figures 6.7 the total magnetization versus the reduced magnetic field for $t = 0.1, 0.3$, and 0.5. It is found that the response of the magnetization to the magnetic field shows hysteresis behaviors with single loops where the reduced magnetic coercive field gets thinner till it disappears when moving from $t = 0.1$ to $t = 5$. This behavior reveals the dependence of the coercive field in terms of the critical temperature and was also found in previous works [49–51]. Then, we have investigated size effects on the coercive field when setting the temperature to $t = 0.3$. For this purpose, we present two graphs in Figure 6.8 showing the variation of the coercive field, respectively, as a function of the nanocube size, L_{nc} (Figure 6.8).a) and the nanosystem size, L_c (Figure 6.8.b). For the first case, we have found a continuous increase of the coercive field when the nanocube size decreased, with a constant sequence between nanocube sizes 5 and 6. This is similar to a multi-domain state of magnetic nanomaterials with dipolar interactions [199,202,203]. However, for the second case, when fixing

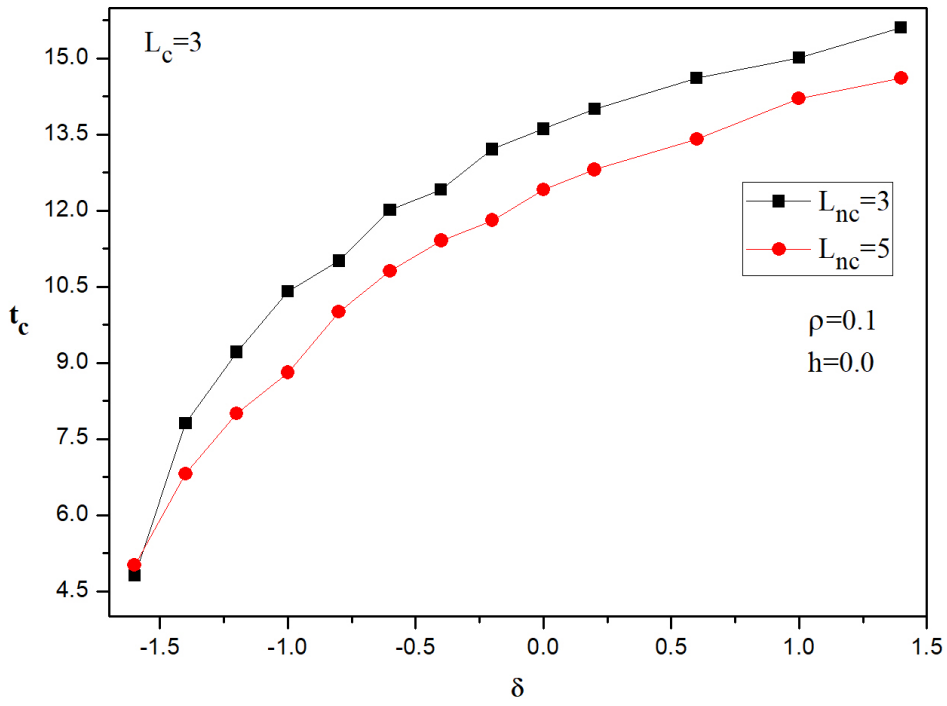

Figure 6.6: Reduced critical temperature versus the reduced magnetic anisotropy $\delta = \Delta/J_1$ for sizes $Lc = 3$ and $L_{nc} = 3$ and 5

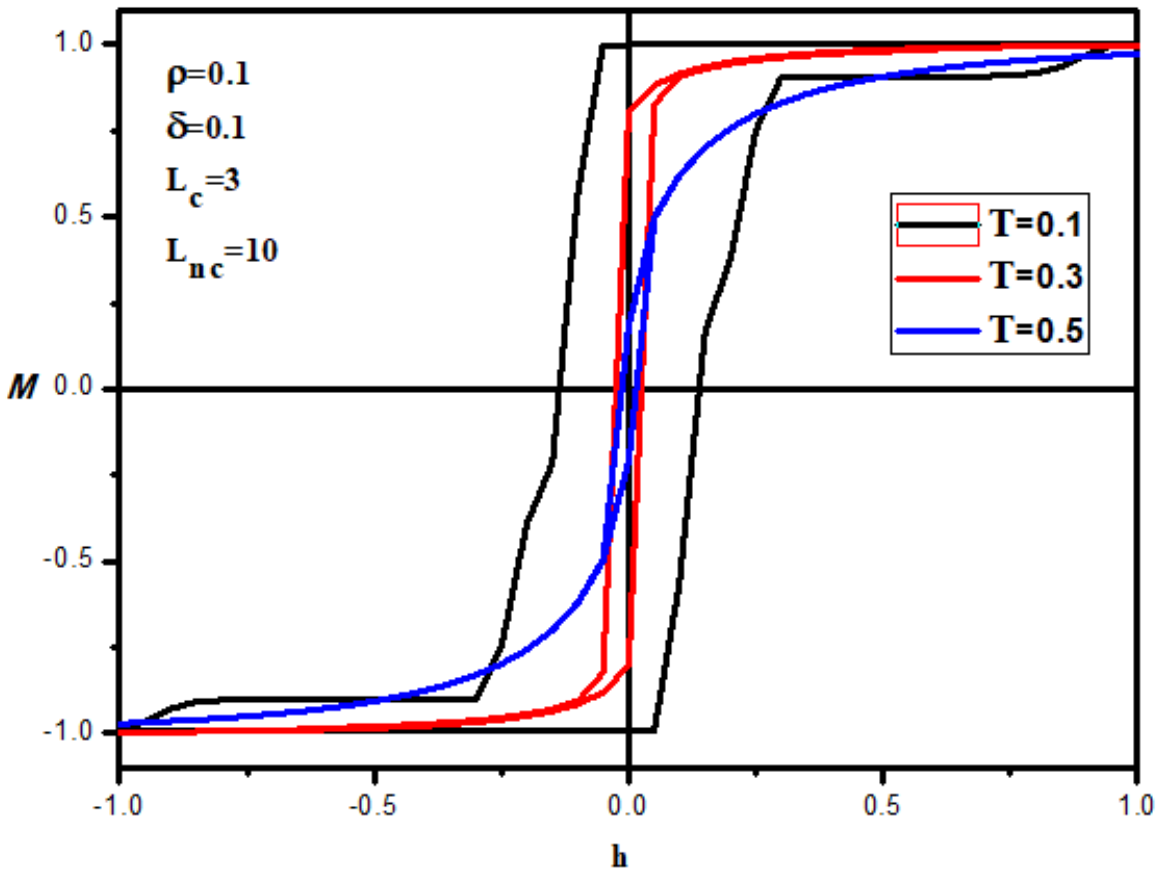

Figure 6.7: Total magnetization versus the reduced external magnetic field for $\rho = 0.1$, $\delta = 0.1$, $L_c = 3$, and $L_{nc} = 10$

the nanocube size to $L_{nc} = 3$ and decreasing the nanosystem size from $L_c = 10$ to $L_c = 2$, we observe a coercivity behavior which increases up to a maximum reaching at $L_c = 4$ and then decreases. But now, this situation reminds the conversion from a multidomain state to a single-domain state observed in magnetic nanomaterials. Note that a like superparamagnetic phase was not found at low nanosystem sizes. We assume that these phenomena are due to the Rubik's cube structure and to the nanometric character of the studied system.

6.1.4 Conclusion

In this work, we have studied size effects on magnetic properties of the ferromagnetic nanoparticles of Ising spin- 1 by using Monte Carlo simulation with the Ising model. The studied system has the particularity to be a Rubik's cube consisting of identical nanocubes. It has been shown that phase diagrams depend on the system parameters and are affected as well as by the nanosystem size than only by the nanocube size. Indeed, depending on the reduced exchange coupling, two regimes have been observed where the reduced critical temperature decreases and increases, respectively. Moreover, the variation of the coercive field as a function of sizes has shown a well-known phenomenon of magnetic nanomaterials with dipolar interactions, where the coercive field increases, reaches a maximum, and then decreases to zero with decreasing nanoparticle size. However, in our case, we have not found the coercive field reduced to zero for low sizes. We attributed these phenomena to the structure and the nature of our system.

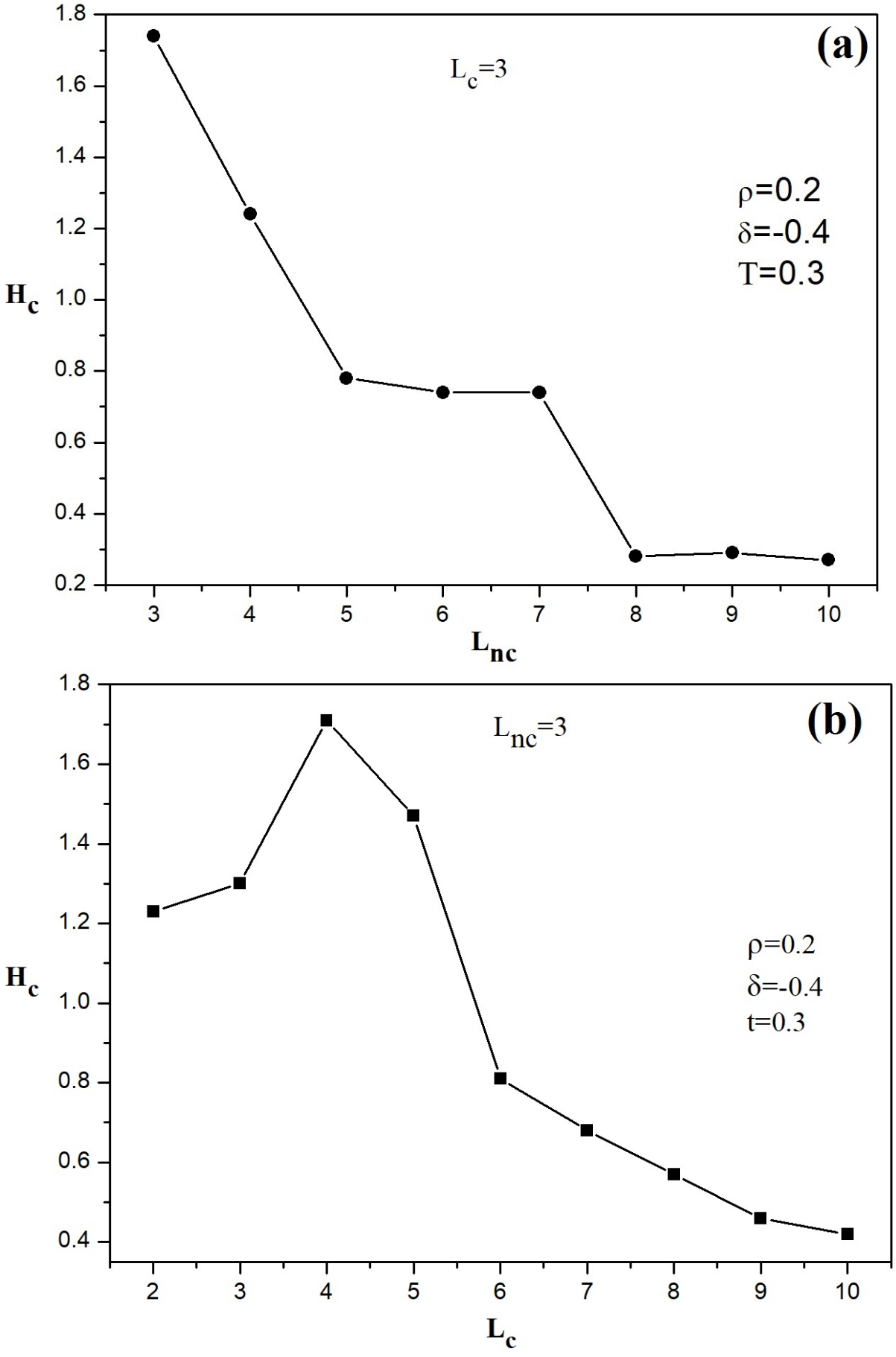

Figure 6.8: Coercive field versus sizes: a) of the nanocubes L_{nc} , b) of the nanosystem (Rubik's cube) L_c

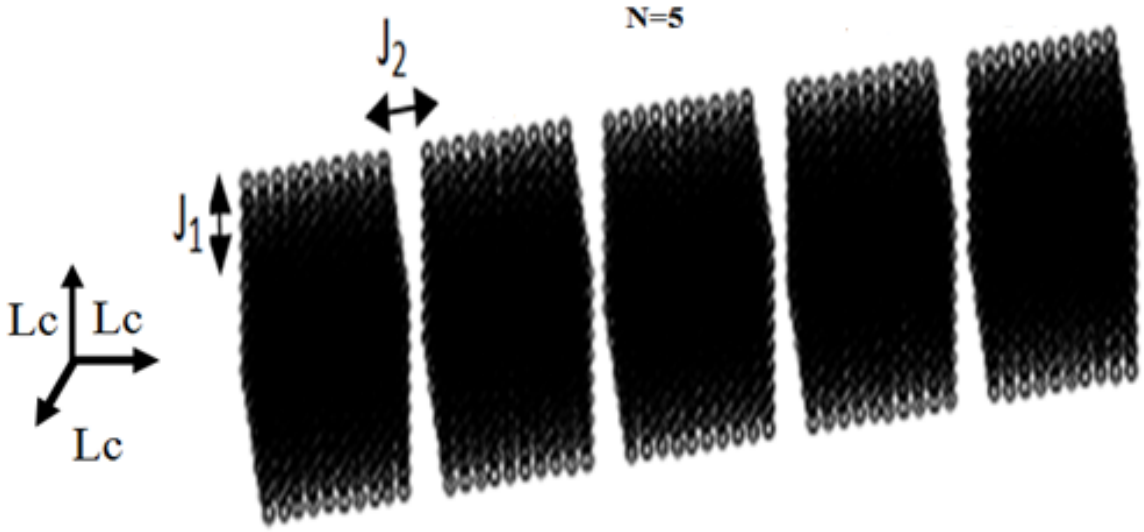

Figure 6.9: Schematic representation of a nanocubic Chain Model with magnetic moment spin $S = 1$ and the number of cube equal $N = 5$ the size of cube $(Lc * Lc * Lc)$

6.2 Magnetic properties of Nanocubic Chain Model (NCCM): Monte Carlo Study.

6.2.1 Introduction

Magnetic nanoparticle assemblies have been the subject of immense scientific activity over the last decade [120, 204, 205]. Magnetic nanoparticles have interesting properties in the scientific world, especially in the area of Spintronics and new technology- namely magnetic storage media and memory devices [206–209]. The importance of the magnetic nanoparticle is attributed to the fact that they represent a critical link between current technologies and future applications, due to their small size, large surface-to-volume ratio and size-dependent properties like superparamagnetism [210]. Today's focus has shifted towards biomedical applications and functional materials [211–213]. From the view point of biophysics, magnetic particles can be considered as a model system for studying the polar organization of microtubules or generate spontaneous helical superstructures reminiscent of DNA molecules [214–216].
The experimental and theoretical studies have done recently in this area of magnetic. Messina, R. et al., they are shown that the attraction and assembly of parallel magnetic chains is the result of a delicate interplay of dipole–dipole interactions and short range excluded volume correlations [217]. Material engineering and emerging applications in lithography and biomedicine are studied by Yuping Bao et al., they are concluded with a succinct discussion of the pharmacokinetics pathways of iron oxide nanoparticles in the human body-an important and required practical consideration for any in vivo biomedical application, followed by a brief outlook of the field [218]. Synthesis, alignment, and magnetic properties of monodisperse Nickel nanocubes are treated by Alec P et al., they are established that the nickel nanocubes have over 4 times enhancement in magnetic saturation compared to spherical superparamagnetic nickel nanoparticles [198].
Herein we reported the magnetic properties of NCCM via The Monte Carlo study. Thank to this method we achieved a several results like: the critical temperature, the effect of the anisotropy on the magnetization, the impact of the temperature and anisotropy on hysteresis loop.
The organization of this work is as follows: in section 2, we presented the model and method. Results are shown and discussed in section 3. The final section is reserved for all in all (conclusion).

6.2.2 Theoretical model and method

This section is devoted to present the model of our system and the method used for determine the magnetic properties of NCCM. First of all, we have considered the NCCM as displayed in Figure 6.9. Each site on the figure is occupied by an Ising spins $S = 1$. The interaction in the cube is expressed by J_1, and the interaction between two cubes is noted by J_2. The Hamiltonian was described this CCM was given by this equation:

$$\mathcal{H} = -J_1 \sum_{\langle i,j \rangle} S_i S_j - J_2 \sum_{\langle i,j \rangle} S_i S_j - \Delta \sum_{i=1}^{N} (S_i)^2 - H \sum_{i=1}^{N} (S_i) \tag{6.5}$$

This Hamiltonian is composed of the following parameters: $\langle i, j \rangle$ correspond to the closest neighbors between $S_i - S_j$. J_1 and J_2, which are the parameters of the equation, represent the exchange coupling in the cube and inter-cubes or between cubes respectively, Δ denotes an anisotropy applied on all the system spins as well as H stands for an external magnetic field.

This subsection treats also the method employed for establishing the magnetic properties of the CCM. We applied a standard sampling method to simulate the Hamiltonian given by (6.5) who is Monte Carlo Simulations with the application of Metropolis algorithm. Cyclic free conditions on the lattice were imposed and were generated by sequentially traversing the lattice and making single-spin flip attempts. The acceptation or rejection is made according to a heat-bath algorithm under the Metropolis approximation. Our data was established with 10^6 Monte Carlo steps per spin, discarding the first 10^4 Monte Carlo steps. Starting from different initial conditions, we executed the average of each parameter and estimate the Monte Carlo simulations, averaging over many initial conditions. Our program calculates the following parameters, namely:
The internal energy per site is determined as:

The magnetization per site is determined as:

$$M = \frac{1}{N} \mid \sum_{i} S_i \mid \tag{6.6}$$

Where N is the total number of spins in all the lattice.

The magnetic susceptibility is given as:

$$\chi = \frac{N}{K_B T} (\langle M^2 \rangle - \langle M \rangle^2) \tag{6.7}$$

K_B is the Boltzmann's constant set to unity.

The relation links the magnetization and the susceptibility:

$$\chi = \frac{\partial M}{\partial H} \mid_{H=0} \tag{6.8}$$

H is the external magnetic field.

6.2.3 Results and discussions

The goal set behind this section is to study and elaborate the magnetic properties of the NCCM by The Monte Carlo study. We analyzed and treated the magnetic properties of the NCCM. We used,

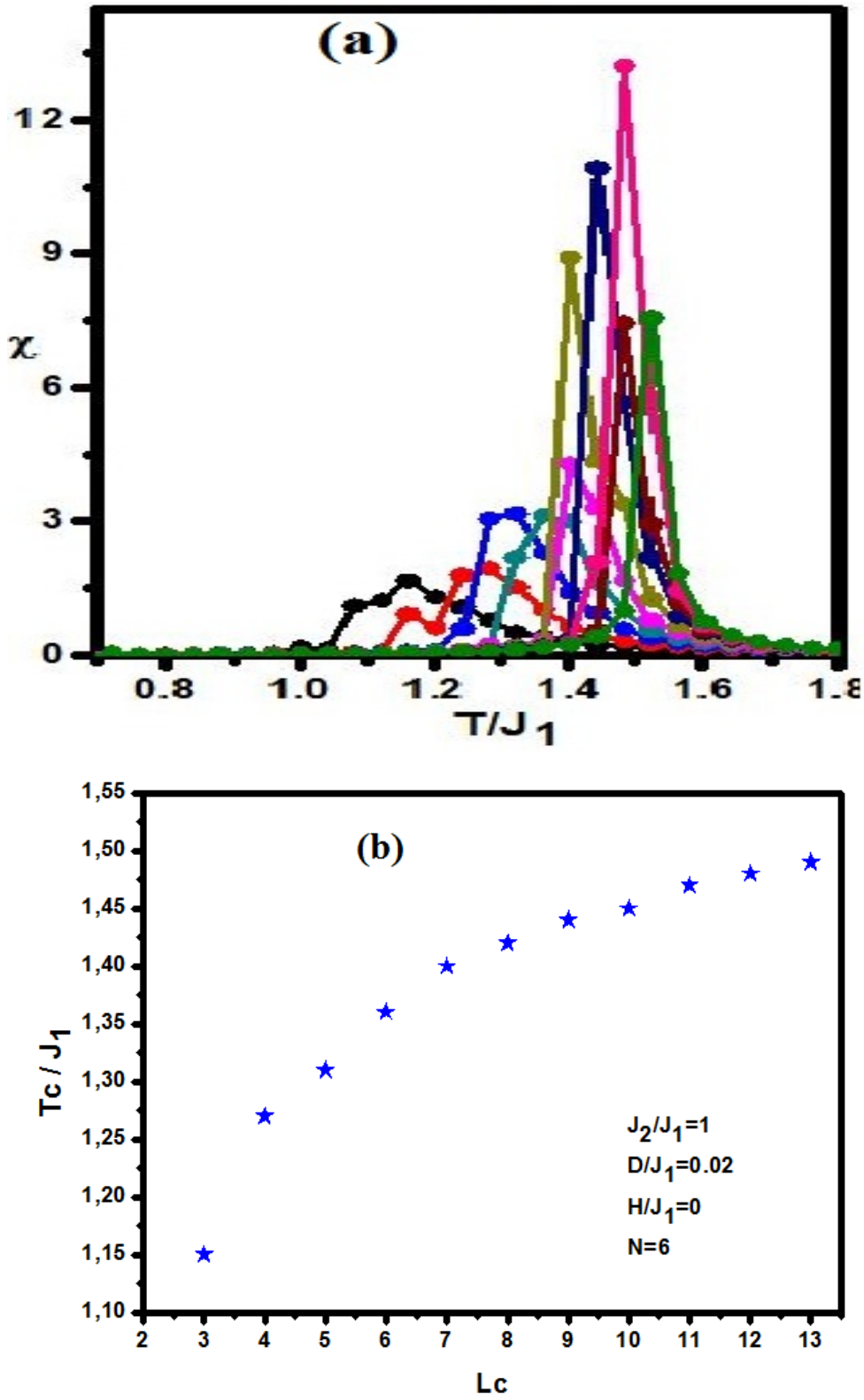

Figure 6.10: (a) Magnetic susceptibility as a function of temperature for various cube size: $Lc = 4, 5, 6, 7, 8, 9, 10, 11, 12$ and 13, in (b) the reduced transition temperature as a function of cubic size for $J_2/J_1 = 1$, $\Delta/J_1 = 0.02$ and $N = 6$.

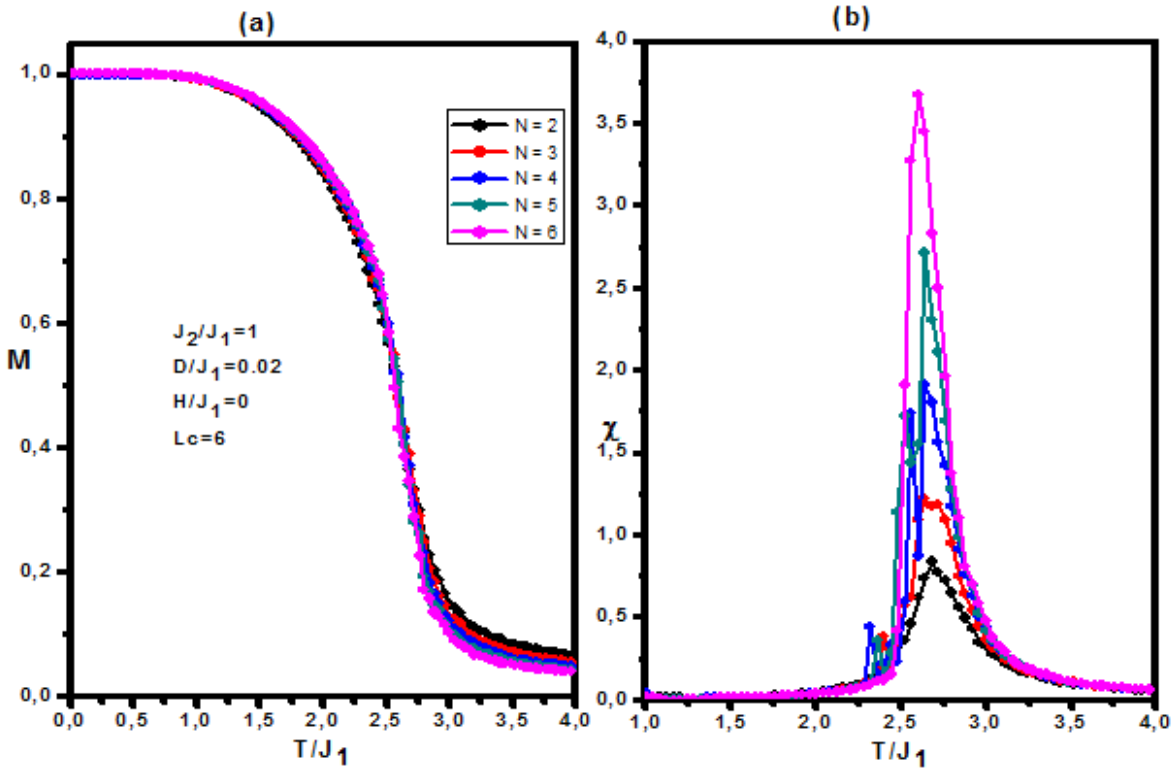

Figure 6.11: Magnetization in (a) and magnetic susceptibility in (b) as a function of temperature for various cube number:$N = 2, 3, 4, 5$ and 6 for $J_2/J_1 = 1$, $\Delta/J1 = 0.02$ and $Lc = 6$.

J_2/J_1,T/J_1, Δ/J_1 and H/J_1 as the reduced parameters. By this method, we achieved several results are given in the following paragraphs.

Figure 6.10(a) illustrated the variation of the magnetic susceptibility as a function of the temperature for the different values of the cube size ($Lc = 3, 4, 5, 6, 7, 8, 9, 10, 11, 12$ and 13) with the reduced exchanges coupling ($J_2/J_1 = 1.0$), the reduced anisotropy ($\Delta/J_1 = 0.02$) and the number's cube ($N = 6$). From this figure, we noticed that the effect of cube size on the magnetization is observed. In other words the reduced transition temperature increases when the size of NCCM increases. On the other side, the all magnetic susceptibilities are situated at the reduced transition temperature Tc/J_1 as presented in the table below (Table:6.1). We can say that this system belongs to the second order transition family because we observed the continuity of the magnetization at transition temperature.

Size	3	4	5	6	7	8	9	10	11	12	13
Tc/J_1	1.15	1.27	1.31	1.36	1.4	1.42	1.44	1.45	1.47	1.48	1.49

Table 6.1: The variation of reduced transition temperature versus cube size

From the Figure 6.10.(c), we observed that the reduced transition temperature increases with the increases of size as said before.

Figure 6.11(a-b) presented the variation of total magnetization and magnetic susceptibility as a function of the temperature for the different values of cube number ($N = 2, 3, 4, 5$ and 6) with the reduced exchanges coupling ($J_2/J_1 = 1.0$), the reduced anisotropy ($\Delta/J_1 = 0.02$) and the cube size ($Lc = 6$). We concluded that the impact of cube number on the magnetization is not observed. In other words, the all magnetic susceptibilities are situated at same the reduced transition temperature even if the number's cube increases.

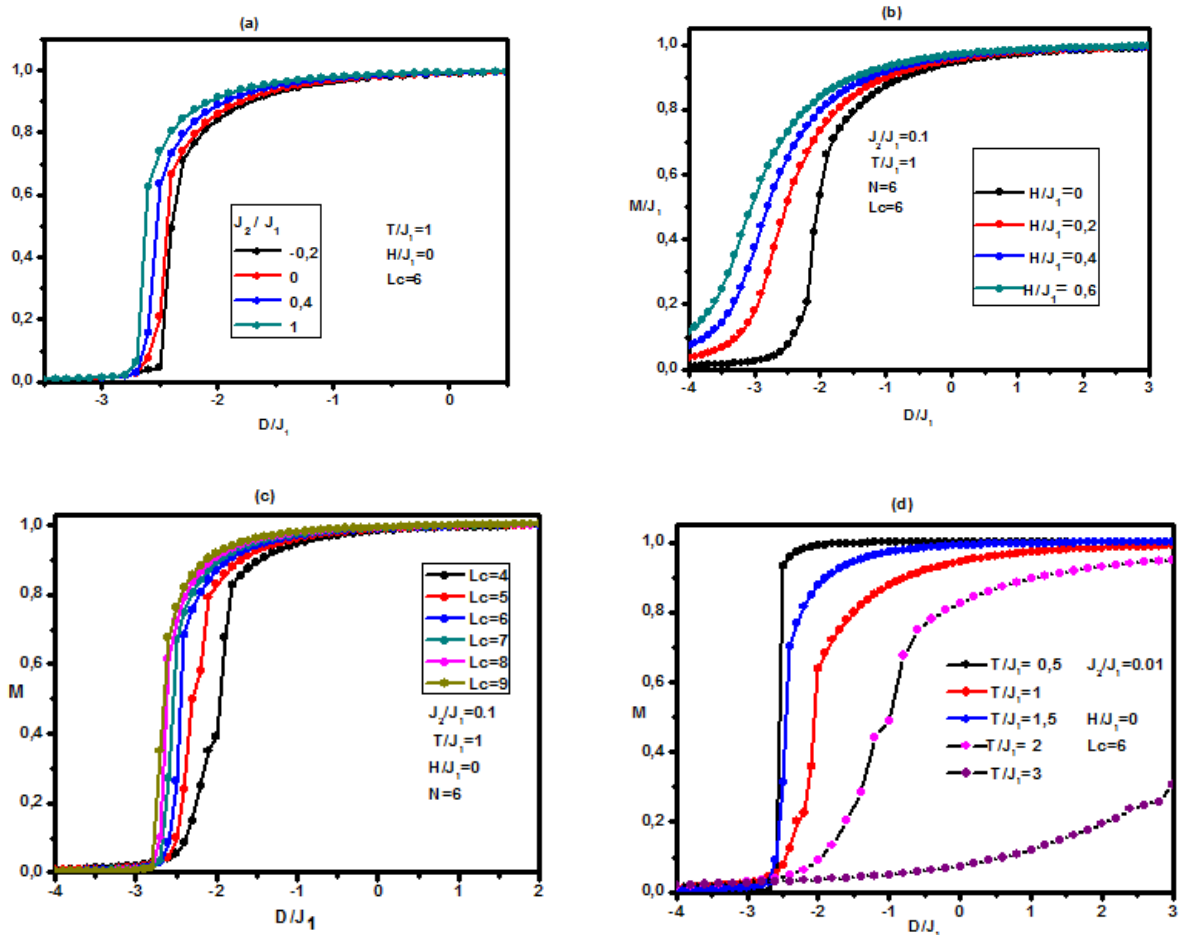

Figure 6.12: (a-d): Magnetization versus reduced anisotropy for various reduced exchange coupling in (a), in (b) for various reduced external field, in (c) for various cube size and in (d) for various reduces temperature with number of cube ($N = 6$).

We plotted the Figure 6.12(a-d) to illustrate the total magnetization versus the reduced anisotropy at the fixed cube number $N = 6$. In the first step, we presented them in Figure 6.12.a with the different values of the reduced exchange coupling ($J_2/J_1 = -0.1, -0.2, -0.4, -0.6, -0.9$ and $-1.0 \text{for} H/J_1 = 0.0, T/J_1 = 1.0$) and as a result we concluded that despite the act of varying the coupling J_2/J_1, the reduced anisotropy for $\Delta/J_1 < -3.5$ does not exert any influence on the total magnetization of the NCCM. Contrastively, the total magnetization shown an abrupt change when $-3.5 < \Delta/J_1 < -1$ and kept a constant value when $\Delta/J_1 > -1$ which is equal $M_s = 1$.

Equally important, the effect made the reduced anisotropy Δ/J_1 on the total magnetization for the different values of the reduced external magnetic field ($H/J_1 = 0.0, 0.5, 0.6, 0.7 \text{and} 0.9$), and for different values of cube size ($Lc = 4, 5, 6, 7, 8 \text{and} 9$) with the reduced exchange coupling interaction $J_2/J_1 = 0.1$ is traced in Figure 6.12(b-c). The magnetization of different cube size increases with increasing the reduced anisotropy and reduced external field until reached their saturation $M_s = 1$. For a high value of cube size and the reduced external field the magnetization increases quickly such as given in Figure 6.12(b-c). Figure 6.12.d. illustrated, the total magnetization versus the reduced anisotropy of different reduced temperatures $T/J_1 = 0.5, 1, 1.5, 2$ and 3 with $J_2/J_1 = 0.1$, $H/J_1 = 0.0$, $Lc = 6$ and $N = 6$. The magnetization doesn't achieved the saturation value when the reduced temperature increases.

As the end section of this article, the effect of the reduced exchange coupling, the reduced temperature and the reduced anisotropy on the magnetic hysteresis loop is elucidated in Figure 6.13(a-c)). Indeed,

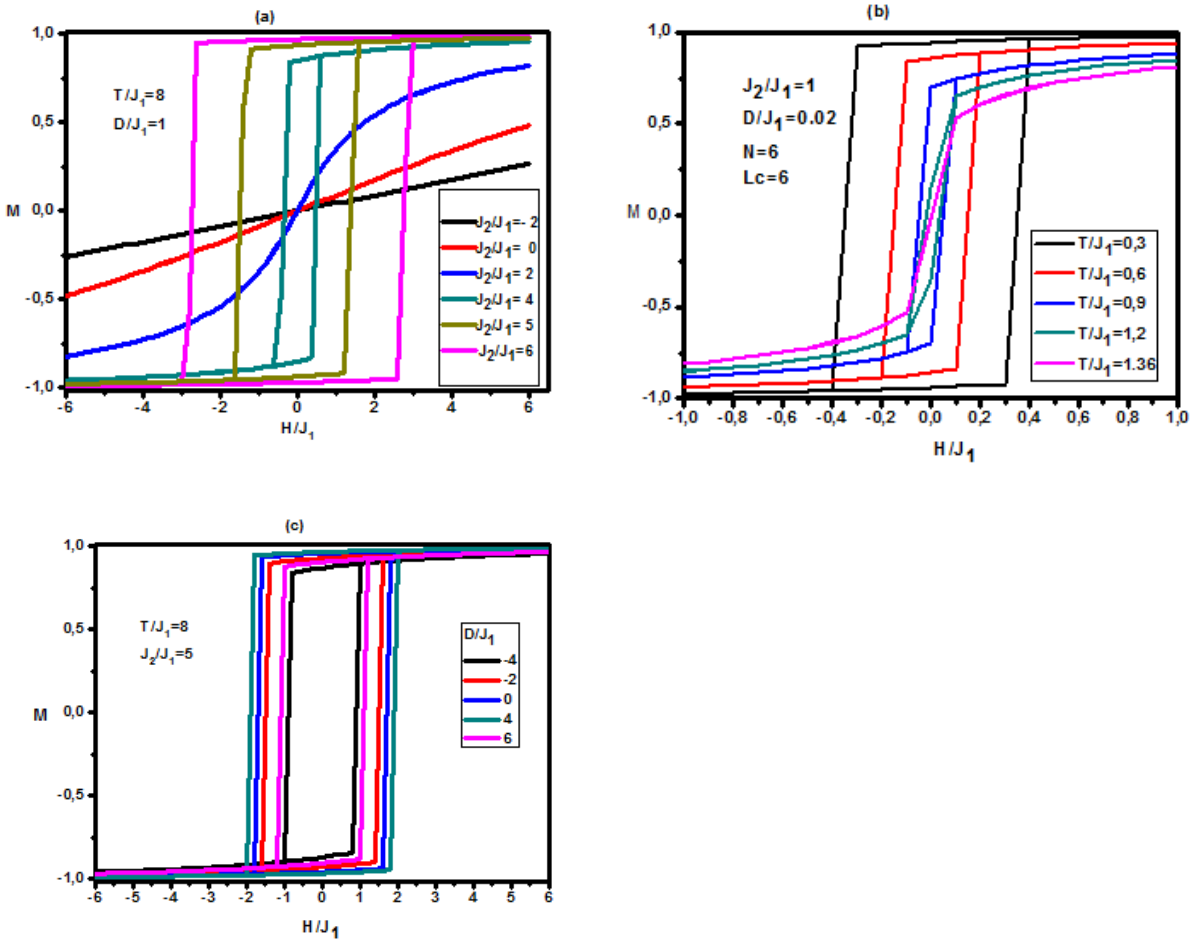

Figure 6.13: The total magnetization hysteresis loop for different reduced exchange coupling (J2/J1=-2, 0, 2, 4,5 and 6) in (a), for different reduced temperatures (T/J1=0.3, 0.6, 0.9, 1.2 and 1.36) in (b) and for different reduced anisotropy ($D/J_1 = -4, -2, 0, 4$ and 6) in (c).

Figure 6.13.a shown clearly the effect that the reduced exchange coupling has applied on the magnetic hysteresis cycle that is the coercive field increases with increasing of the reduced exchange coupling. From, the Figure 6.13.b, we concluded that the coercive field decreases with the increasing of the reduced temperature and it was despaired at the reduced transition temperature ($T/J_1 = 1.36$) [146,174,219,220]. For the different values of the reduced anisotropy with $T/J_1 = 8$ and $J_2/J_1 = 5$ as illustrated in Figure 6.13.c. This figure allows us to conclude that the coercive field increases when the anisotropy increasing.

6.2.4 Conclusion

The magnetic properties of the NCCM have investigated by the Monte Carlo simulations. The reduced transitions temperatures are established for different cube size of NCCM ($Lc*Lc*Lc$). The result achieved is that the reduced transition temperature increases with the increases of the cube size (Lc). As second results, the magnetization versus the reduced anisotropy for different values of the reduced exchange interaction, size of the NCCM, the reduced external magnetic field as well as the reduced temperature. The magnetic hysteresis cycle are found for different reduced temperature value, for different reduced exchange interaction value as well as for different reduced anisotropy. The magnetic coercive field increases with increasing of the reduced exchange coupling and the reduced anisotropy while the coercive field decreases when increases the reduced temperature.

6.3 Effects of size for an assembly of Core-Shell nanoparticles with the cubic structure: Monte Carlo simulations.

6.3.1 Introduction

Recent technological tendencies have motivated [6] the invention of new magnetic material properties, which requires that the known materials be structured in all three dimensions at various scale lengths to exploit these magnetic properties due to their nanoscale structure [4,5]. In the last decade, the magnetic nanoparticles have been a main subject for several theoretical and experimental investigations thanks to of their potential nanotechnological and industrial applications in the following domains : information storage [27, 29], biomedical applications [132, 221, 222], shielding [223] , sensors [185], permanent magnets [135] and magneto-resistive devices [186]. Particularly in the domain of information storage, the possibility to control the coercivity in magnetic nanomaterials has led, particularly in the domain of information storage, to many significant technological applications. The magnetic nanoparticles are promising candidates for a further increase in the density of the magnetic storage devices.

On the other hand, many theoretical studies have been devoted to investigating the magnetic properties of various types of the magnetic nanoparticle systems such as nanocubes [144, 146, 147, 165, 193], nanorods [168], nanofilms [170, 187, 224], nanowire [171, 225], dendrimer [174–177] , nanotube [189, 226], nanospheric [180, 191] and skyrmion [227]. These studies use the following different types of methods: Monte Carlo (MC), Mean Field Approximation (MFA), Effective Field Theory (EFT), Green function formalism, Cluster Variation Method (CVM) and Micromagnetic Simulations.

The magnetic nanoparticles with the core-shell morphology have received particular attention because of their physical properties, which are highly dependent on the structure of the core-shell and the interface exchange [228]. During the last few years, numerous works have been devoted to the investigation and to the synthesis of the nanoparticles that consist of core-shell architecture in order to understand their thermodynamic and magnetic properties. For example, Iron/Iron oxide Core/Shell have been synthesized [194], and Abedini et al [229] , in turn, have been synthesized using Fe/Ni nanoparticles in the core/shell structure by Radiolytic Reduction Method. Rafique et al [230] reported that the magnetic properties and effects of NaOH on the formation of FeCo alloy nanostructures were assembled, and Lu et al [231] studied, in turn, the magnetic properties of the size-controlled CoNi alloy nanoparticles. This growing interest in these systems with cubic shapes is mainly due to the beneficial effects (as a lower surface spin disorder, higher crystallinity and higher magnetic moments) of the cubic shape [232, 233] compared with those of the spherical shape. Recently, it has been found that cubic nanoparticles have a higher degree of crystallization, and larger single crystal and higher saturation magnetization compared to spherical nanoparticles of the same size [234]. However, due to the combination of their characteristics such as (i) their cubic shape and core-shell structure; (ii) the high coercivity and (iii) magnetization saturation, they are considered promising candidates as heat mediators for in vivo hyperthermia and MRI applications [199].

Magnetism of an assembly of particles differs from that of a single particle. Particularly, because the giant magnetic moment of a particle radiates a dipolar magnetic field which is felt at a greater distance by the moment of the other particles. Furthermore, at high concentrations, the particles can be in direct magnetic interaction (ferromagnetic) because of their proximity. This implies that the macroscopic properties of the assembly (coercive field, blocking temperature ...) vary depending on the metal concentration and the particle size and to a lesser extent on the size distribution [235–237].

In our study, we propose to investigate an assembly of Ising Ferromagnetic / antiferromagnetic core-shell nanoparticles with a cubic shape, using Monte Carlo simulations. For this spin system, we aim to study the effects of the interface exchange and interparticle coupling exchange, as well as of the anisotropy parameter and size effects on the critical temperature and the coercive field. From this structure, a number of interesting magnetic properties as compared to those observed in the magnetic nanoparticles with dipolar interactions and non-colinearity of spins have emerged. These phenomena are due to the side effects.

The outline of the remaining parts of the paper is as follows: In section 2 we described the Hamiltonian model and the method used. In section 3, we presented the results achieved along with the discussion. Finally, in section 4 we present the conclusion.

6.3.2 Theoretical model and method

We considered the assembly of cubic nanoparticles as the structural model for the studied system. As shown in Figure 6.14 , the model contains n-identical nanocubes of Size L^3 with $L = 2Ls + Lc$. Three regions describe each nanocube: a ferromagnetic core with side Lc, a ferromagnetic shell of thickness Ls and a ferromagnetic core-shell interface that is constituted by the core (shell) spins having its nearest neighbours on the shell (core). The sites of the core are occupied by coupled spins $\sigma = 1/2$. The spins $S = 3/2$ occupy those of the Shell and are assumed to interact inside nanocubes and between two adjacent nanocubes. The Hamiltonian method, which governs the system studied, is expressed by:

$$H = -J_1 \sum_{\langle i,j \rangle}^{N} \sigma_i \sigma_j - J_2 \sum_{\langle k,l \rangle}^{N} \sigma_k S_l - J_3 \sum_{\langle m,n \rangle}^{N} S_m S_n - J_4 \sum_{\langle h,p \rangle}^{N} S_h S_p - D \sum_{i}^{N} (S_i)^2 + H \sum_{\langle i,j \rangle}^{N} (\sigma_i + S_j) \quad (6.9)$$

Where, σ_i and σ_j are the nearest-neighbours, the spins of sites i and j represent the core. While S_h and S_p denote the nanocube's side-last spin and the side-first spin of the following adjacent nanocube. J_1 and J_3 are the exchange couplings between the nearest-neighbours of the spins which belong to the core and shell of each nanocube. J_2 and J_4 are exchange couplings interactions between the nearest-neighbours spins across the core-shell interface of the nanocube and consecutive adjacent nanocubes in any direction x, y or z. D is the magnetic anisotropy parameter, and H is the external magnetic field that acts on all the spins S_j and σ_i. The Hamiltonian (1) is solved numerically.In the following, we used normalized parameters: J_2/J_1, J_3/J_1, J_4/J_1, D/J_1 and H/J_1.

To compute the thermodynamic quantities, we have used the Metropolis algorithm within framework of the context of the Ising model. The lattice is considered with free boundary conditions, and the program was performed for different lattice sizes. The program runs a sufficient amount of time using 18.10^5 Monte Carlo steps (MCS), and the equilibrium is reached after 12.10^5 MCS steps per site.
The total magnetization is expressed by:

$$M = \frac{1}{N} \mid \sum_{i} S_i \mid \quad (6.10)$$

Where N is the total number of spins in all the lattice.

The magnetic susceptibility is given as:

$$\chi = \frac{N}{K_B T} (\langle M^2 \rangle - \langle M \rangle^2) \quad (6.11)$$

K_B is the Boltzmann's constant set to unity.

The relation links the magnetization and the susceptibility:

$$\chi = \frac{\partial M}{\partial H} \mid_{H=0} \quad (6.12)$$

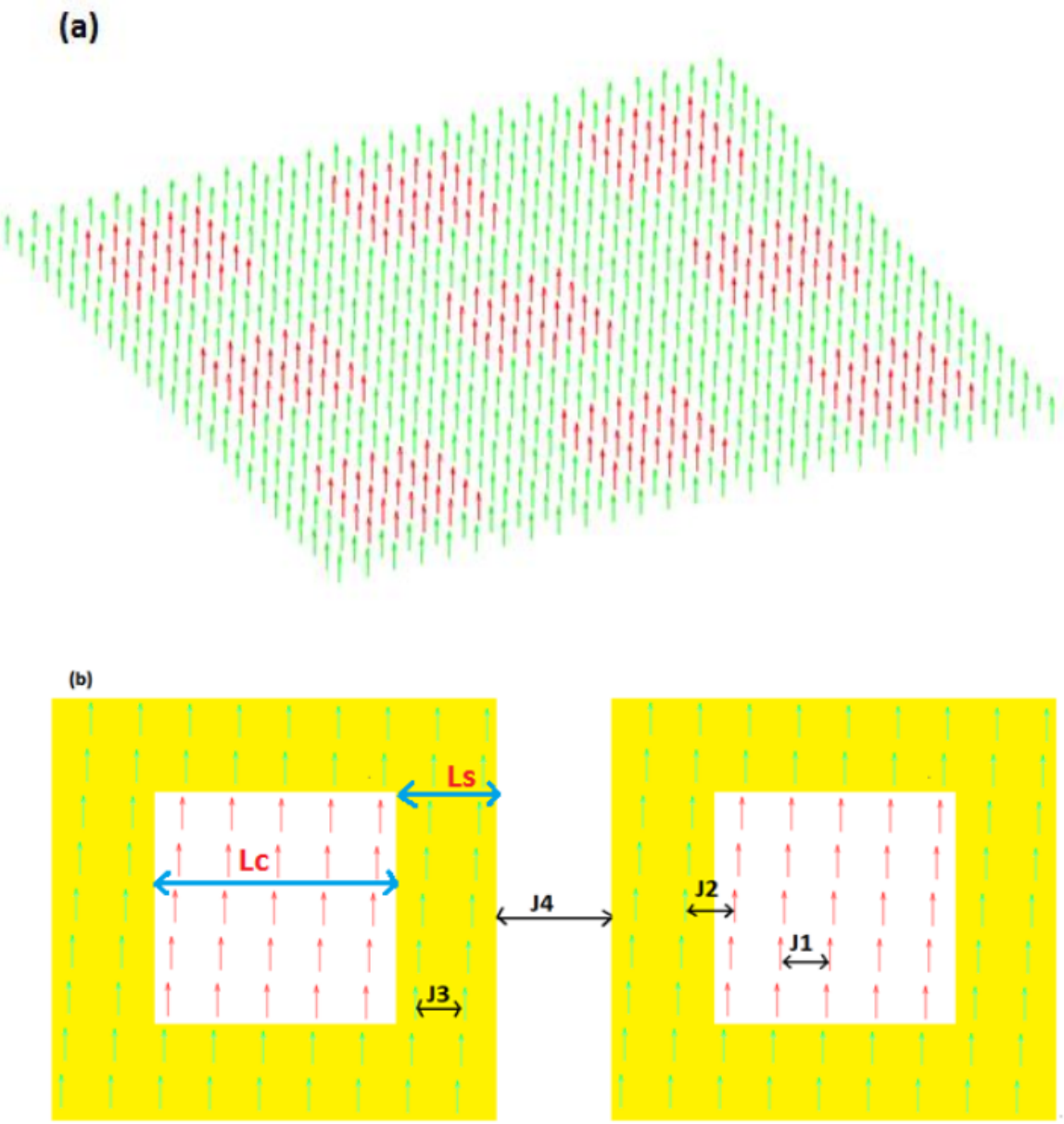

Figure 6.14: Structure of an assembly of cubic nanoparticles Core-Shell

H is the external magnetic field.

6.3.3 Results and discussions

The effect of the core-shell interaction (J_2/J_1) on the critical temperature (Tc/J_1) is presented in Figure 6.15.a, for the sizes $Lc = 6$ and $Ls = 2$ with the different values of the exchange coupling of the core-shell: $J_2/J_1(-3 \leq J2/J1 \leq 3)$ and J_4/J_1 positive. This figure represents a paramagnetic $(3/2, 1/2)$ and $(3/2, -1/2)$ (see figure.3.c and in Figure 6.15.b) phases. The dotted line represents the first order transition between (3/2,1/2) and (3/2,-1/2). We remark from this that the transition temperature increases when the $\mid J_2/J_1 \mid$ increases. The phase diagram shows a symmetric behavior for the positive and negative values of the core-shell interaction (J_2/J_1). The critical temperature (Tc/J_1) takes a minimum of the value ($Tc/J_1 = 4.2$) in case of the absence of $J_2/J_1 = 0$. Furthermore, the positive values J_2/J_1 favor the $(3/2, 1/2)$ phase (see Figure.3.c). For the negative values, the phase $(3/2, -1/2)$ is favoured. The spins of the shell and those of the core interact antiferromagnetically.

Figure 6.16.a shows the phase diagram in the plane $Tc/J_1 - J_4/J_1$ of the system with sizes $Lc = 6$ and $Ls = 2$ with different values of the core-shell coupling exchange J_4/J_1 $(-3 \leq J_4/J_1 \leq -3)$. This figure contains two ordered phases -phase (1), phase (2)- and the paramagnetic phase. The phase (1) corresponds to the nanocubes that are in the antiferromagnetic order;that's, in this phase, the spins of one nanocube are up and the spins of the adjacent nanocube are down (see Figure 6.16.b) . In phase (2), all the nanocubes are, as Figure 6.16.c shows, in the ferromagnetic order and this means that all the spins of the nanocubes are in the same orientation. In the case of the weak interparticle interaction, the contribution of this interaction decreases, and then the critical temperature decreases to a minimum value of Tc/J_1 (for $J_4/J_1 = 0$, $Tc/J_1 = 4.48$). We observe that the interparticle interaction $\mid J_4/J_1 \mid$ increases as the critical temperature, between the ordered phases and the paramagnetic phase, increases symmetrically for the positive and negative values of J_4/J_1 . A similar phase has been plotted in refs [156, 238]. The high critical temperatures Tc/J1 are due to the contribution of the interactions between the different constituents of system $(\sigma_i\sigma_j, \sigma_l S_k, S_m S_n, S_h S_p)$.

Figure 6.17 shows the phase diagram in the plane $Tc/J_1 - D/J_1$ of the system studied with the sizes Lc=6 and Ls=2. It exhibits phases $(1/2, 1/2), (3/2, 1/2)$ and the paramagnetic phase. Negative values of D/J_1 promote the spin-1/2 , and concurrently the critical temperatures become constant and minimum $Tc = 1.1/J_1$. When D/J1 increases the critical temperature increases continuously from the negative values of D/J_1 to the positive values of D/J_1. The dotted line presents the transition phase between $(1/2, 1/2)$ and $(3/2, 1/2)$ phases because the large positive value of D/J_1 promotes the spin-3/2.

The total magnetization behavior as a function of the temperature is presented in Figure 6.18.a for the different values of the shell size $Ls = 2, 3, 4, 6, 8$ with the fixed size of the core $Lc = 2$. We observe both a second order phase transition for all a shift at $T/J1 = 2.96$ for $Ls = 2$.As the value of Ls increases, the critical temperature also increases and the shift gradually disappears. 6.18.b shows the magnetic susceptibility as a function of the temperature. The peaks of the susceptibilities, which correspond to the critical temperature, clearly shows the increase of $Tc/J_1$when Ls increases.

Figure 6.19.a shows remanent and saturation magnetizations (Mr and Ms) as function of sizes $!Ls = 2, 3, 4, 5, 6$ with fixed Lc and for two values of temperatures $T/J_1 = 1, 4$. For $T/J_1 = 1$ For $T/J_1 = 1$, we notice that the variations of the remanent and saturation magnetization are unchanged when the size Ls increases. Thus, the values of the magnetizations experience a slight increase of $(Ls = 2; Mr = Ms = 1.46)$ up to $(Ls = 6; Mr = Ms = 1.48)$, and from Ls, the magnetization becomes almost constant:$Mr = Ms = 1.48$. Consequently, the effect of Ls on the magnetization is almost negligible at $T/J_1 = 1$.However, for $T/J_1 = 4$, the behavior of the saturation magnetization (Ms) as a function of Ls is identical to that of the case $T/J_1 = 4$ but with lower values. This shows the effect of the temperature on the saturation magnetization. In fact, the higher the temperature increases, the more Ms decreases. The same effect of the temperature is noticed on the remanent magnetization (blue line). Figure 6.19.b illustrates the effect of the size Ls on the critical temperature Tc/J_1. Indeed, when Ls increases, the Tc/J_1 values increase logarithmically.

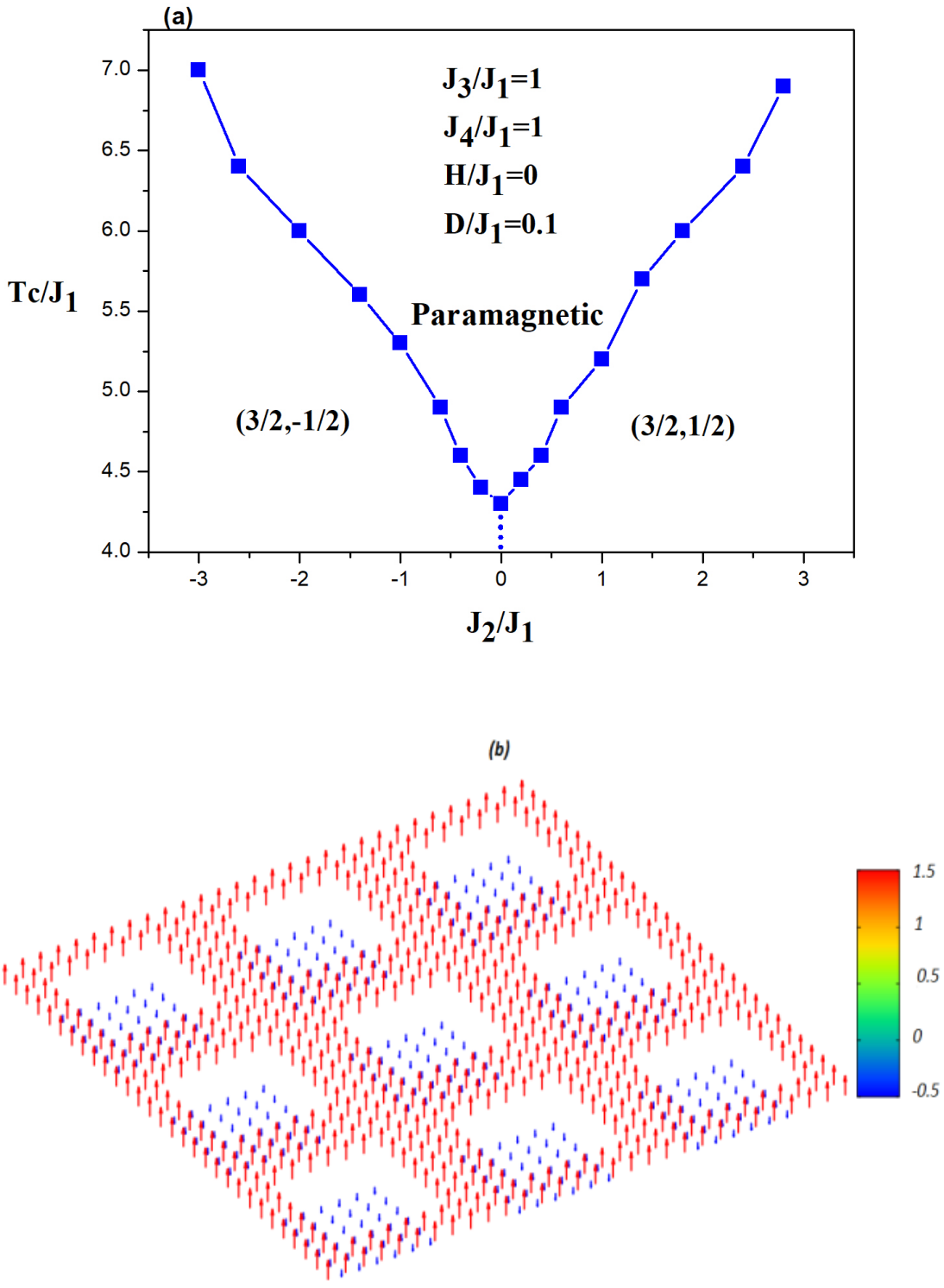

Figure 6.15: (a) Phase diagram in the plane Tc/J_1 versus J_2/J_1. Square points indicate critical temperatures between the $(3/2, -1/2)$, $(3/2, -1/2)$ phases and the paramagnetic phase(b) Simulation snapshot of spin systems of $Ls = 2$ and $Lc = 6$ at $T/J_1 = 1$ and $J_2/J_1 = -3$, the lattice of spins shows a transversal cut of the whole system of nanocubes and spin vectors are represented by colored arrows where the color scales linearly with the z component of the vector to highlight spin textures, it is show $(3/2, -1/2)$ for $J_4/J_1 = 2$.

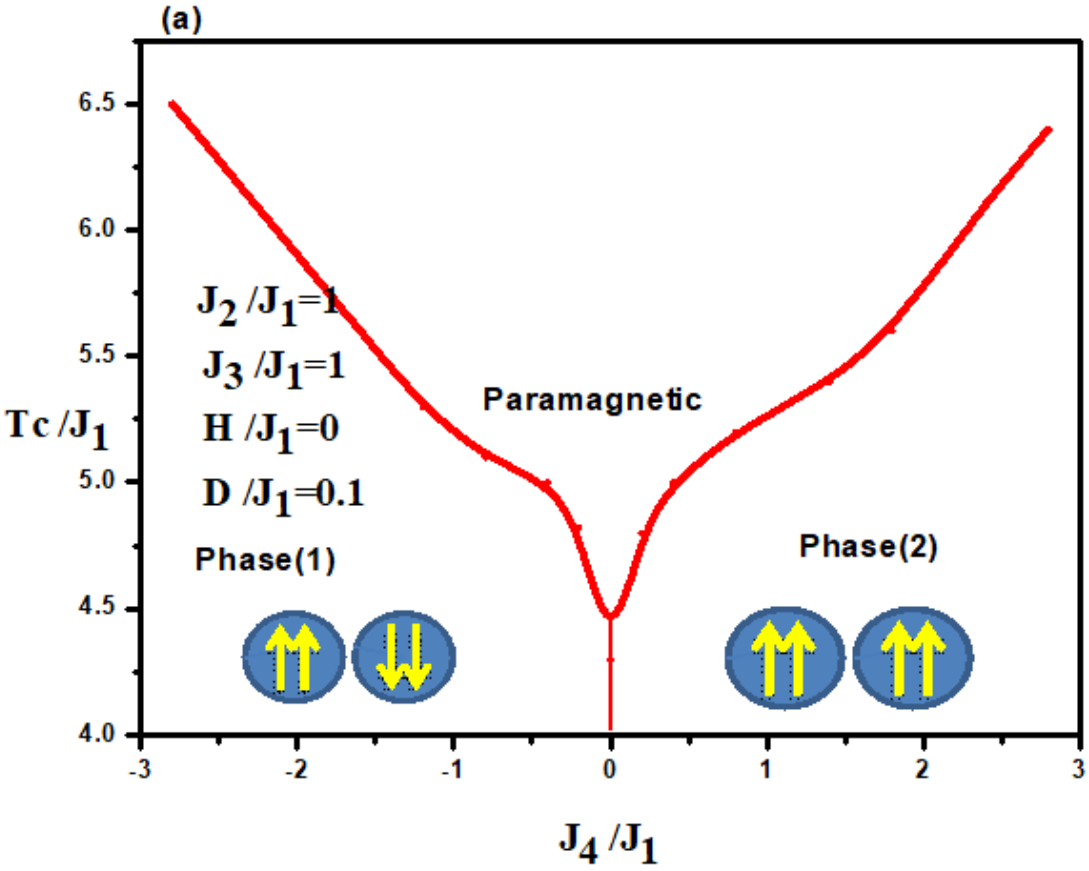
(a)
6.5
6.0
5.5
5.0
4.5
4.0
Tc /J1
J2 /J1=1
J3 /J1=1
H /J1=0
D /J1=0.1
Paramagnetic
Phase(1)
Phase(2)
-3
-2
-1
0
1
2
3
J4 /J1

(b)

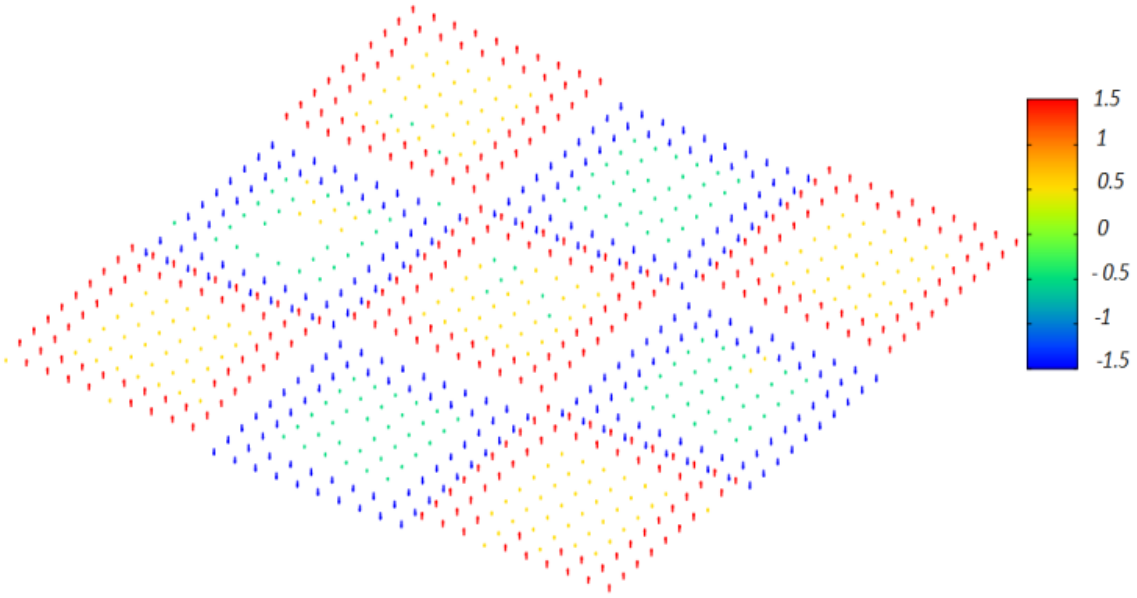
1.5
1
0.5
0
-0.5
-1
-1.5

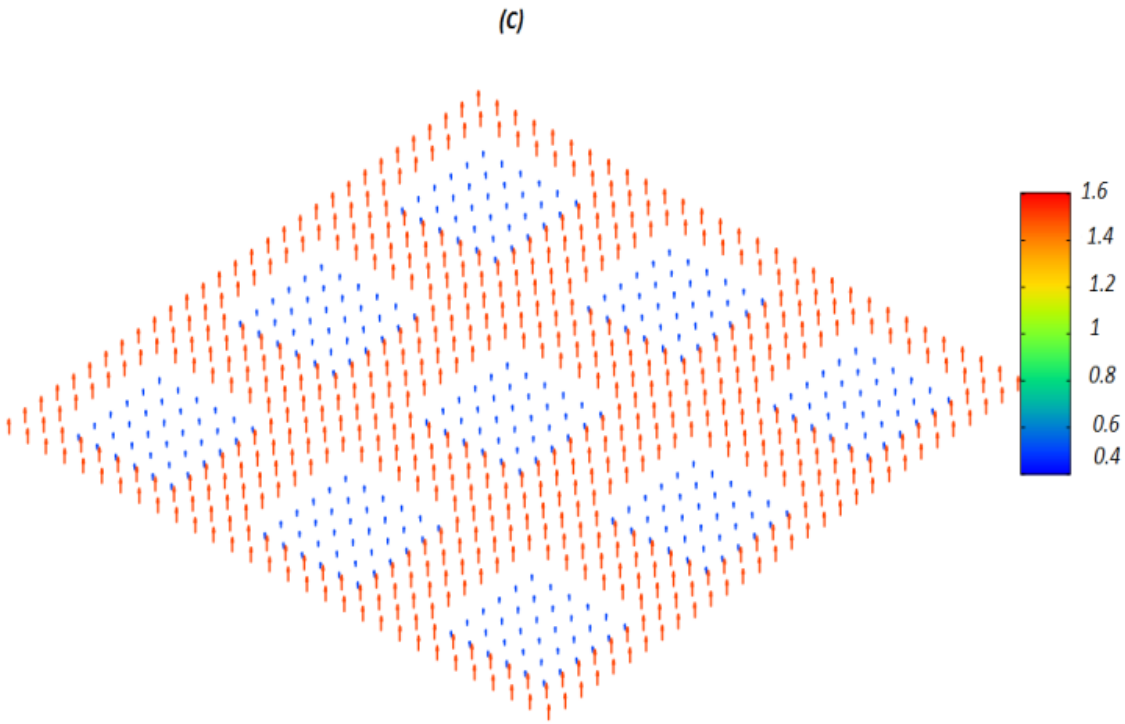

Figure 6.16: (a) Phase diagram in the plane $Tc/J_1 - J_4/J_1$.Square points indicate critical temperatures between phase (1), phase (2) and the paramagnetic phase. $(b-c)$ Simulations snapshots of spin systems of $Ls = 2$ and $Lc = 6$ at $T/J_1 = 1$, the lattice of spins shows a transversal cut of the whole system of nanocubesand spin vectors are represented by colored arrows where the color scales linearly with the z component of the vector to highlight spin textures .(b) schematic of phase (1) for $J_4/J_1 = -1.4$ and (c) of phase (2) for $J_4/J_1 = 2$.

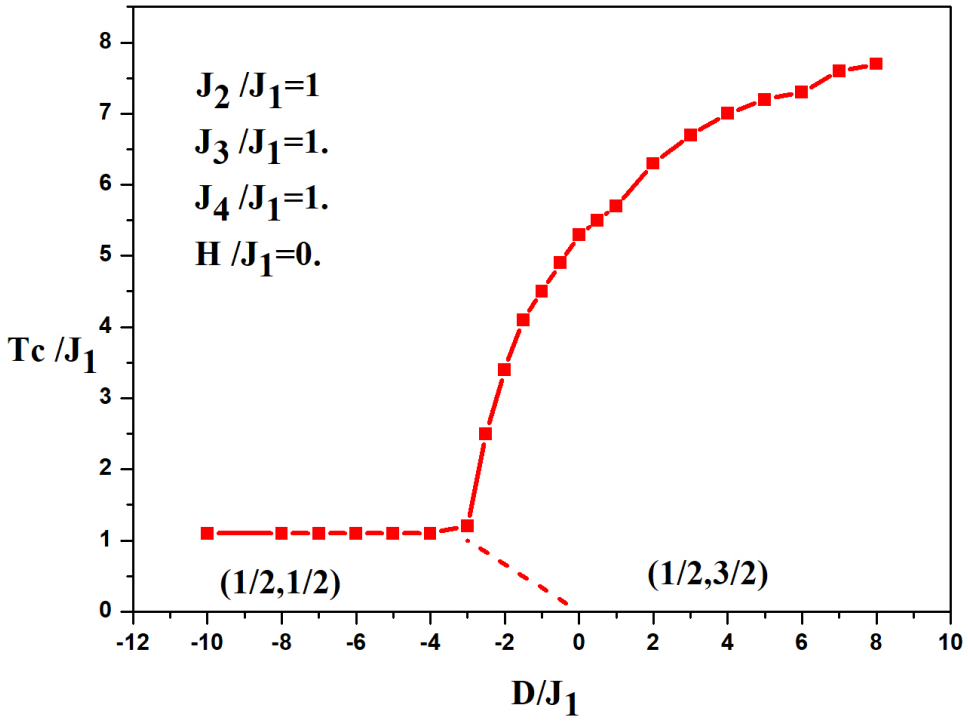

Figure 6.17: Phase diagram displaying the reduced critical temperature, Tc/J_1 versus the reduced anisotropy D/J_1. Square points indicate second-order phase transition points. They limit $(1/2, 1/2)$, $(1/2, 3/2)$ phases from the paramagnetic phase.

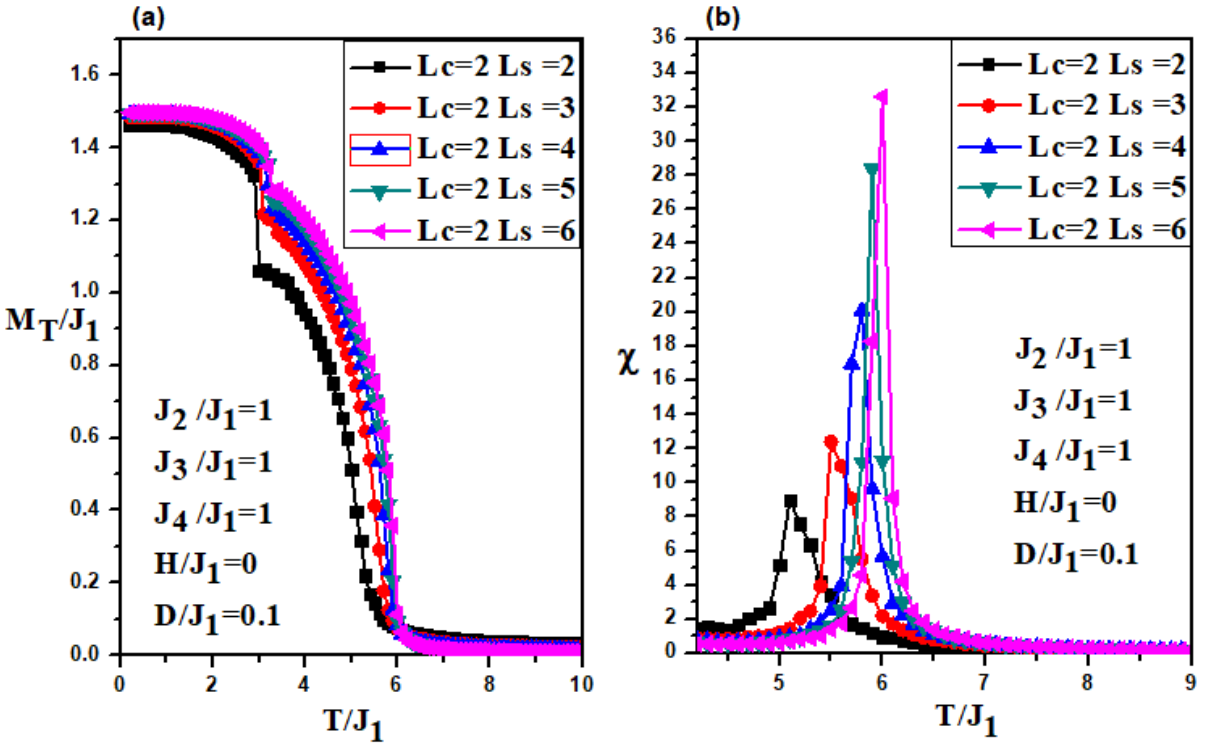

Figure 6.18: Total Magnetization as a function of temperature for different Ls values with fixed Lc. Magnetization and Tc/J_1 as a function of Ls. (b) Magnetic susceptibility as a function of temperature for various Ls values with fixed Lc.

Figure 6.20.a shows the temperature dependence of magnetization obtained for the different Lc values with the fixed Ls. It is seen that magnetization decreases when Lc increases because the core spin increases ($\sigma = 1/2$) and they vanish at the critical temperature by presenting a second-order phase transition. Figure 6.20.b shows, in turn, the magnetic susceptibility as a function of the temperature. The maximum of the peak of the susceptibility corresponds to the critical temperature which shifts to higher temperature when Lc increases. Figure 6.21.a shows the remanent and saturation magnetization as a function of the size of $Lc = 2, 4, 6, 8, 10$ with the fixed Ls and for the two values of temperatures $T/J_1 = 1$ and 4. When the size of Ls increases, the remanent and saturation magnetization decreases. Figure 6.21.b illustrates the effect of the size Lc on the critical temperature Tc/J_1, and thus when Ls increases, the Tc/J_1 values increase.

Figures 6.22.(a-b) show the hysteresis loops as a function of the size of the shell (Ls) with a fixed size of the core (Lc), for the two temperatures: (a) $T/J_1 = 1$ and (b) $T/J_1 = 4$. We note that the remanent and saturation magnetization increase slightly with the increase in Ls and become gradually narrower when T/J_1 increases [194]. Figures 6.23(a-b), we study the effect of the size of the core (Lc) on the hysteresis loops for the two temperatures: (a) $T/J_1 = 1$ and (b) $T/J_1 = 4$. We observe that the remanent and saturation magnetization show an obvious decrease, simultaneously with the increase in Lc. This behavior is due to the dominance of the spins-1/2 over the spins-3/2 rate, and this fact leads to the decrease in Mr.

In Figures 6.24(a-b), we have studied the effect of the interparticle interaction J_4/J_1 on the hysteresis loops behavior for different values of J_4/J_1. It is obvious that the shape of the hysteresis loops of the core and shell becomes narrower as J_4/J_1 decreases. in comparison to positive values J_4/J_1, when J_4/J_1 takes a negative values, the hysteresis loops shefted to positive values of H/J_1. As we increasing J_4/J_1, the coercivity increases symmetrically for both negative and positive of J_4/J_1 and presenting a minimum at $J_4/J_1 = 0$ (see In Figures 6.24.c).

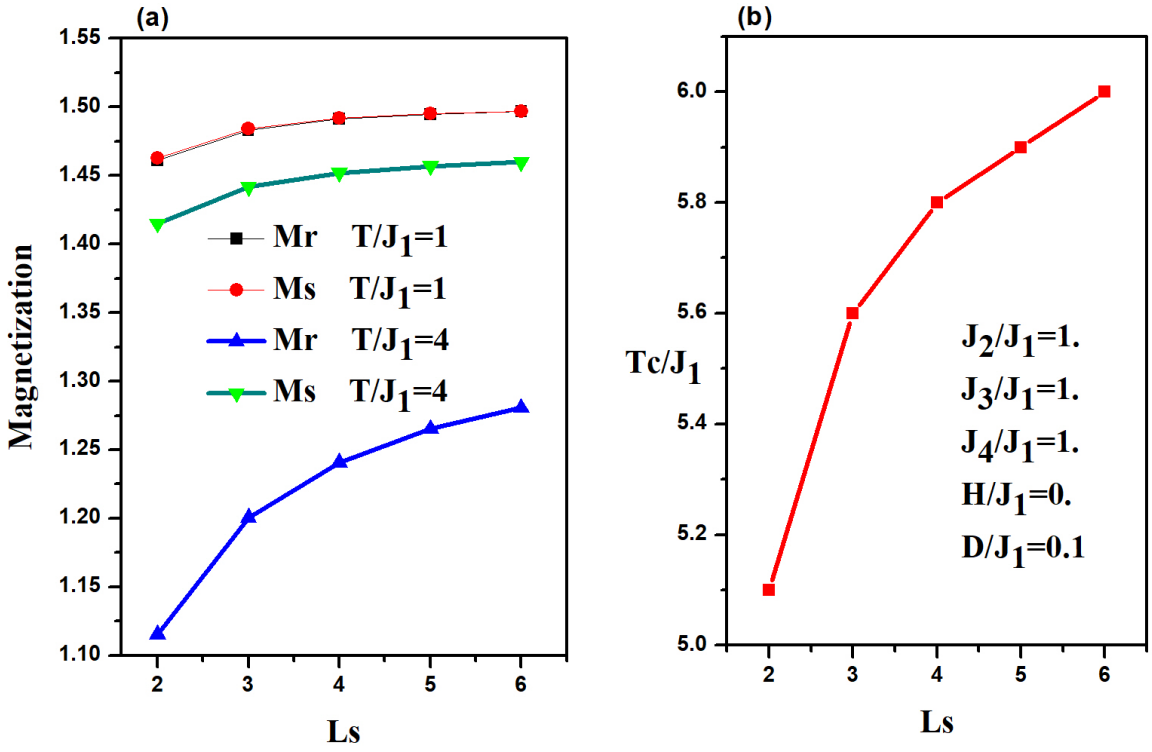

Figure 6.19: Remanent and saturation magnetizations as a function of Ls for temperatures $T/J_1 = 1$ and $T/J_1 = 4$ with fixed Lc. For $T/J_1 = 1$, remanent and saturation magnetizations are illustrated by the black and red lines, respectively, and for $T/J_1 = 4$, they are presented in blue and green line, respectively.(b) The critical temperature Tc/J_1 as a function of different values of Ls with fixed Lc.

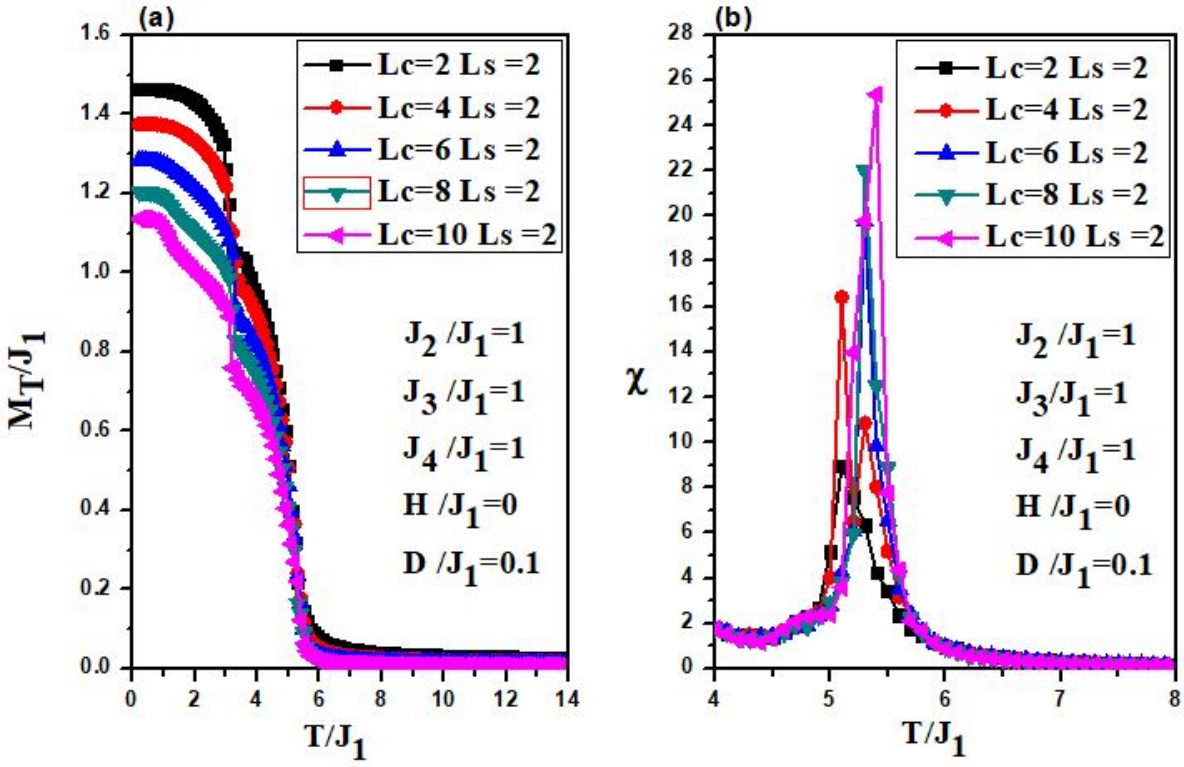

Figure 6.20: (a)magnetization as a function of temperature for different Lc values with fixed Ls. Magnetization and Tc as a function of Ls (b) magnetic susceptibility as a function of temperature for various Lc values with fixed Ls.

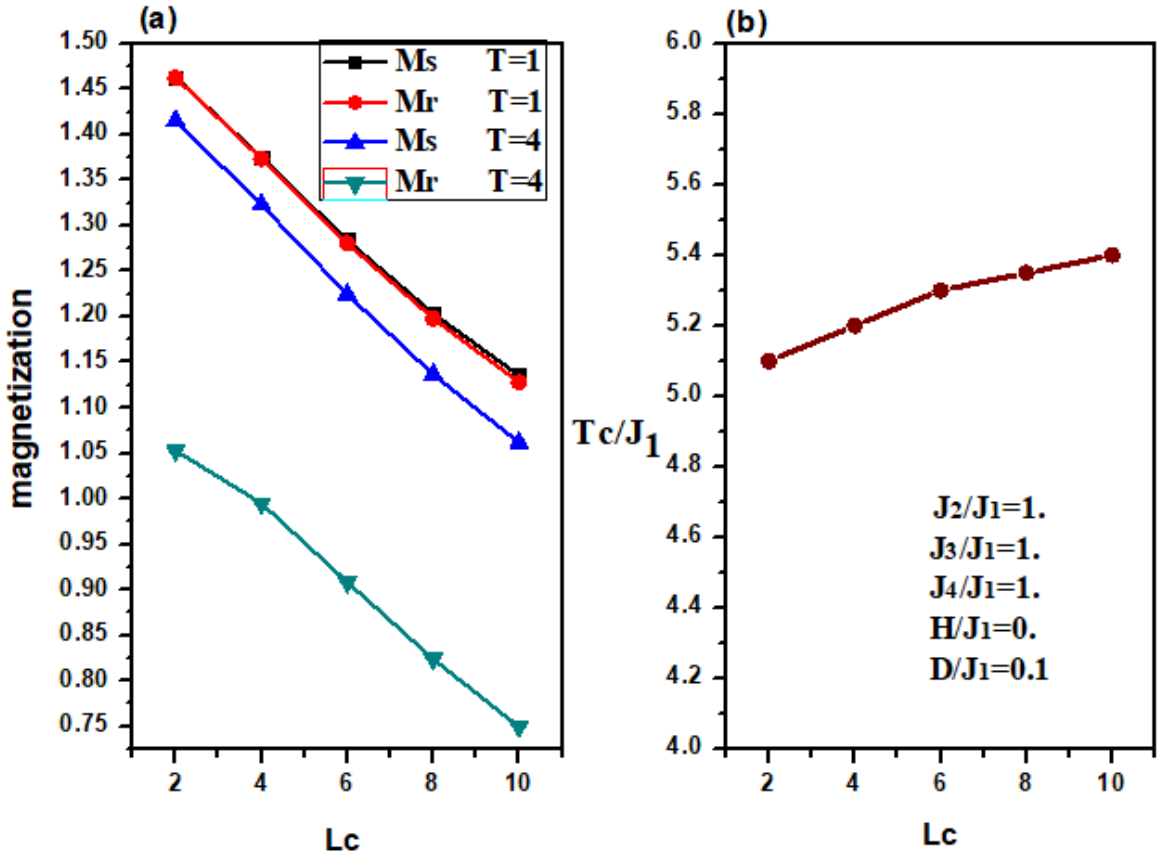

Figure 6.21: Remanent and saturation magnetizations as a function of Lc for temperatures$T/J_1 = 1$ and $T/J_1 = 4$ with fixed Ls (black line) show remanent magnetization with $T/J_1 = 1$ (red line) saturation magnetization with $T/J_1 = 1$(blue line) remanent magnetization with $T/J_1 = 4$ (green line) saturation magnetization with $T/J_1 = 1$. (b) critical temperatures Tc/J_1 as a function of the different value of Lc with fixed Ls.

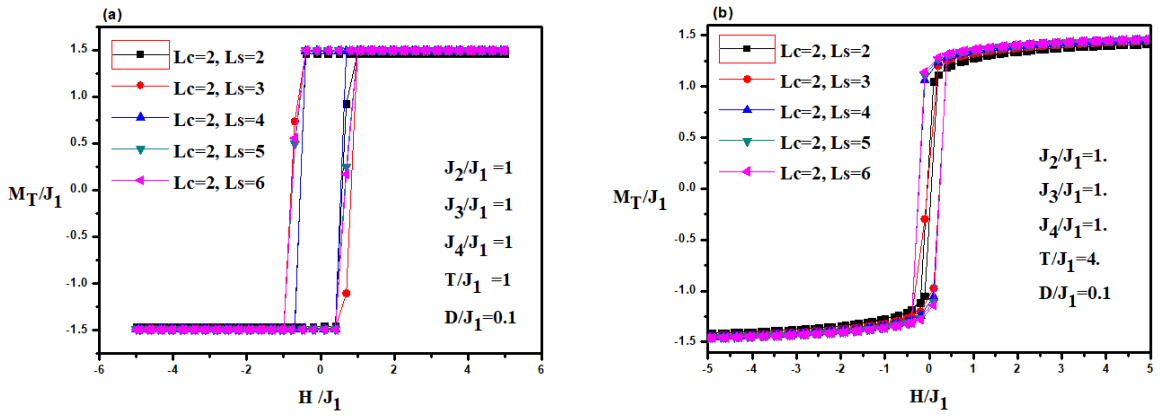

Figure 6.22: Hysteresis loops as a function of Ls with fixed Lc, (a) T/J1=1 and (b) T/J1=4.

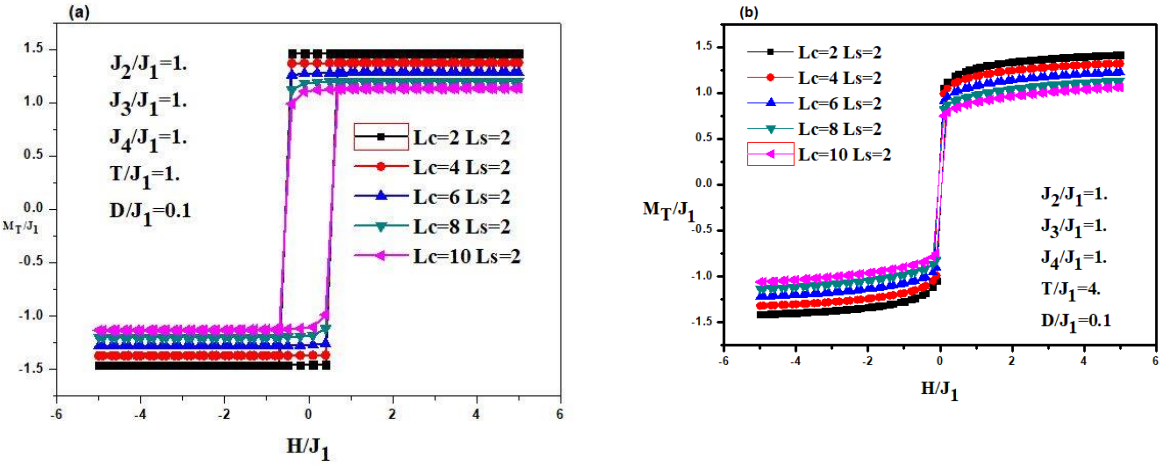

Figure 6.23: Hysteresis loops as a function of Lc with fixed Ls, (a) $T/J_1 = 1$ and (b) $T/J_1 = 4$

The influence of the magnetic anisotropy on the hysteresis behavior is shown in In Figures 6.25.a), which presents the variation of the total magnetization versus the external magnetic field, for different values of the reduced magnetic anisotropy, $D/J_1 = -3, 0$ and 3. It appears that the central loop width of the hysteresis curve increases proportionally with D/J_1. We show in Figures 6.25.b the effect of D/J_1 on the coercivity. We can see that the coercivity Hc/J_1 increases continuously from negative to positive values of D/J_1. In fact, low negative values of D/J_1 tend to vanish the magnetization and as a consequence, low fields are needed to demagnetize the system; contrary to the case of high negative values and positive values of D/J_1, where coercive fields becomes higher. In particular, for negative values of D/J_1, the Hc/J_1 becomes constant and minimum $Hc/J_1 = 0.5$, because D/J_1 promote the $(1/2, 1/2)$ phase. On the other hand, with large positive values of D/J_1, the Hc/J_1 becomes constant and maximum $Hc/J_1 = 0.87$, because D/J_1 promotes the $(3/2, 1/2)$ phase. The results show that as the anisotropy D/J_1 increases as Hc/J_1 increases. This behavior is reported by N. Hachem et al [239] and agrees with Figure 6.17.

Now, the effect of the exchange coupling J_2/J_1on the hysteresis behavior is investigated. In Figure 6.26.a, the hysteresis loops are plotted for different values of $J_2/J_1 = \pm 3, \pm 2$ and ± 1. We can see that when J_2/J_1 takes negative values, the remnant and saturation magnetizations decrease, on the other hand, for positives values of J_2/J_1, the remnant and saturation magnetizations are constant, while, the width of the hysteresis curves increases. This behavior is explicit in Figure 6.26.b, presenting the coercive field as a function of the exchange coupling J_2/J_1. Two regions are observed: The first, going from $J_2/J_1 = -3$ to 1, where the coercive field decreases until the minimum value $Hc/J_1 = 1/2$. Figure 6.15.a is in a good agreement with Figure 6.26.b.

6.3.4 Conclusion

In this work, we have used Monte Carlo Simulations based on an adapted Metropolis algorithm, to study magnetic properties of a core-shell nanosystem having a Rubik's cube structure. We have investigated system parameters effects on phase diagrams for different system sizes and the hysteresis behaviors when applying the external magnetic field. We have observed that, both, the exchange couplings and the magnetic anisotropy affect phase diagrams. The increase of positive exchange interactions between spins core and shell, on one hand and between nanocubes on the other hand, has the particularity to increase the critical temperature, favoring the stable phase (3/2, 1/2). The same phase is also advantaged by positive values of the magnetic anisotropy. Furthermore, the increase of the system size has the effect to increase the critical temperature, which is a typical behavior observed with nanosystems. The hysteresis behavior investigation has shown that, exchange couplings and the magnetic anisotropy control the coercivity.

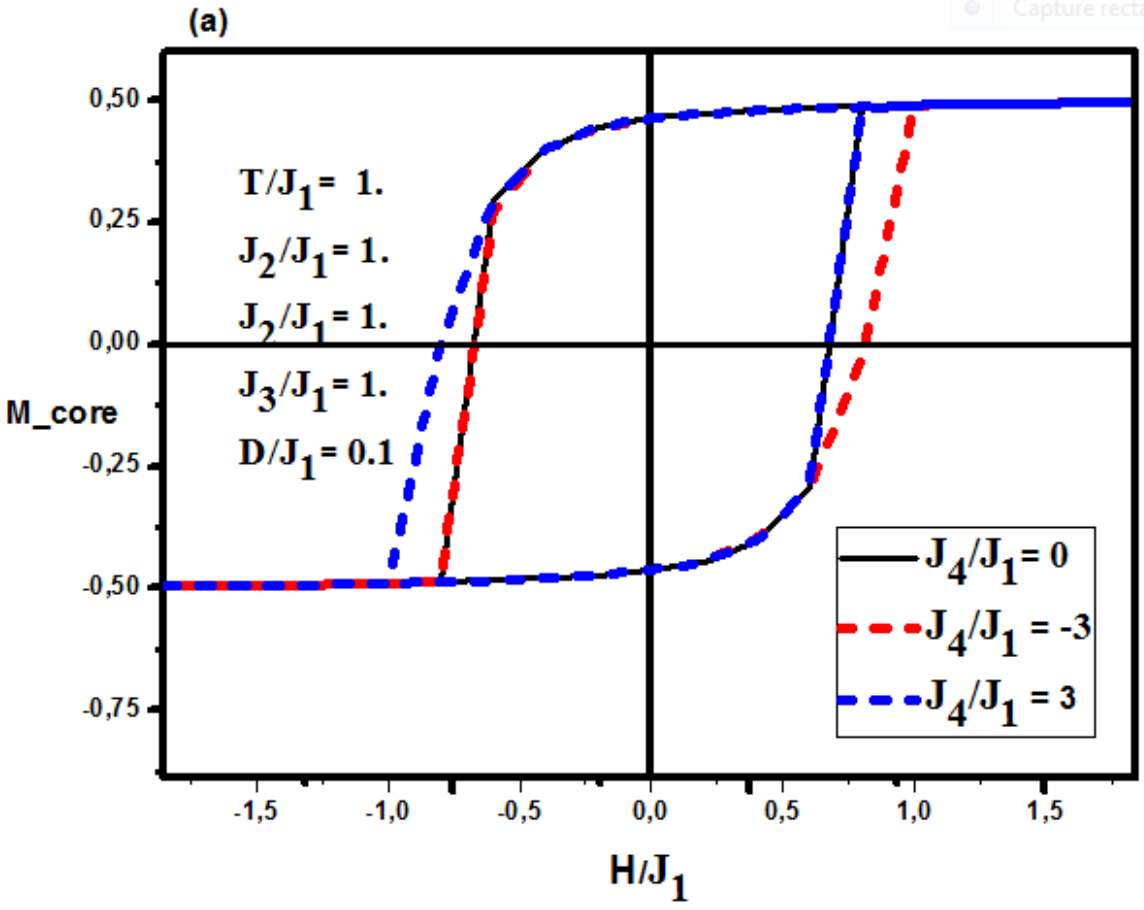
(a)
0,50
0,25
0,00
-0,25
-0,50
-0,75
M_core
T/J1= 1.
J2/J1= 1.
J2/J1= 1.
J3/J1= 1.
D/J1= 0.1
J4/J1= 0
J4/J1 = -3
J4/J1 = 3
-1,5
-1,0
-0,5
0,0
0,5
1,0
1,5
H/J1

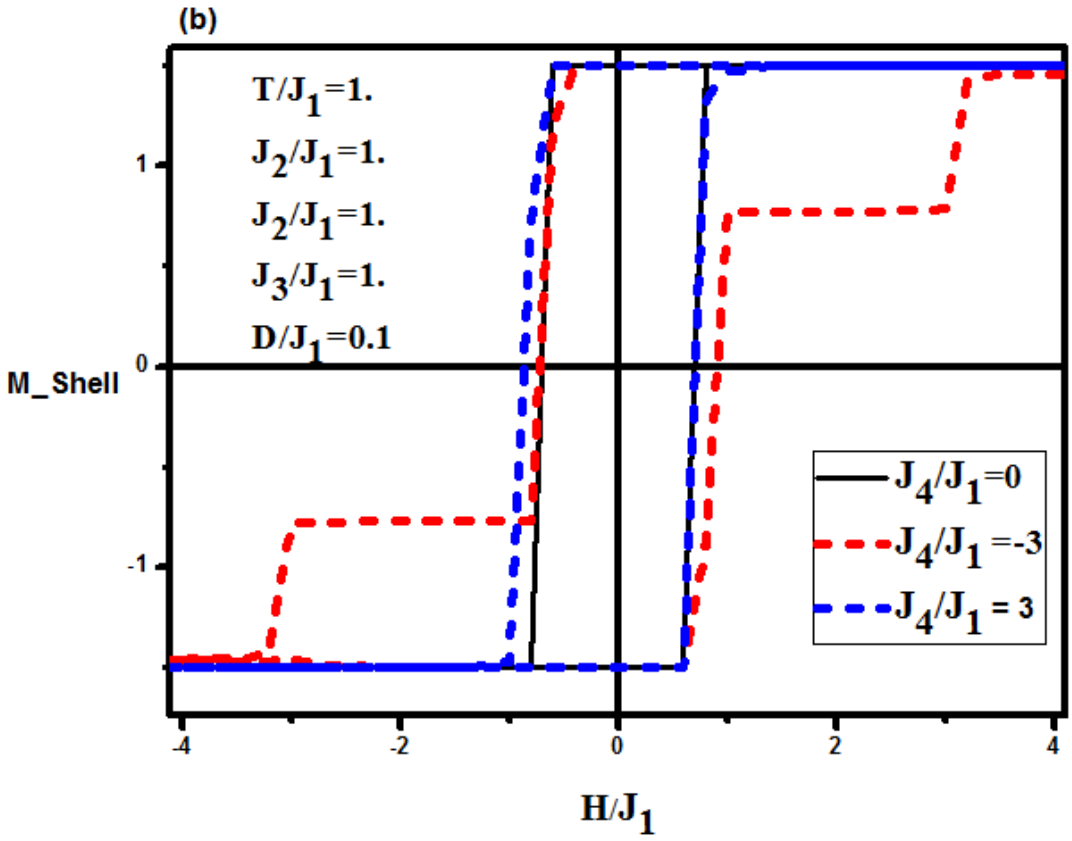
(b)
T/J1=1.
J2/J1=1.
J2/J1=1.
J3/J1=1.
D/J1=0.1
M_Shell
1
0
-1
-4
-2
0
2
4
H/J1
J4/J1=0
J4/J1 =-3
J4/J1 = 3

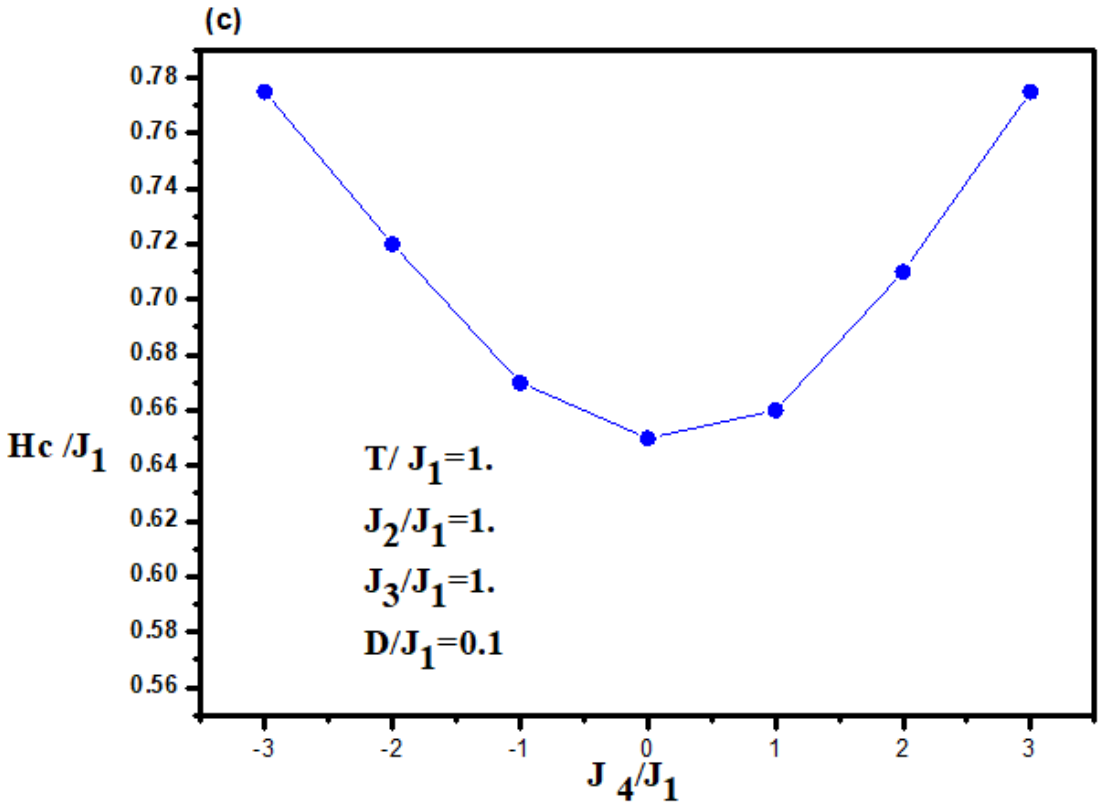

Figure 6.24: Hysteresis loops (a) core and (b) shell as a function of H/J_1, for $Lc = 6$ and $Ls = 2$, (c) J_4/J_1-dependent coercivity

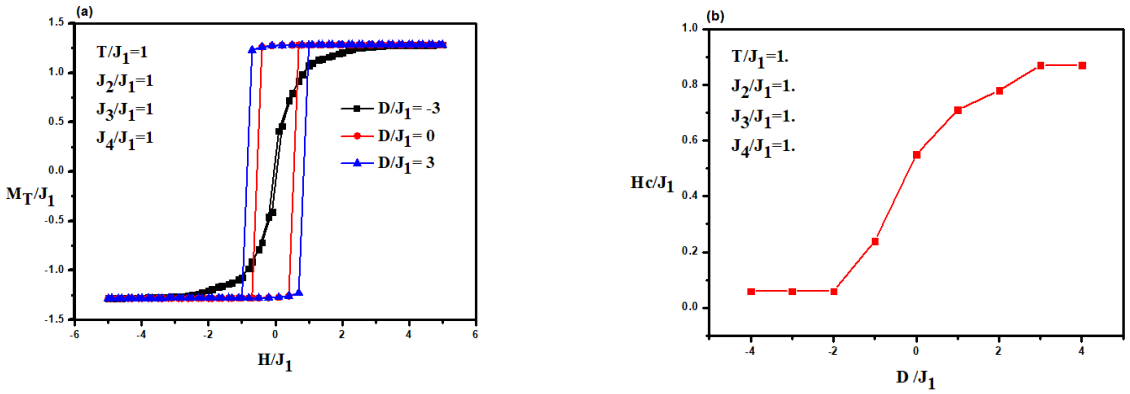

Figure 6.25: (a) Hysteresis loops as a function of D/J_1, for $Lc = 6$ and $Ls = 2$, (b) D/J_1-dependent coercivity.

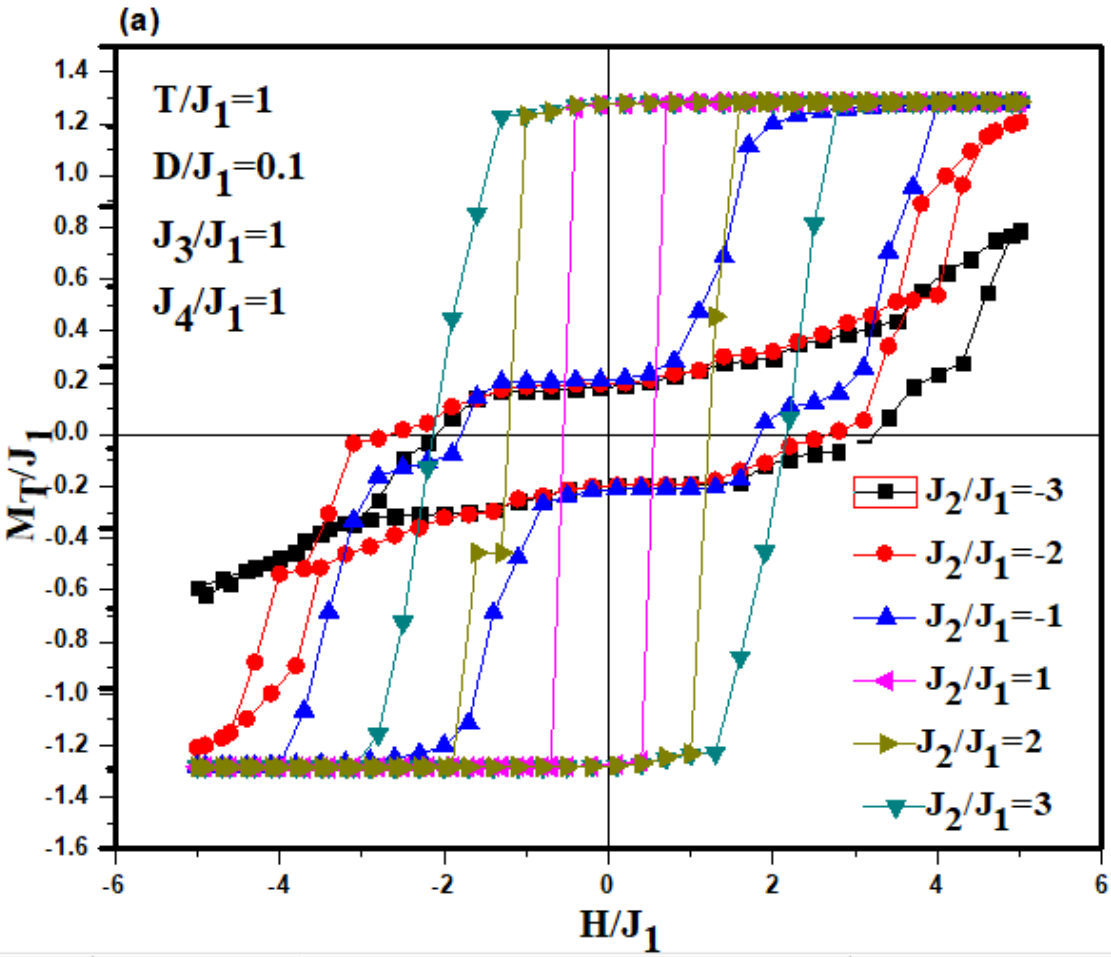
(a)
T/J1=1
D/J1=0.1
J3/J1=1
J4/J1=1
J2/J1=-3
J2/J1=-2
J2/J1=-1
J2/J1=1
J2/J1=2
J2/J1=3
MT/J1
H/J1
1.4
1.2
1.0
0.8
0.6
0.4
0.2
0.0
-0.2
-0.4
-0.6
-0.8
-1.0
-1.2
-1.4
-1.6
-6
-4
-2
0
2
4
6

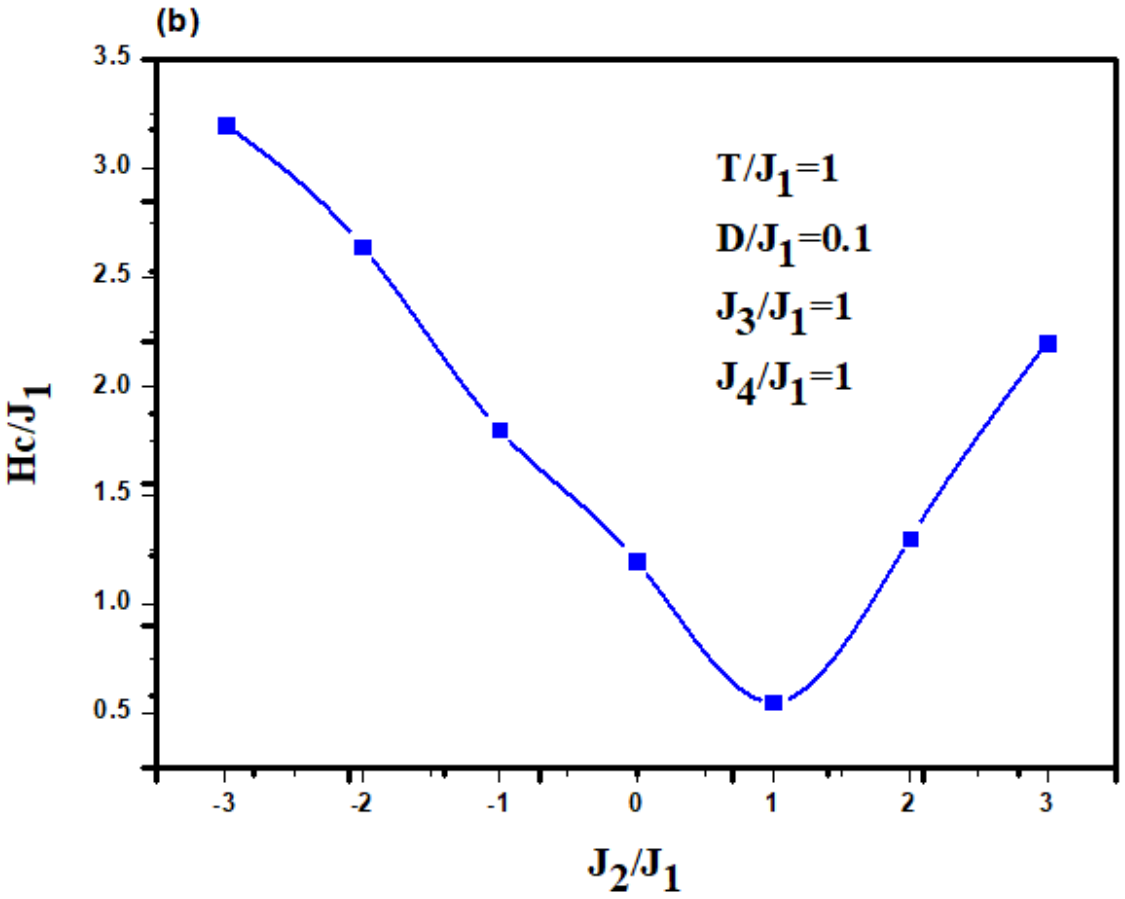

Figure 6.26: (a) Hysteresis loops as a function of J_2/J_1, for $Lc = 6$ and $Ls = 2$, (b) J_2/J_1-dependent coercivity

General conclusion

The aim of this thesis is the study of the behavior of the magnetic properties of isolated and interacting nanoparticles. Throughout this study, we have considered the cubic nanoparticles with uniaxial anisotropy. We have sought to control the overall magnetic properties of the nanoparticles. The effects of different factors have been considered intrinsic as the constant of anisotropy or extrinsic as the temperature and type of external excitation.

First, we have presented the generalities on magnetism and magnetic nanoparticles along with the discussion of the general magnetic properties of the magnetic nanoparticles and their prominence in the biomedical field, the storage of information and the magnetic sensors. These magnetic nanoparticles derive that importance from the above-mentioned properties and from their structures and morphologies. Then, we have given the description of both the Ising Hamiltonian model that we have used in our work and that of the Monte Carlo method. It is worth-mentioning that the fundamentals for Monte Carlo have been discussed starting from the principle of application to the measurement calculations balance through the implementation of the Metropolis algorithm.

In the following, we summarize the main results and the possible perspectives of each chapter:

In the fourth chapter, we have studied the magnetic properties, the phase diagrams of the fundamental state, the examination of the phase diagrams in the ground state and the exploration of the partial and total magnetization, the susceptibility and specific heat as a function of temperature and the critical behavior of simple perovskite $PbVO_3$ with spin $S = 1/2$ which is an important material used as a component in electronic devices. The study has been conducted by Monte Carlo simulation using the Ising 3D model. By scanning the different reduced values of the exchange interactions and the reduced parameter of the magnetic anisotropy, it has been shown that the phase diagrams of the system depend on the parameters mentioned above. These results correspond to the development and discussion of stable phases. Additionally, the transition temperature determined in this work ($T_N = 182K$) is in good agreement with the experimental value, $T_N = 190K$. The temperature transition also increases along with the increasing absolute value of the exchange coupling interactions. (J_{ab}, J_c). Further, by studying the effects of the system size, we have found that the peak of the magnetic susceptibility increases as the size of the network increases. To study the critical behavior of the material highlighted, we have calculated the critical exponents corresponding to the correlation length, the total magnetization and the susceptibility magnetic.

In the fifth chapter, using Monte Carlo simulation, we studied a trilayer spin (5/2;3/2;5/2) Ising nanocube. We have investigated the effects of the exchange couplings, the parapetre of anisotropy, the external magnetic field, the thickness ratio size r on the magnetic and thermodynamic properties. The phase diagrams are obtained for different reduced exchange couplings J_2/J_1 ($\sigma - \sigma$ interaction), J_3/J_1 ($\sigma - S$ interlayer intercation) and reduced parameter of anisotropy D/J_1 , where the exchange couplings between spins σ and between spins S respectivly J_1,J_2 are considered ferromagnetic while the interlayer exchange coupling J_3 is considered antiferromagnetic. According to the results, it is demonstrated that the system can exhibit the compensation behavior. For the present system, it is found whether the compensation point (T_{com}) appears in the system, depending on the existence of the critical exchange coupling J_2/J_1 and anisotropic parameter D/J_1. Decreasing J_2/J_1 and D/J_1 will be beneficial to the compensation behavior, whereas increasing J_2/J_1 and D/J_1 will promote the increase of the transition temperature (T_C). The phase diagram that present the T_C and T_{com} as a function of the reduced exchange coupling J2/J1 for different ratio thickness size r , we remark an inverse behavior concerning

transition temperature, in which there is a critical value of $J_2/J_1 = 0.45$. if $(J_2/J_1 > 0.45)$ we found that by increasing the ration thickness r ,the transition temperation T_C also increases. In contrary when $(J_2/J_1 < 0.45)$ increasing the ration thickness size r, T_C decreases. The combination of more than one magnetic element constituting a nanocube influences its magnetic behavior.

The sixth Chapter treat the case of the nanoparticles assemblies. In the first section we have studied the size effects and the coupling and anisotropy parameters on the magnetic properties of the ferromagnetic nanoparticles of Ising spin-1. It is already known that the studied system has the particularity of being a Rubik's cube that is composed of identical nanocubes This has been done using Monte Carlo simulation as part of the Ising 3D model. It has been shown that the phase diagrams depend on the parameters of the system and are affected not only by the size of the nano-system, but also by its size. Indeed, depending on the reduced exchange coupling, two regimes have been observed where the reduced critical temperature decreases and increases, respectively. The system presents second-order phase transitions at finite temperatures. Furthermore, an external magnetic field has been applied and we have studied the hysteresis loops for the selected low values of the temperature. then, It has been found that the response of the magnetization to the strength of the magnetic field shows hysteresis behaviors with simple loops where the reduced magnetic coercive field gets thinner and thinner till it is disappeared when going from t = 0,1 to t = 5. Finally, the variation of the coercive field as a function of size has revealed a well-known phenomenon of magnetic nano-materials with dipolar interactions, where the coercive field increases to reach the maximum and then decreases to zero when the size of the nanoparticles decreases. However, in our case, we have not found a coercive field reduced to zero for small sizes. We have attributed these phenomena to the structure and nature of our system. However, we have found that our results are qualitatively in agreement with other works.

In the seconde section, we have studied, in the same context of the nanocubes, the magnetic properties of the magnetic nanocubes chain (NCCM) of spin-1 using Monte Carlo simulations. The magnetic properties have been determined by scanning the values of the system parameters. The reduced transition temperatures have been established for the different sizes of NCCM cube $(Lc * Lc * Lc)$. It has been clear that the reduced transition temperature increases along with the increasing cube size (Lc).The coercive magnetic field increases with the increasing reduced exchange coupling and reduced anisotropy, while the coercive field decreases as the reduced temperature increases.

As for the third section, we investigated the magnetic properties of a nano-system with a Rubik's cube structure that consists of core/shell morphology nano-cubes, with spin-1/2 in the core and spin-3/2 on the Shell. This has been simulated by Monte Carlo method using the Ising 3D model based on a Metropolis algorithm. We have studied the effects of the system parameters on the phase diagrams for the different system sizes and hysteresis behaviors when we have applied the external magnetic field. It has been observed that the exchange couplings and magnetic anisotropy affect the phase diagrams. The increase of the positive exchange interactions between the core and shell spins, on the one hand, and between the nano-cubes, on the other hand, has the particularity of increasing the critical temperature, along with favoring the stable phase (3/2, 1/2). The same phase is also favored by the positive values of the magnetic anisotropy. For each phase, we have presented the configuration of the spins of our studied system. Moreover, the increase in the size of the system has caused the increase in the critical temperature, and as a result a typical behavior has been observed with the nano-systems. The study of the hysteresis behavior has shown that both the exchange coupling and the magnetic anisotropy control the coercivity.

Finally, this work has demonstrated that it is possible to control the magnetic order in cubic NPs by varying the sizes and numbers of the nanoparticles. In addition, the results obtained can serve as a point of comparison for the theoretical calculations on these types of systems to better understand the relationship between their magnetic properties and their structural and size factors.

As perspectives and to complete our work, other forms of assemblies of nanoparticles such as nanosphere, nanotubes could be modeled by the Monte Carlo method. Thus other properties such as electrical properties could be explored in other research works. In addition we plan to introduce other terms in the Hamiltonians namely the dipolar interaction and the interaction of Dzyaloshinskii-Moriya to explore other atypical properties caused by the nanostructure systems.

Publications

In This Thesis

Some of the research leading to this thesis has appeared previously in the following publications.

Journal Articles

- A.Kadiri,G. Dimitri.Ngantso, Y. EL Amraoui, H. Ez-Zahraouyet al **"Ferromagnetic Nanoparticles of Ising Spin-1 with a Rubik's Cube Structure: Monte Carlo Simulations."**. – *Journal of Superconductivity and Novel Magnetism*, (2018): 1-6.

- A.Kadiri, M. Arejdal ,M. Ait Tamerd,M.Bouadi,G. Dimitri Ngantso, Y. EL Amraoui, H. Ez-Zahraouy ,A. Benyoussef **"Effect of thickness size on magnetic behavior of layered Ising nanocube with Spins (5/2,3/2, 5/2):Monte Carlo simulations."**. –

- A.Kadiri,M. Arejdal, A. Abbassi, Y. EL Amraoui, H. Ez-Zahraouy et al **"Calculated Magnetic Properties of the Compound** $PbVO_3$**."**. – *Journal of Superconductivity and Novel Magnetism*, 30(8)(2017):2247-2253.

- M. Arejdal, A.AbbassiA.Kadiri et al **"The magnetic properties and magneto-caloric effect in the compound MnBi: The Monte Carlo study"**.. – *Journal of Magnetism and Magnetic Materials*, 466 (2016):463-468.

- M. Arejdal, A.Kadiri et al **"Magnetic Properties of the DoublePerovskite Ba2CoUO6: Ab Initio Method, Mean Field Approximation, and Monte Carlo Study."**. – *Journal of Superconductivity and Novel Magnetism*, 29.10(2016):2659-2667.

Bibliography

[1] D. Gatteschi, O. Kahn, J. S. Miller, and F. Palacio, *Magnetic molecular materials*, vol. 198. Springer Science & Business Media, 2012. 1, 46

[2] S.-B. Wang, Y.-L. Min, and S.-H. Yu *The Journal of Physical Chemistry C*, vol. 111, no. 9, pp. 3551–3554, 2007. 1, 59

[3] M. Vomir, R. Turnbull, I. Birced, P. Parreira, D. A. MacLaren, S. L. Lee, P. André, and J.-Y. Bigot *Nano Lett.*, vol. 16, no. 8, pp. 5291–5297, 2016. 1, 59

[4] M. E. McHenry *et al. Phys. Rev. B*, vol. 49, no. 16, pp. 11358–11363, 1994. 1, 76

[5] M. E. McHenry *et al. Bull Mater Sci*, vol. 22, no. 3, pp. 495–501, 1999. 1, 76

[6] V. F. Cardoso *et al. Adv Healthc Mater*, vol. 7, no. 5, 2018. 1, 76

[7] C. Kittel, P. McEuen, *et al.*, *Introduction to solid state physics*, vol. 8. Wiley New York, 1996. 1, 15

[8] C. Kittel *Reviews of modern Physics*, vol. 21, no. 4, p. 541, 1949. 1, 15

[9] V. V. Mody *et al. European Journal of Nanomedicine*, vol. 5, no. 1, pp. 11–21, 2013. 1, 19

[10] K. L. Kelly, E. Coronado, L. L. Zhao, and G. C. Schatz, "The optical properties of metal nanoparticles: the influence of size, shape, and dielectric environment," 2003. 1

[11] S. Pourmasoud, A. Sobhani-Nasab, M. Behpour, M. Rahimi-Nasrabadi, and F. Ahmadi, "Investigation of optical properties and the photocatalytic activity of synthesized ybyo4 nanoparticles and ybvo4/niwo4 nanocomposites by polymeric capping agents," *Journal of Molecular Structure*, vol. 1157, pp. 607–615, 2018. 1

[12] X. Ning, H. Yu, F. Peng, and H. Wang, "Pt nanoparticles interacting with graphitic nitrogen of n-doped carbon nanotubes: Effect of electronic properties on activity for aerobic oxidation of glycerol and electro-oxidation of co," *Journal of Catalysis*, vol. 325, pp. 136–144, 2015. 1

[13] A. López-Ortega, E. Lottini, C. d. J. Fernandez, and C. Sangregorio, "Exploring the magnetic properties of cobalt-ferrite nanoparticles for the development of a rare-earth-free permanent magnet," *Chemistry of Materials*, vol. 27, no. 11, pp. 4048–4056, 2015. 1

[14] D. Lisjak and A. Mertelj, "Anisotropic magnetic nanoparticles: A review of their properties, syntheses and potential applications," *Progress in Materials Science*, vol. 95, pp. 286–328, 2018. 1

[15] M.-C. Daniel and D. Astruc, "Gold nanoparticles: assembly, supramolecular chemistry, quantum-size-related properties, and applications toward biology, catalysis, and nanotechnology," *Chemical reviews*, vol. 104, no. 1, pp. 293–346, 2004. 1

[16] L. Gao and X. Yan, "Nanozymes: an emerging field bridging nanotechnology and biology," *Sci China Life Sci*, vol. 59, no. 4, pp. 400–402, 2016. 1

[17] S. Ahmed, M. Ahmad, B. L. Swami, and S. Ikram, "A review on plants extract mediated synthesis of silver nanoparticles for antimicrobial applications: a green expertise," *Journal of advanced research*, vol. 7, no. 1, pp. 17–28, 2016. 1

[18] S. Hasan, "A review on nanoparticles: their synthesis and types," *Research Journal of Recent Sciences* _____ *ISSN*, vol. 2277, p. 2502, 2015. 1

[19] T. Hyeon, "Chemical synthesis of magnetic nanoparticles," *Chemical Communications*, no. 8, pp. 927–934, 2003. 1

[20] A.-H. Lu, E. e. Salabas, and F. Schüth, "Magnetic nanoparticles: synthesis, protection, functionalization, and application," *Angewandte Chemie International Edition*, vol. 46, no. 8, pp. 1222–1244, 2007. 1

[21] Z. Shaterabadi, G. Nabiyouni, and M. Soleymani *Progress in biophysics and molecular biology*, vol. 133, pp. 9–19, 2018. 1, 46

[22] M. Shisode, P. B. Kharat, D. N. Bhoyar, V. Vinayak, M. Babrekar, and K. Jadhav, "Structural and multiferroic properties of ba2+ doped bifeo3 nanoparticles synthesized via sol-gel method," in *AIP Conference Proceedings*, vol. 1953, p. 030276, AIP Publishing, 2018. 1

[23] J. Frankel, "J. frankel and j. dorfman, nature (london) 126, 274 (1930)," *Nature (London)*, vol. 126, p. 274, 1930. 1

[24] L. Bogani and W. Wernsdorfer, "Molecular spintronics using single-molecule magnets," in *Nanoscience And Technology: A Collection of Reviews from Nature Journals*, pp. 194–201, World Scientific, 2010. 1

[25] W. Wernsdorfer, "Molecular nanomagnets: towards molecular spintronics," *International Journal of Nanotechnology*, vol. 7, no. 4, p. 497, 2010. 1

[26] R. Elilarassi and G. Chandrasekaran, "Optical, electrical and ferromagnetic studies of zno: Fe diluted magnetic semiconductor nanoparticles for spintronic applications," *Spectrochimica Acta Part A: Molecular and Biomolecular Spectroscopy*, vol. 186, pp. 120–131, 2017. 1

[27] V. Skumryev *et al. Nature*, vol. 423, no. 6942, pp. 850–853, 2003. 1, 59, 76

[28] R. H. Kodama *Journal of Magnetism and Magnetic Materials*, vol. 200, no. 1, pp. 359–372, 1999. 1, 46, 59

[29] S. P. Gubin, *Magnetic nanoparticles*. John Wiley & Sons, 2009. 1, 18, 76

[30] P. Tartaj, M. Morales, T. Gonzalez-Carreno, S. Veintemillas-Verdaguer, and C. Serna, "Advances in magnetic nanoparticles for biotechnology applications," *Journal of Magnetism and Magnetic Materials*, vol. 290, pp. 28–34, 2005. 1

[31] A. Hütten, D. Sudfeld, I. Ennen, G. Reiss, W. Hachmann, U. Heinzmann, K. Wojczykowski, P. Jutzi, W. Saikaly, and G. Thomas, "New magnetic nanoparticles for biotechnology," *Journal of biotechnology*, vol. 112, no. 1-2, pp. 47–63, 2004. 1

[32] S. C. McBain, H. H. Yiu, and J. Dobson, "Magnetic nanoparticles for gene and drug delivery," *International journal of nanomedicine*, vol. 3, no. 2, p. 169, 2008. 1

[33] S. V. Otari, S. K. Patel, S.-Y. Kim, J. R. Haw, V. C. Kalia, I.-W. Kim, and J.-K. Lee, "Copper ferrite magnetic nanoparticles for the immobilization of enzyme," *Indian journal of microbiology*, vol. 59, no. 1, pp. 105–108, 2019. 1

[34] M. Nikitin, A. Orlov, S. Znoyko, V. Bragina, B. Gorshkov, T. Ksenevich, V. Cherkasov, and P. Nikitin, "Multiplex biosensing with highly sensitive magnetic nanoparticle quantification method," *Journal of Magnetism and Magnetic Materials*, vol. 459, pp. 260–264, 2018. 1

[35] M. Hasanzadeh, N. Shadjou, and M. de la Guardia, "Iron and iron-oxide magnetic nanoparticles as signal-amplification elements in electrochemical biosensing," *TrAC Trends in Analytical Chemistry*, vol. 72, pp. 1–9, 2015. 1

[36] J. Kudr, Y. Haddad, L. Richtera, Z. Heger, M. Cernak, V. Adam, and O. Zitka, "Magnetic nanoparticles: From design and synthesis to real world applications," *Nanomaterials*, vol. 7, no. 9, p. 243, 2017. 1

[37] O. L. Gobbo, K. Sjaastad, M. W. Radomski, Y. Volkov, and A. Prina-Mello, "Magnetic nanoparticles in cancer theranostics," *Theranostics*, vol. 5, no. 11, p. 1249, 2015. 1

[38] J. Gallo, N. J. Long, and E. O. Aboagye, "Magnetic nanoparticles as contrast agents in the diagnosis and treatment of cancer," *Chemical Society Reviews*, vol. 42, no. 19, pp. 7816–7833, 2013. 1

[39] B. Thiesen and A. Jordan, "Clinical applications of magnetic nanoparticles for hyperthermia," *International journal of hyperthermia*, vol. 24, no. 6, pp. 467–474, 2008. 1

[40] Q. A. Pankhurst, J. Connolly, S. Jones, and J. Dobson, "Applications of magnetic nanoparticles in biomedicine," *Journal of physics D: Applied physics*, vol. 36, no. 13, p. R167, 2003. 1

[41] Q. Pankhurst, N. Thanh, S. Jones, and J. Dobson, "Progress in applications of magnetic nanoparticles in biomedicine," *Journal of Physics D: Applied Physics*, vol. 42, no. 22, p. 224001, 2009. 1, 46

[42] S. Spirou, S. Costa Lima, P. Bouziotis, S. Vranješ-Djurić, E. Efthimiadou, A. Laurenzana, A. Barbosa, I. Garcia-Alonso, C. Jones, D. Jankovic, *et al.*, "Recommendations for in vitro and in vivo testing of magnetic nanoparticle hyperthermia combined with radiation therapy," *Nanomaterials*, vol. 8, no. 5, p. 306, 2018. 1

[43] P. Tartaj, M. del Puerto Morales, S. Veintemillas-Verdaguer, T. González-Carreño, and C. J. Serna, "The preparation of magnetic nanoparticles for applications in biomedicine," *Journal of physics D: Applied physics*, vol. 36, no. 13, p. R182, 2003. 1

[44] R. M. Ferguson, A. P. Khandhar, S. J. Kemp, H. Arami, E. U. Saritas, L. R. Croft, J. Konkle, P. W. Goodwill, A. Halkola, J. Rahmer, *et al.*, "Magnetic particle imaging with tailored iron oxide nanoparticle tracers," *IEEE transactions on medical imaging*, vol. 34, no. 5, pp. 1077–1084, 2015. 1

[45] E. B. Ehlerding, P. Grodzinski, W. Cai, and C. H. Liu, "Big potential from small agents: nanoparticles for imaging-based companion diagnostics," *ACS nano*, vol. 12, no. 3, pp. 2106–2121, 2018. 1

[46] C. Yang, G. Lin, C. Zhu, X. Pang, Y. Zhang, X. Wang, X. Li, B. Wang, H. Xia, and G. Liu, "Metalla-aromatic loaded magnetic nanoparticles for mri/photoacoustic imaging-guided cancer phototherapy," *Journal of Materials Chemistry B*, vol. 6, no. 17, pp. 2528–2535, 2018. 1

[47] K. Ulbrich, K. Hola, V. Subr, A. Bakandritsos, J. Tucek, and R. Zboril, "Targeted drug delivery with polymers and magnetic nanoparticles: covalent and noncovalent approaches, release control, and clinical studies," *Chemical reviews*, vol. 116, no. 9, pp. 5338–5431, 2016. 1

[48] X. Mou, Z. Ali, S. Li, and N. He, "Applications of magnetic nanoparticles in targeted drug delivery system," *Journal of nanoscience and nanotechnology*, vol. 15, no. 1, pp. 54–62, 2015. 1

[49] K. Hola, Z. Markova, G. Zoppellaro, J. Tucek, and R. Zboril, "Tailored functionalization of iron oxide nanoparticles for mri, drug delivery, magnetic separation and immobilization of biosubstances," *Biotechnology advances*, vol. 33, no. 6, pp. 1162–1176, 2015. 1

[50] L. H. Reddy, J. L. Arias, J. Nicolas, and P. Couvreur, "Magnetic nanoparticles: design and characterization, toxicity and biocompatibility, pharmaceutical and biomedical applications," *Chemical reviews*, vol. 112, no. 11, pp. 5818–5878, 2012. 2

[51] H.-M. Yang, C. W. Park, S. Park, and J.-D. Kim, "Cross-linked magnetic nanoparticles with a biocompatible amide bond for cancer-targeted dual optical/magnetic resonance imaging," *Colloids and Surfaces B: Biointerfaces*, vol. 161, pp. 183–191, 2018. 2

[52] A. Winter, S. Engels, L. Reinhardt, C. Wasylow, H. Gerullis, and F. Wawroschek, "Magnetic marking and intraoperative detection of primary draining lymph nodes in high-risk prostate cancer using superparamagnetic iron oxide nanoparticles: additional diagnostic value," *Molecules*, vol. 22, no. 12, p. 2192, 2017. 2

[53] J. Haegele, N. Panagiotopoulos, S. Cremers, J. Rahmer, J. Franke, R. L. Duschka, S. Vaalma, M. Heidenreich, J. Borgert, P. Borm, *et al.*, "Magnetic particle imaging: A resovist based marking technology for guide wires and catheters for vascular interventions," *IEEE transactions on medical imaging*, vol. 35, no. 10, pp. 2312–2318, 2016. 2

[54] V. Nabaei, R. Chandrawati, and H. Heidari, "Magnetic biosensors: Modelling and simulation," *Biosensors and Bioelectronics*, vol. 103, pp. 69–86, 2018. 2

[55] X. Li, J. Wei, K. E. Aifantis, Y. Fan, Q. Feng, F.-Z. Cui, and F. Watari, "Current investigations into magnetic nanoparticles for biomedical applications," *Journal of Biomedical Materials Research Part A*, vol. 104, no. 5, pp. 1285–1296, 2016. 2

[56] S. Bharath, A. R. Sam, and K. Kalaivani, "Detection and quantification of pathogenic bacteria using giant magnetic resistance sensor," in *2015 IEEE Technological Innovation in ICT for Agriculture and Rural Development (TIAR)*, pp. 160–164, IEEE, 2015. 2

[57] I. Ennen, D. Kappe, T. Rempel, C. Glenske, and A. Hütten, "Giant magnetoresistance: Basic concepts, microstructure, magnetic interactions and applications," *Sensors*, vol. 16, no. 6, p. 904, 2016. 2

[58] C. Reig, S. Cardoso, and S. C. Mukhopadhyay, "Giant magnetoresistance (gmr) sensors," *SSMI6*, vol. 1, pp. 157–80, 2013. 2

[59] X. Zhang, N. Vernier, Z. Cao, Q. Leng, A. Cao, D. Ravelosona, and Z. Weisheng, "Magnetoresistive sensors based on the elasticity of domain walls," *Nanotechnology*, 2018. 2

[60] S. Fathi Karkan, M. Mohammadhosseini, Y. Panahi, M. Milani, N. Zarghami, A. Akbarzadeh, E. Abasi, A. Hosseini, and S. Davaran, "Magnetic nanoparticles in cancer diagnosis and treatment: a review," *Artificial cells, nanomedicine, and biotechnology*, vol. 45, no. 1, pp. 1–5, 2017. 3

[61] S. A. A. Imhmed *et al.*, *Application of magnetic susceptibility measurements to oilfield scale management.* PhD thesis, Heriot-Watt University, 2012. 5

[62] A. Guinier and R. Jullien, *La Matière à l'état solide: des supraconducteurs aux superalliages.* Hachette, 1987. 5

[63] É. d. T. de Lacheisserie, *Magnétisme*, vol. 2. Edp Sciences, 2012. 5

[64] U. Jeong, X. Teng, Y. Wang, *et al. Advanced Materials*, vol. 19, no. 1, pp. 33–60, 2007. 6

[65] P. Mohn, *Magnetism in the solid state: an introduction*, vol. 134. Springer Science & Business Media, 2006. 7

[66] "Archive Larousse : Grande Encyclopédie Larousse." 8

[67] M. Altunbulak, *The Pauli principle, representation theory, and geometry of flag varieties.* PhD thesis, Ph. D. thesis, Bilkent University, 2008.[11] AA Klyachko, The Pauli . . . , 2008. 9

[68] R. L. Conte, "Magnetic nanostructures with structural inversion asymmetry," 2015. 9

[69] I. Dzyaloshinsky *Journal of Physics and Chemistry of Solids*, vol. 4, no. 4, pp. 241–255, 1958. 10

[70] T. Moriya *Physical Review*, vol. 120, no. 1, p. 91, 1960. 10

[71] P. Robert, *Traité d'électricité : Matériaux de l'électrotechnique Volume 2.* Lausanne : Presses polytechniques et universitaires Romandes, 1989. 12

[72] P. BRISSONNEAU, "Aimants permanents: Principes et circuits magnétiques," *Techniques de l'ingénieur. Génie électrique*, vol. 2, no. D2090, pp. 2090–1, 1990. 12

[73] R. Skomski, *Simple models of magnetism*. Oxford University Press on Demand, 2008. 14

[74] S. Mustafa, *Chapter 4 Size–dependent structure parameter for silicon nanowires and nanoparticles 4.1. Introduction*. PhD thesis, 10 2010. 16

[75] https://www.tf.uni-kiel.de/matwis/amat/admat$_e n/kap_4/backbone/r4_{33}.html$. 17

[76] W. F. Brown *Annals of the New York Academy of Sciences*, vol. 147, no. 12, pp. 463–488, 1969. 18

[77] L.-M. Lacroix, S. Lachaize, A. Falqui, T. Blon, J. Carrey, M. Respaud, F. Dumestre, C. Amiens, O. Margeat, B. Chaudret, *et al.*, "Ultrasmall iron nanoparticles: Effect of size reduction on anisotropy and magnetization," *Journal of Applied Physics*, vol. 103, no. 7, p. 07D521, 2008. 18

[78] O. Popov and M. Mikhov *physica status solidi (a)*, vol. 118, no. 1, pp. 289–294, 1990. 19

[79] R. Sappey, *Etude de la dynamique de nanoparticules magnetiques dans la limite des tres basses temperatures*. PhD thesis, Paris 11, 1997. 19

[80] J. Osborn, "Demagnetizing factors of the general ellipsoid," *Physical review*, vol. 67, no. 11-12, p. 351, 1945. 20

[81] E.-D. Ciuculescu, *Synthèse et étude des propriétés de nanoparticules magnétiques de type coeur-coquille*. PhD thesis, Université de Toulouse, Université Toulouse III-Paul Sabatier, 2007. 20

[82] *Chemical Communications*, vol. 47, no. 43, pp. 11954–11956, 2011. 21

[83] *Journal of Non-Crystalline Solids*, vol. 353, no. 8-10, pp. 743–747, 2007. 21

[84] S. Oldenburg *et al. Chemical Physics Letters*, vol. 288, no. 2-4, pp. 243–247, 1998. 21

[85] R. Ghosh Chaudhuri and S. Paria *Chemical reviews*, vol. 112, no. 4, pp. 2373–2433, 2011. 21

[86] N. L. Dhas *et al.* in *Inorganic Frameworks as Smart Nanomedicines*, pp. 387–448, Elsevier, 2018. 22, 23

[87] I. A. Hadjiagapiou, A. Malakis, and S. Martinos *Physica A: Statistical Mechanics and its Applications*, vol. 387, no. 10, pp. 2256–2266, 2008. 24

[88] W. Heisenberg, "Zur theorie des ferromagnetismus," in *Original Scientific Papers Wissenschaftliche Originalarbeiten*, pp. 580–597, Springer, 1985. 24

[89] E. Ising *Zeitschrift für Physik*, vol. 31, no. 1, pp. 253–258, 1925. 24, 27

[90] M. Blume, "Theory of the first-order magnetic phase change in u o 2," *Physical Review*, vol. 141, no. 2, p. 517, 1966. 24

[91] S. Capponi *et al. Physical Review E*, vol. 89, no. 6, p. 062136, 2014. 24

[92] U. Lucia *Physica A: Statistical Mechanics and its Applications*, vol. 392, no. 5, pp. 1051–1062, 2013. 24

[93] R. Bennett, "100 Years of Moore's Law," 2015. 25

[94] "The best of the 20th century: Editors name Top 10 Algorithms." 26

[95] A. Knapp, "Chinese supercomputer is now the world's fastest-by a lot," 2013. 26

[96] L. Wilhelm *PhysikalischeZeitschrift*, vol. 21, pp. 613–615, 1920. 27

[97] R. B. Potts vol. 48, no. 1, pp. 106–109, 1952. 27

[98] J. Ashkin and E. Teller *Physical Review*, vol. 64, no. 5-6, p. 178, 1943. 27

[99] H. E. Stanley, "Phase transitions and critical phenomena," 1971. 27

[100] R. J. Baxter, *Exactly solved models in statistical mechanics*. Elsevier, 2016. 27

[101] L. Onsager *Physical Review*, vol. 65, no. 3-4, p. 117, 1944. 28

[102] Y. Velenik, "Le modèle d'ising," 2009. 28

[103] N. Metropolis *et al. The journal of chemical physics*, vol. 21, no. 6, pp. 1087–1092, 1953. 28

[104] B. Alder and T. Wainwright, "Statistical mechanical theory of transport properties," *Proceedings of the international union of pure and applied physics, Brussels*, 1956. 28

[105] F. James *Reports on progress in Physics*, vol. 43, no. 9, p. 1145, 1980. 31, 59

[106] M. P. Allen, D. J. Tildesley, *et al.*, *Computer simulation of liquids*. Oxford University Press, Oxford New York, 1987. 32, 59

[107] M. Arejdal, "Theoretical study of the magnetic properties and the magnetocaloric effect of materials: Spintronics materials (dendrimer models) and magnetic refrigeration materials (mnas/mnbi)," 2017. 34

[108] J. Ashkin, "J. ashkin and e. teller, phys. rev. 64, 178 (1943).," *Phys. Rev.*, vol. 64, p. 178, 1943. 36

[109] R. V. Shpanchenko, V. V. Chernaya, *et al. Chemistry of materials*, vol. 16, no. 17, pp. 3267–3273, 2004. 38

[110] N. A. Spaldin, S.-W. Cheong, and R. Ramesh, "Multiferroics: Past, present, and future," *Phys. Today*, vol. 63, no. 10, pp. 38–43, 2010. 38

[111] M. Fiebig *J. Phys. D: Appl. Phys.*, vol. 38, no. 8, p. R123, 2005. 38

[112] A. A. Belik *et al. Chemistry of materials*, vol. 17, no. 2, pp. 269–273, 2005. 38, 39, 42

[113] A. A. Belik, S. Iikubo, *et al.*, "Neutron powder diffraction study on the crystal and magnetic structures of bicoo3," *Chemistry of materials*, vol. 18, no. 3, pp. 798–803, 2006. 38, 39

[114] K. Oka, I. Yamada, *et al.*, "Magnetic ground-state of perovskite pbvo3 with large tetragonal distortion," *Inorganic chemistry*, vol. 47, no. 16, pp. 7355–7359, 2008. 38

[115] P. Ravindran, R. Vidya, O. Eriksson, and H. Fjellvåg *Advanced Materials*, vol. 20, pp. 1353–1356, 2008. 38

[116] S. Alam, J. Ahmad, Y. Ohya, *et al. J. Phys. Soc. Jpn.*, vol. 81, no. 7, p. 074709, 2012. 38

[117] I. V. Solovyev *Phys. Rev. B*, vol. 85, no. 5, p. 054420, 2012. 38

[118] J. B. Goodenough and J. Zhou *Sci Technol Adv Mater*, vol. 16, no. 3, 2015. 38

[119] A. A. Tsirlin, A. A. Belik, R. V. Shpanchenko, E. V. Antipov, E. Takayama-Muromachi, and H. Rosner *Phys. Rev. B*, vol. 77, no. 9, p. 092402, 2008. 38

[120] M. A. Boles, M. Engel, and D. V. Talapin *Chem. Rev.*, vol. 116, no. 18, pp. 11220–11289, 2016. 38, 70

[121] S. yao Yan, Y. Xie, T. Liu, and H. tao Yu *Journal of Physics: Condensed Matter*, vol. 22, no. 12, p. 125501, 2010. 38

[122] X. Ming, J.-W. Yin, X.-L. Wang, C.-Z. Wang, Z.-F. Huang, and G. Chen *Solid State Sciences*, vol. 12, no. 5, pp. 938 – 945, 2010. 38

[123] D. J. Singh *Phys. Rev. B*, vol. 73, p. 094102, 2006. 38

[124] M. Lane W. *Applied Physics Letters*, vol. 90, no. 6, 2007. 38

[125] A. Kumar, L. W. Martin, *et al. Phys. Rev. B*, vol. 75, p. 060101, 2007. 38

[126] A. Kumar, N. J. Podraza, S. Denev, J. Li, L. W. Martin, Y.-H. Chu, R. Ramesh, R. W. Collins, and V. Gopalan *Applied Physics Letters*, vol. 92, no. 23, p. 231915, 2008. 38

[127] R. V. Shpanchenko *ChemInform*, vol. 35, 2004. 38

[128] Y. Uratani, T. Shishidou, F. Ishii, and T. Oguchi *Japanese Journal of Applied Physics*, vol. 44, no. 9S, p. 7130, 2005. 38

[129] M.-Q. Cai, J.-C. Liu, *et al. The Journal of chemical physics*, vol. 126, no. 15, p. 154708, 2007. 38

[130] L. P. Kadanoff, *Statistical physics: statics, dynamics and renormalization*. World Scientific Publishing Company, 2000. 43

[131] V. Skumryev, S. Stoyanov, Y. Zhang, G. Hadjipanayis, D. Givord, and J. Nogués *Nature*, vol. 423, no. 6942, pp. 850–853, 2003. 46

[132] R. Zou, S. Gong, *et al. Chemistry of Materials*, vol. 29, no. 9, pp. 3938–3946, 2017. 46, 76

[133] D. Matatagui, O. Kolokoltsev, N. Qureshi, E. Mejía-Uriarte, C. Ordoñez-Romero, A. Vázquez-Olmos, and J. Saniger, "Magnonic sensor array based on magnetic nanoparticles to detect, discriminate and classify toxic gases," *Sensors and Actuators B: Chemical*, vol. 240, pp. 497–502, 2017. 46

[134] X. Du and J. Zhou, "Application of biosensors to detection of epidemic diseases in animals," *Research in veterinary science*, 2018. 46

[135] H. Zeng, J. Li, J. P. Liu, Z. L. Wang, and S. Sun *Nature*, vol. 420, no. 6914, pp. 395–398, 2002. 46, 59, 76

[136] M. Angelakeris, "Magnetic nanoparticles: A multifunctional vehicle for modern theranostics," *Biochimica et Biophysica Acta (BBA)-General Subjects*, vol. 1861, no. 6, pp. 1642–1651, 2017. 46

[137] A. Lopez-Ortega, M. Estrader, G. Salazar-Alvarez, A. G. Roca, and J. Nogues, "Applications of exchange coupled bi-magnetic hard/soft and soft/hard magnetic core/shell nanoparticles," *Physics Reports*, vol. 553, pp. 1–32, 2015. 46

[138] A. Tovstolytkin, M. Kulyk, V. Kalita, S. Ryabchenko, V. Zamorskyi, O. Fedorchuk, S. Solopan, and A. Belous, "Nickel-zinc spinel nanoferrites: Magnetic characterization and prospects of the use in self-controlled magnetic hyperthermia," *Journal of Magnetism and Magnetic Materials*, vol. 473, pp. 422–427, 2019. 46

[139] O. L. Lanier, A. G. Monsalve, P. S. McFetridge, and J. Dobson, "Magnetically triggered release of biologics," *International Materials Reviews*, pp. 1–28, 2018. 46

[140] K. Chesnel, D. Griner, D. Smith, Y. Cai, M. Trevino, B. Newbold, T. Wang, T. Liu, E. Jal, A. Reid, *et al.*, "Unraveling nanoscale magnetic ordering in fe3o4 nanoparticle assemblies via x-rays," *Magnetochemistry*, vol. 4, no. 4, p. 42, 2018. 46

[141] I. Lyubutin, S. Starchikov, A. Baskakov, N. Gervits, C.-R. Lin, Y.-T. Tseng, W.-J. Lee, and K.-Y. Shih, "Exchange-coupling of hard and soft magnetic sublattices and magnetic anomalies in mixed spinel nife0. 75cr1. 25o4 nanoparticles," *Journal of Magnetism and Magnetic Materials*, vol. 451, pp. 336–343, 2018. 46

[142] W. Wang, D.-d. Chen, D. Lv, J.-p. Liu, Q. Li, and Z. Peng, "Monte carlo study of magnetic and thermodynamic properties of a ferrimagnetic ising nanoparticle with hexagonal core-shell structure," *Journal of Physics and Chemistry of Solids*, vol. 108, pp. 39–51, 2017. 46

[143] H. Magoussi, A. Zaim, and M. Kerouad *Solid State Communications*, vol. 200, pp. 32–41, 2014. 46, 59

[144] E. Vatansever *Physics Letters A*, vol. 381, no. 18, pp. 1535–1542, 2017. 46, 59, 76

[145] Y. Yüksel, E. Aydıner, and H. Polat *Journal of Magnetism and Magnetic Materials*, vol. 323, pp. 3168–3175, 2011. 46, 59

[146] A. Kadiri, G. D. Ngantso, Y. EL Amraoui, H. Ez-Zahraouy, A. Elkenz, and A. Benyoussef *J Supercond Nov Magn*, 2018. 46, 75, 76

[147] A. F. Schäffer, A. Sukhov, and J. Berakdar *Journal of Magnetism and Magnetic Materials*, vol. 438, pp. 70–75, 2017. 46, 59, 76

[148] I. J. L. Diaz and N. d. S. Branco, "Monte carlo simulations of an ising bilayer with non-equivalent planes," *Physica A: Statistical Mechanics and its Applications*, vol. 468, pp. 158–170, 2017. 46

[149] I. Diaz and N. Branco, "Ferrimagnetism and compensation temperature in spin-1/2 ising trilayers," *Physica B: Condensed Matter*, vol. 529, pp. 73–79, 2018. 46, 50

[150] R. E. Camley and J. Barnaś, "Theory of giant magnetoresistance effects in magnetic layered structures with antiferromagnetic coupling," *Physical review letters*, vol. 63, no. 6, p. 664, 1989. 46

[151] A. Berkowitz, J. Mitchell, M. Carey, A. Young, S. Zhang, F. Spada, F. Parker, A. Hutten, and G. Thomas, "Giant magnetoresistance in heterogeneous cu-co alloys," *Physical Review Letters*, vol. 68, no. 25, p. 3745, 1992. 46

[152] M.-H. Phan and S.-C. Yu, "Review of the magnetocaloric effect in manganite materials," *Journal of Magnetism and Magnetic Materials*, vol. 308, no. 2, pp. 325–340, 2007. 46

[153] K. El Maalam, M. Balli, S. Habouti, M. Dietze, M. Hamedoun, E.-K. Hlil, M. Es-Souni, A. El Kenz, A. Benyoussef, and O. Mounkachi, "Composite (la0. 45nd0. 25) sr0. 3mno3/5cuo materials for magnetic refrigeration applications," *Journal of Magnetism and Magnetic Materials*, vol. 449, pp. 25–32, 2018. 46

[154] K. Das and I. Das, "Magnetocaloric effect study of ferromagnetic-charge ordered core-shell type manganite nanostructures," *Journal of Magnetism and Magnetic Materials*, vol. 436, pp. 97–100, 2017. 46

[155] L. Jiang, J. Zhang, Z. Chen, Q. Feng, and Z. Huang, "Monte carlo study of magnetic properties for the mixed spin-3/2 and spin-1 ferrimagnetic nanoparticles," *Physica B: Condensed Matter*, vol. 405, no. 1, pp. 420–424, 2010. 47

[156] B. Boughazi, M. Boughrara, and M. Kerouad *Physica A: Statistical Mechanics and its Applications*, vol. 465, pp. 628–635, 2017. 47, 79

[157] T. Kaneyoshi, "Ferrimagnetism in an ising bilayer film with a transverse field and nonmagnetic interlayers," *Journal of Superconductivity and Novel Magnetism*, vol. 31, no. 6, pp. 1949–1954, 2018. 47

[158] N. Sehdev, R. Medwal, R. Malik, A. Kandasami, D. Kanjilal, and S. Annapoorni, "Thermal annealing and transient electronic excitations induced interfacial and magnetic effects on pt/co/pt trilayer," *Nuclear Instruments and Methods in Physics Research Section B: Beam Interactions with Materials and Atoms*, vol. 420, pp. 50–56, 2018. 47

[159] J. P. Santos and F. S. Barreto, "An effective-field theory study of trilayer ising nanostructure: Thermodynamic and magnetic properties," *Journal of Magnetism and Magnetic Materials*, vol. 439, pp. 114–119, 2017. 47

[160] I. J. L. Diaz and N. d. S. Branco, "Monte carlo study of an anisotropic ising multilayer with antiferromagnetic interlayer couplings," *Physica A: Statistical Mechanics and its Applications*, vol. 490, pp. 904–917, 2018. 47

[161] N. De La Espriella, J. Madera, and G. Buendía, "Critical phenomena in a mixed spin-3/2 and spin-5/2 ising ferro-ferrimagnetic system in a longitudinal magnetic field," *Journal of Magnetism and Magnetic Materials*, vol. 442, pp. 350–359, 2017. 50

[162] M. Keskin and M. Ertaş, "Frequency-dependent dynamic magnetic properties of the ising bilayer system consisting of spin-3/2 and spin-5/2 spins," *Physica A: Statistical Mechanics and its Applications*, vol. 496, pp. 79–89, 2018. 50

[163] A. Özkılıç and Ü. Temizer, "Dynamic phase transitions and compensation temperatures in the mixed spin-1 and spin-5/2 ising system on alternate layers of a hexagonal lattice," *Journal of Magnetism and Magnetic Materials*, vol. 330, pp. 55–65, 2013. 50

[164] X.-W. Wei, G.-X. Zhu, Y.-J. Liu, Y.-H. Ni, Y. Song, and Z. Xu, "Large-scale controlled synthesis of feco nanocubes and microcages by wet chemistry," *Chemistry of Materials*, vol. 20, no. 19, pp. 6248–6253, 2008. 56

[165] A. Zaim, M. Kerouad, and Y. E. Amraoui *Journal of Magnetism and Magnetic Materials*, vol. 321, no. 8, pp. 1077–1083, 2009. 59, 76

[166] D. Kechrakos, K. N. Trohidou, and M. Vasilakaki *Journal of Magnetism and Magnetic Materials*, vol. 316, no. 2, pp. e291–e294, 2007. arXiv: cond-mat/0607038. 59

[167] S. Venkateswarlu, B. N. Kumar, B. Prathima, Y. SubbaRao, and N. V. V. Jyothi *Arabian Journal of Chemistry*, 2014. 59

[168] Y. Ichino, Y. Yoshida, and S. Miura *Jpn. J. Appl. Phys.*, vol. 56, no. 1, p. 015601, 2016. 59, 76

[169] K. Slyusarenko, D. Constantin, and P. Davidson *The Journal of Chemical Physics*, vol. 140, no. 10, p. 104904, 2014. 59

[170] A. Zaim, M. Kerouad, Y. E. Amraoui, and D. Baldomir *Journal of Magnetism and Magnetic Materials*, vol. 316, no. 2, pp. e306–e308, 2007. 59, 76

[171] T. Kaneyoshi *Physica A: Statistical Mechanics and its Applications*, vol. 390, no. 21-22, pp. 3697–3703, 2011. 59, 76

[172] A. Ghaddar, F. Gloaguen, and J. Gieraltowski *J. Phys.: Conf. Ser.*, vol. 200, no. 7, p. 072032, 2010. 59

[173] Y. P. Ivanov, A. Alfadhel, *et al. Sci Rep*, vol. 6, p. 24189, 2016. 59

[174] M. Arejdal, A. Jabar, *et al. J Supercond Nov Magn*, vol. 28, no. 11, pp. 3371–3378, 2015. 59, 75, 76

[175] M. Arejdal, A. Jabar, *et al. Journal of Superconductivity and Novel Magnetism*, vol. 29, no. 10, pp. 2553–2558, 2016. 59, 76

[176] M. Arejdal *et al. Physica B: Condensed Matter*, vol. 504, pp. 116–120, 2017. 59, 76

[177] R. Masrour *et al. Journal of Magnetism and Magnetic Materials*, vol. 417, pp. 397–400, 2016. 59, 76

[178] H. Matsumura and T. Ando *J. Phys. Soc. Jpn.*, vol. 70, no. 9, pp. 2657–2665, 2001. 59

[179] A. Zaim, M. Kerouad, M. Boughrara, A. Ainane, and J. J. d. Miguel *J Supercond Nov Magn*, vol. 25, no. 7, pp. 2407–2414, 2012. 59

[180] E. Vatansever and H. Polat *Journal of Magnetism and Magnetic Materials*, vol. 343, pp. 221–227, 2013. 59, 76

[181] T.-J. Yoon, H. Lee, H. Shao, and R. Weissleder *Angew. Chem. Int. Ed. Engl.*, vol. 50, no. 20, pp. 4663–4666, 2011. 59

[182] C. Alexiou, A. Schmidt, R. Klein, P. Hulin, C. Bergemann, and W. Arnold *Journal of Magnetism and Magnetic Materials*, vol. 252, pp. 363–366, 2002. 59

[183] J.-H. Lee, J.-T. Jang, J.-S. Choi, S. H. Moon, S.-H. Noh, J.-W. Kim, J.-G. Kim, I.-S. Kim, K. I. Park, and J. Cheon *Nat Nanotechnol*, vol. 6, no. 7, pp. 418–422, 2011. 59

[184] L. Xi, Z. Wang, Y. Zuo, and X. Shi *Nanotechnology*, vol. 22, no. 4, p. 045707, 2011. 59

[185] G. Kurlyandskaya, M. Sanchez, B. Hernando, V. Prida, P. Gorria, and M. Tejedor *Applied physics letters*, vol. 82, no. 18, pp. 3053–3055, 2003. 59, 76

[186] I. Groza, R. Morel, A. Brenac, C. Beigne, and L. Notin *IEEE Transactions on Magnetics*, vol. 47, no. 10, pp. 3355–3357, 2011. 59, 76

[187] T. Kaneyoshi *Journal of Magnetism and Magnetic Materials*, vol. 321, no. 20, pp. 3430–3435, 2009. 59, 76

[188] T. Kaneyoshi *physica status solidi (b)*, vol. 246, no. 10, pp. 2359–2365, 2009. 59

[189] T. Kaneyoshi *physica status solidi (b)*, vol. 248, no. 1, pp. 250–258, 2011. 59, 76

[190] T. Kaneyoshi *Journal of Magnetism and Magnetic Materials*, vol. 323, no. 9, pp. 1145–1151, 2011. 59

[191] D. A. Garanin and H. Kachkachi *Phys. Rev. Lett.*, vol. 90, no. 6, p. 065504, 2003. 59, 76

[192] H.-Y. Wang, Y.-S. Zhou, E. Wang, and D. Lin *Chinese Journal of Physics*, vol. 39, no. 1, pp. 85–89, 2001. 59

[193] H. Wang, Y. Zhou, D. L. Lin, and C. Wang *physica status solidi (b)*, vol. 232, no. 2, pp. 254–263, 2002. 59, 76

[194] A. Shavel *et al. Advanced Functional Materials*, vol. 17, no. 18, pp. 3870–3876, 2007. 59, 76, 84

[195] B. P. Pichon *et al. Chem. Mater.*, vol. 23, no. 11, pp. 2886–2900, 2011. 59

[196] F. Kronast *et al. Nano Lett.*, vol. 11, no. 4, pp. 1710–1715, 2011. 59

[197] E. Wetterskog, C.-W. Tai, *et al. ACS nano*, vol. 7, no. 8, pp. 7132–7144, 2013. 59

[198] A. P. LaGrow, B. Ingham, *et al. J. Am. Chem. Soc.*, vol. 134, no. 2, pp. 855–858, 2012. 59, 70

[199] A. Sathya, P. Guardia, R. Brescia, *et al. Chem. Mater.*, vol. 28, no. 6, pp. 1769–1780, 2016. 59, 65, 76

[200] Y. Wang, Y. Zheng, C. Z. Huang, and Y. Xia *J Am Chem Soc*, vol. 135, no. 5, pp. 1941–1951, 2013. 59

[201] H. J. Han, T. Yu, W.-S. Kim, and S. H. Im *Journal of Crystal Growth*, vol. 469, pp. 48–53, 2017. 59

[202] Y. Yu *et al. Adv. Mater. Weinheim*, vol. 25, no. 22, pp. 3090–3094, 2013.

[203] A. E. Berkowitz, R. H. Kodama, S. A. Makhlouf, F. T. Parker, F. E. Spada, E. J. McNiff, and S. Foner *Journal of Magnetism and Magnetic Materials*, vol. 196-197, pp. 591–594, 1999. 65

[204] Z. Nie, A. Petukhova, and E. Kumacheva *Nat Nanotechnol*, vol. 5, no. 1, pp. 15–25, 2010. 70

[205] K. J. Bishop, C. E. Wilmer, S. Soh, and B. A. Grzybowski, "Nanoscale forces and their uses in self-assembly," *small*, vol. 5, no. 14, pp. 1600–1630, 2009. 70

[206] G. A. Prinz, "Magnetoelectronics," *science*, vol. 282, no. 5394, pp. 1660–1663, 1998. 70

[207] R. H. Kodama *Journal of Magnetism and Magnetic Materials*, vol. 200, no. 1, pp. 359–372, 1999. 70

[208] H. F. Hamann, M. O'Boyle, Y. C. Martin, M. Rooks, and H. K. Wickramasinghe *Nature materials*, vol. 5, no. 5, p. 383, 2006. 70

[209] A. Chanthbouala, A. Crassous, *et al. Nature nanotechnology*, vol. 7, no. 2, p. 101, 2012. 70

[210] M. Marolt, "Superparamagnetic materials," in *Proceeding of Seminar Ib-4th Year (Old Program), University of Ljubljana Faculty of Mathematics and Physics*, 2014. 70

[211] M. Coïsson, G. Barrera, F. Celegato, L. Martino, F. Vinai, P. Martino, G. Ferraro, and P. Tiberto *Journal of Magnetism and Magnetic Materials*, vol. 415, pp. 2–7, 2016. 70

[212] A. E. Deatsch and B. A. Evans *Journal of Magnetism and Magnetic Materials*, vol. 354, pp. 163 – 172, 2014. 70

[213] Q. Dai, D. Berman, K. Virwani, J. Frommer, P.-O. Jubert, M. Lam, T. Topuria, W. Imaino, and A. Nelson *Nano letters*, vol. 10, no. 8, pp. 3216–3221, 2010. 70

[214] E. D. Spoerke, G. D. Bachand, J. Liu, D. Sasaki, and B. C. Bunker *Langmuir*, vol. 24, no. 14, pp. 7039–7043, 2008. 70

[215] G. Singh, H. Chan, A. Baskin, E. Gelman, N. Repnin, P. Král, and R. Klajn *Science*, vol. 345, no. 6201, pp. 1149–1153, 2014. 70

[216] I. Stanković, M. Dašić, and R. Messina *Soft Matter*, vol. 12, no. 12, pp. 3056–3065, 2016. 70

[217] R. Messina and I. Stanković *Physica A: Statistical Mechanics and its Applications*, vol. 466, pp. 10–20, 2017. 70

[218] Y. Bao, T. Wen, A. C. S. Samia, A. Khandhar, and K. M. Krishnan *J Mater Sci*, vol. 51, no. 1, pp. 513–553, 2016. 70

[219] M. Arejdal *et al. Physica A: Statistical Mechanics and its Applications*, vol. 437, pp. 375–381, 2015. 75

[220] M. Arejdal, A. Jabar, *et al. J Supercond Nov Magn*, vol. 29, no. 10, pp. 2553–2558, 2016. 75

[221] A. J. McGrath *et al. Chem. Commun.*, vol. 53, no. 84, pp. 11548–11551, 2017. 76

[222] M. P. Boroon *et al. Journal of Thermal Biology*, vol. 72, pp. 127–136, 2018. 76

[223] Y. Qing, L. Ma, X. Hu, *et al. Ceramics International*, vol. 44, no. 7, pp. 8706–8709, 2018. 76

[224] T. Kaneyoshi *Phase Transitions*, vol. 90, no. 2, pp. 131–142, 2017. 76

[225] N. Zaim, A. Zaim, and M. Kerouad *Journal of Alloys and Compounds*, vol. 663, pp. 516–523, 2016. 76

[226] T. Kaneyoshi *J Supercond Nov Magn*, vol. 31, no. 2, pp. 483–492, 2018. 76

[227] P. Sutcliffe *Physical review letters*, vol. 118, no. 24, p. 247203, 2017. 76

[228] S. Bedanta, A. Barman, *et al. Journal of nanomaterials*, vol. 2013, p. 169, 2013. 76

[229] A. Abedini *et al. Journal of Alloys and Compounds*, vol. 711, pp. 190–196, 2017. 76

[230] M. Y. Rafique *et al. Journal of Alloys and Compounds*, vol. 550, pp. 423–430, 2013. 76

[231] W. Lu, D. Sun, and H. Yu *Journal of Alloys and Compounds*, vol. 546, pp. 229–233, 2013. 76

[232] P. Guardia *et al. ACS Nano*, vol. 6, no. 4, pp. 3080–3091, 2012. 76

[233] H. Yang, T. Ogawa, *et al. Journal of Applied Physics*, vol. 103, no. 7, p. 07D526, 2008. 76

[234] G. Zhen *et al. The Journal of Physical Chemistry C*, vol. 115, no. 2, pp. 327–334, 2010. 76

[235] J. Vernieres, S. Steinhauer, *et al. Advanced Functional Materials*, vol. 27, no. 11, p. 1605328, 2017. 76

[236] D. Kechrakos and K. N. Trohidou *Phys. Rev. B*, vol. 58, no. 18, pp. 12169–12177, 1998. 76

[237] D. Kechrakos and K. Trohidou *Journal of Applied Physics*, vol. 89, no. 11, pp. 7293–7295, 2001. 76

[238] O. Dakir, A. El Kenz, and A. Benyoussef *Physica A: Statistical Mechanics and its Applications*, vol. 426, pp. 45–55, 2015. 79

[239] N. Hachem, M. Madani, *et al. J Supercond Nov Magn*, vol. 31, no. 7, pp. 2165–2172, 2018. 88

Résumé

Les nanoparticules magnétiques ont été largement étudiées pour leurs applications variées, allant du stockage d'information aux applications biomédicales. Cette multitude de fonctionnalités des nanoparticules magnétiques est due à leurs tailles nanométriques qui génèrent des phénomènes atypiques. Dans ce contexte plusieurs travaux théoriques et expérimentaux ont été consacrés à l'exploration des propriétés magnétiques de ce type de matériaux. Cependant, plusieurs problèmes ne sont pas encore résolus, en particulier la nature des interactions intra et inter-nanoparticules ainsi que les différentes morphologies des nanoparticules.

Cette thèse porte sur l'étude des propriétés magnétiques des nanoparticules en fonction de la température, à l'aide de la simulation numérique Monte et Carlo. Les effets de la dispersion, la morphologie des nanoparticules, les interactions surface-Cœur intra-nanoparticule et les interactions entre les nanoparticules ont été étudiés pour différentes tailles. Ainsi pour des nanoparticules cubiques, la température de critique, l'aimantation rémanente, les champs coercitifs et le cycle Hystérésis, dépendent fortement, des couplages d'échange, de l'anisotropie magnétique et de la taille des nanoparticules. De plus la température de compensation prend lieu pour des valeurs bien précises des interactions magnétiques surface-cœur et entre particules, en bon accord qualitatif avec les travaux expérimentaux.

Mots-clefs : Nanopaticules magnétiques; Nanocubes ; Propriétés magnétiques ;Modèle d'Ising; Effets de taille ; Diagrammes de phases ; Simulation Monte Carlo.

Abstract

Magnetic nanoparticles were widely studied for their varied applications, ranging from information storage to biomedical applications. This multitude of functionalities of magnetic nanoparticles is due to their nanometric sizes, which generate atypical phenomena. In this context, several theoretical and experimental works have been devoted to the exploration of the magnetic properties of this type of material. However, various problems have not yet been solved, in particular the nature of the intra- and inter-nanoparticle interactions as well as the different morphologies of the nanoparticles.

This thesis focuses on the study of the magnetic properties of nanoparticles as a function of temperature, using numerical Monte Carlo simulation. The effects of dispersion, the morphology of the nanoparticles, the intra-nanoparticle interactions and the interactions between the nanoparticles have been studied for different sizes. Thus, for cubic nanoparticles, the critical temperature, the residual magnetization, the coercive fields and the Hysteresis cycle strongly depend on the exchange couplings, the magnetic anisotropy and the size of the nanoparticles. Moreover, the compensation temperature takes place for very precise values of magnetic interactions Core-Shell and between particles, in good agreement, qualitatively, with the experimental works.

Key Words : Magnetic nanoparticles ; Nanocubes; Magnetic properties ; Ising Model ; Size effect ; Diagram phases ; Monte Carlo simulations.